NAVAL POSTGRADUATE SCHOOL

MONTEREY, CALIFORNIA

THESIS

ATMOSPHERIC RIVERS AND THEIR ROLE IN EXTREME PRECIPITATION IN THE MIDWEST U.S.

by

Stephanie L. Hedstrom

March 2013

Thesis Advisor: Wendell Nuss
Second Reader: Heather Archambault

Approved for public release;distribution is unlimited

THIS PAGE INTENTIONALLY LEFT BLANK

REPORT DOCUMENTATION PAGE

Form Approved OMB No. 0704-0188

1. AGENCY USE ONLY *(Leave blank)*	**2. REPORT DATE** March 2013	**3. REPORT TYPE AND DATES COVERED** Master's Thesis

4. TITLE AND SUBTITLE
ATMOSPHERIC RIVERS AND THEIR ROLE IN EXTREME PRECIPITATION IN THE MIDWEST U.S.

5. FUNDING NUMBERS

6. AUTHOR(S) Stephanie L. Hedstrom

7. PERFORMING ORGANIZATION NAME(S) AND ADDRESS(ES)
Naval Postgraduate School
Monterey, CA 93943-5000

8. PERFORMING ORGANIZATION REPORT NUMBER

9. SPONSORING /MONITORING AGENCY NAME(S) AND ADDRESS(ES)
N/A

10. SPONSORING/MONITORING AGENCY REPORT NUMBER

11. SUPPLEMENTARY NOTES The views expressed in this thesis are those of the author and do not reflect the official policy or position of the United States Air Force, Department of Defense or the U.S. Government. IRB Protocol number ____N/A____.

12a. DISTRIBUTION / AVAILABILITY STATEMENT
Approved for public release;distribution is unlimited

12b. DISTRIBUTION CODE

13. ABSTRACT (maximum 200 words)

Two case studies are presented of atmospheric rivers (ARs) that produced heavy precipitation in the Midwest U.S. during March 2008 and October 2009. A third case study demonstrating an AR with normal precipitation in the Midwest is also included for comparison. The analyses used the Climate Forecast System Reanalysis (CFSR) data sets for identification of ARs and analysis. The study documents several key ingredients that contribute to differentiating between events of extreme precipitation and normal precipitation. The primary findings of this study are as follows: 1) the induced flow due to the low-level/surface temperature anomaly plays an important role in transporting moisture from the Caribbean northward to the Midwest, 2) the induced wind field from a strong upper-level potential vorticity (PV) anomaly increases moisture flux from the Gulf and decreases static stability, which favors convective precipitation, and 3) heavy precipitation events are preceded approximately 9 hours by an increasing, positive moisture flux occurring across the northern Gulf Coast.

14. SUBJECT TERMS atmospheric river, heavy precipitation	**15. NUMBER OF PAGES** 113
	16. PRICE CODE

17. SECURITY CLASSIFICATION OF REPORT	**18. SECURITY CLASSIFICATION OF THIS PAGE**	**19. SECURITY CLASSIFICATION OF ABSTRACT**	**20. LIMITATION OF ABSTRACT**
Unclassified	Unclassified	Unclassified	UU

NSN 7540-01-280-5500

Standard Form 298 (Rev. 2-89)
Prescribed by ANSI Std. 239-18

THIS PAGE INTENTIONALLY LEFT BLANK

Approved for public release;distribution is unlimited

ATMOSPHERIC RIVERS AND THEIR ROLE IN EXTREME PRECIPITATION IN THE MIDWEST U.S.

Stephanie L. Hedstrom
Captain, United States Air Force
B.S., University of North Dakota, 2004

Submitted in partial fulfillment of the
requirements for the degree of

MASTER OF SCIENCE IN METEOROLOGY

from the

NAVAL POSTGRADUATE SCHOOL
March 2013

Author: Stephanie L. Hedstrom

Approved by: Wendell Nuss
Thesis Advisor

Heather Archambault
Second Reader

Wendell Nuss
Chair, Department of Meteorology

THIS PAGE INTENTIONALLY LEFT BLANK

ABSTRACT

Two case studies are presented of atmospheric rivers (ARs) that produced heavy precipitation in the Midwest U.S. during March 2008 and October 2009. A third case study demonstrating an AR with normal precipitation in the Midwest is also included for comparison. The analyses used the Climate Forecast System Reanalysis (CFSR) data sets for identification of ARs and analysis. The study documents several key ingredients that contribute to differentiating between events of extreme precipitation and normal precipitation. The primary findings of this study are as follows: 1) the induced flow due to the low-level/surface temperature anomaly plays an important role in transporting moisture from the Caribbean northward to the Midwest, 2) the induced wind field from a strong upper-level potential vorticity (PV) anomaly increases moisture flux from the Gulf and decreases static stability, which favors convective precipitation, and 3) heavy precipitation events are preceded approximately 9 hours by an increasing, positive moisture flux occurring across the northern Gulf Coast.

THIS PAGE INTENTIONALLY LEFT BLANK

TABLE OF CONTENTS

THIS PAGE INTENTIONALLY LEFT BLANK

LIST OF FIGURES

LIST OF TABLES

THIS PAGE INTENTIONALLY LEFT BLANK

I. INTRODUCTION

Over the weekend of 1–2 May 2010, record-breaking rainfall occurred over Kentucky and Tennessee. As much as 18–20 inches fell locally, in areas to the west and south of Nashville, TN, and amounts of 11-13 inches throughout much of middle and western Tennessee. Flash flooding and flooding of the Cumberland River and its tributaries caused 26 fatalities. Preliminary estimates of property damage in the greater Nashville area exceeded $2 billion (NWS, 2011). Fort Campbell Army Installation, located approximately 60 miles north of Nashville and also affected by the heavy precipitation, was open to mission-essential personnel only, including only mission-essential services at the Blanchfield Army Community Hospital (The Leaf Chronicle, 2010). The washed-out roads and sinkholes created dangerous situations for both on- and off-base transportation, limiting access to training areas and impacting the already tight land-use resources on the installation.

This heavy and long-lived precipitation event was caused by two successive, quasi-stationary mesoscale convective systems (MCSs). The MCSs were supported by a stream of moisture-abundant air from the Caribbean Sea and Gulf of Mexico, also known as an atmospheric river (AR). The event described here is an example of a heavy precipitation event fueled by an AR. The forecast challenge with this situation is: How do we accurately forecast where the extreme precipitation will occur? Is merely identifying the existence of an AR enough to warrant heavy precipitation warnings? From observations of West Coast ARs, not all are extreme precipitation makers, hinting at the importance of identifying key dynamical processes for extracting the moisture from the atmosphere. If heavy precipitation were forecast based solely on the presence of an AR, false alarm rates would be high.

Studies of severe flooding on the West Coast have indicated that ARs play an important role (Ralph et al. 2006). However, ARs impacting precipitation in the Midwest have not been as thoroughly studied. Direct application of the results

from West Coast studies regarding the involved dynamics may not apply, since topography plays a significant role in forcing vertical motion in that region. ARs with a deep moisture tap into the Caribbean have the potential to produce extreme precipitation, which causes impacts to transportation, property and life. Understanding the critical dynamical processes in which heavy precipitation is extracted from ARs extending from the Caribbean is crucial in accurately forecasting impacts to personnel and resources for military installations in the central U.S.

II. BACKGROUND

A. DEFINITION

An atmospheric river (AR) is defined as strong, horizontal moisture fluxes with a filamentary form, with a length several times larger than the width (Zhu and Newell, 1998). The majority of the mid-latitude moisture flux occurs in these filamentary features, yet the fraction of the globe they cover is 10% or less (Zhu and Newell, 1998; Ralph et al. 2004). When AR conditions occur, they are typically located in the warm sector of extratropical cyclones (warm conveyor belt) and can be characterized by strong winds (low level jet) and large water vapor contents at low altitudes (Ralph et al. 2004), with roughly 75% of the meridional moisture transport occurring in the lowest 2.25 km (Ralph et al. 2004). The combination of the filamentary form and high water vapor content lends itself to the term “atmospheric river.”

Classifying an AR strictly on the water vapor content has not yet been standardized, and may require different thresholds based on the region in which the AR occurs. For U.S. West Coast ARs that spanned an 8-year period, Neiman et al. (2008) specified that a long (>2000km) and narrow (<1000km) plume with integrated water vapor (IWV) exceeding 20mm was a good indicator of an AR. A strong wintertime AR exceeded a threshold of 30mm of IWV. For the Midwest U.S., a recent study of an extreme precipitation event in May 2010 attributed IWV values in the range of 30–55mm (Moore et al. 2012) extending from Central America to the Great Lakes region (~3000km). Therefore, the exact definition may be regionally dependent and depend on the circumstances to be fully defined.

An AR over the Pacific Ocean extending toward the West Coast is often called the “Pineapple Express,” as it is a warm, moist air that flows northeastward near the Hawaiian Islands (Lackman et al. 1999). Similarly, Dirmeyer and Kinter (2009) dubbed the AR equivalent impacting the central U.S. as the “Maya Express.”

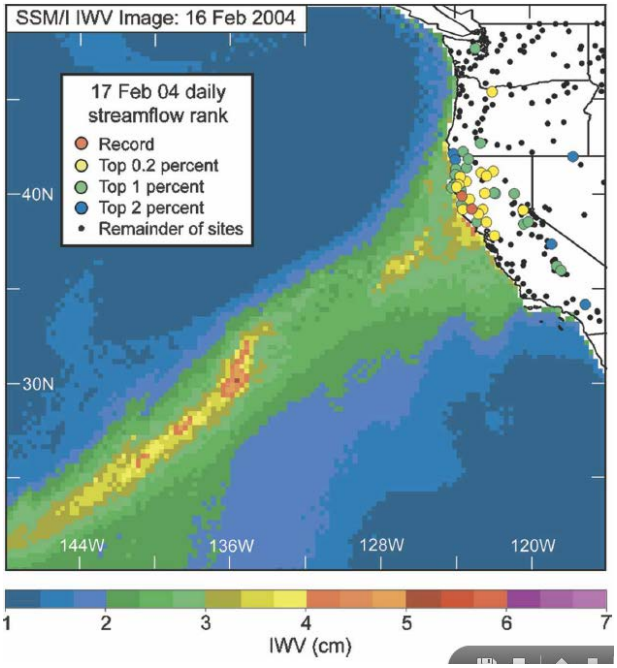

Figure 1. Pineapple Express Feb 2004. Integrated Water Vapor Values Exceeding 20mm, with Local IWV Exceeding 40mm (From Neiman et al. 2008).

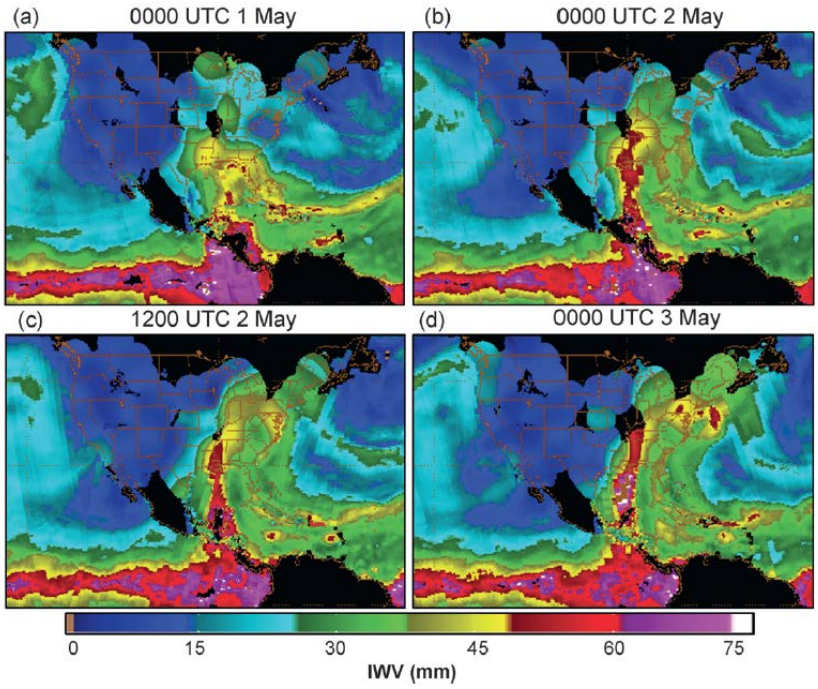

Figure 2. Maya Express May 2010. Integrated Water Vapor Values Exceeding 50mm (From Moore et al. 2012).

Zhu and Newell (1998) found that four to five ARs exist at any given time, corresponding to a planetary wave number four to five. This may be due to the associated synoptic-scale extratropical cyclone and subsequent frontal processes of each planetary wave, resulting in narrow regions of moisture transport. The location of these features, whether over land or ocean, affects the amount of poleward moisture transport (Ralph et al. 2004).

B. WEST COAST U.S. ATMOSPHERIC RIVERS

Lackman et al. (1999) did a composite analysis of ARs to determine the planetary/synoptic flow patterns associated with Pineapple Express events. They found a negative sea level pressure (SLP) anomaly was located west of British Columbia and a positive SLP anomaly centered over the southwest U.S. The pressure gradient flow associated with this orientation created an AR with a southwest to northeast orientation in which moisture could be transported from the tropics to the West Coast. They also noted that the surface temperature anomaly was aligned so that initially a cold anomaly existed over Yukon and Northwest Territories and a warm anomaly stretched from the Hawaiian Islands toward the Pacific NW. As the pattern evolved, the warm anomaly amplified and advanced northeastward to the Pacific Northwest, eventually shifting eastward to encompass much of the U.S. (Lackman et al. 1999). As a result of the anomalously warm conditions, land-falling ARs in the winter lead to rain-on-snow to melt snowpacks, which increased the likelihood of flooding (Neiman et al. 2008). Neiman et al. (2008) showed that roughly twice as much precipitation as normal falls during AR storms during the winter on the West Coast. During the summer, precipitation enhancements were not as significant (mostly due to the IWV content being less as it originates over the cool Pacific).

1. Orographic Enhancement

It is widely documented that interaction of an AR with steep, mountainous terrain (commonly found along the West Coast) provides strong and concentrated upslope water vapor flux, leading to heavy orographic precipitation

and flooding when sufficient dynamics to extract the moisture that exists (e.g., Ralph et al. 2004, 2011; Lackman et al. 1999).

2. Frontal Wave Enhancement

In studies of an extreme event in California, Ralph et al. (2004) and Neiman et al. (2004) have documented the presence of a mesoscale frontal wave of roughly 500–1000km horizontal wavelength along the primary cold front, but did not necessarily document the impact that frontal wave had on the AR and subsequent focusing of extreme rainfall. Ralph et al. (2011) found that in their study of a single case, a mesoscale frontal wave increased the duration of AR conditions at landfall in the Pacific Northwest.

C. MIDWEST U.S. ATMOSPHERIC RIVERS

As identified by Moore et al. (2012), considerable attention has been placed on ARs impacting the western coasts of continents, but very little on those impacting the Central U.S. In a water cycle perspective of Midwest floods, Dirmeyer and Kinter (2010) found that the patterns that produced flood and drought conditions were not mirror images of each, but rather that flood cases were often associated with a proportionally larger transport of moisture from the Caribbean or Gulf of Mexico compared to normal conditions. Climate studies linking extreme precipitation to ARs are also limited for the Midwest. Higgins et al. (2011) conducted a climate analysis of two months of heavy precipitation events, which is a start, but far from all-encompassing.

Terrain is not a significant precipitation extractor for Midwest ARs. Therefore, knowledge of the dynamics to extract moisture from an AR is crucial for understanding the likelihood and location of heavy precipitation. In the recent case of the Tennessee flood in May 2010, two persistent and stationary MCSs (fueled by an AR) caused heavy precipitation. The persistent mesoscale lifting associated with the quasi-stationary convectively generated outflow boundaries and a persistent strong integrated water vapor flux (integrated vapor transport – (IVT)) with the stationary AR combined to cause rain in excess of 13” throughout

middle Tennessee. In this case, it was also documented that a local acceleration of the winds in the low levels accompanied the passage of a mesoscale frontal wave (Moore et al. 2012).

Higgins et al. (2011) studied high precipitation events impacting the south central U.S. during May–June 2010 and found that all of the cases were associated with warm, moist air masses (with record-breaking temperatures occurring in the surrounding regions) and that deep moisture plumes extended deep in to the Caribbean, typical of a "Maya Express." Again, do all ARs produce extreme precipitation? Merely recognizing an AR and forecasting heavy precipitation may overforecast the situation and lead to false alarms, as implied by the discussion by Dirmeyer and Kinter (2010).

Key processes that enhanced precipitation on the West Coast have been identified as terrain (Neiman et al. 2008) and frontal waves (Ralph et al. 2011). The difference between ARs in the Midwest and those impacting the West Coast are not well understood and may represent fundamental differences in their forcing. The critical dynamical processes associated with ARs in the Midwest that produce extreme precipitation have not been widely documented and certainly will be different from West Coast ARs.

D. DYNAMICS

The study by Moore et al. (2012) documented the meteorological conditions and physical processes associated with an AR extending into the central U.S., but being based on only one case, further studies or additional cases (such as this study) are needed to support their findings and/or provide additional insight to the processes involved in heavy precipitation associated with ARs.

Schumacher and Johnson (2005) found that 65% of extreme precipitation events in the Midwest were caused by mesoscale convective systems and 27% resulted from synoptic weather systems. While Schumacher and Johnson (2005) selected their cases based on 24-hour rainfall totals, their events were not

necessarily related to ARs. In contrast, the selection process for this thesis is to determine cases of existing ARs in the Midwest and examine which dynamical processes enabled efficient extraction of moisture in the form of precipitation (not all of the strong ARs may have produced significant precipitation). This is important for the forecaster in order to determine whether an AR will be an extreme precipitation producer, and to recommend actions accordingly based on the forecasted impact.

Based on preliminary numerical model results, Ralph et al. (2004) suggested that the primarily geostrophic horizontal frontal confluence contributes significantly to the development of IWV plumes, and ageostrophic secondary vertical frontal circulations focus the narrower cloud liquid water (CLW) and rain rate (RR) peaks within the plumes. This implies that the broad area of moisture that is typically present over the Gulf of Mexico and the Caribbean can be concentrated into a narrow plume and advected into the Midwest, increasing the average precipitation.

This study hypothesizes that the following concepts are pivotal in extreme precipitation events associated with Midwest ARs: 1) the low-level/surface temperature anomaly plays an important role in transporting moisture from the Caribbean northward to the Midwest, 2) the induced wind field from a strong upper-level potential vorticity (PV) anomaly increases moisture flux from the Gulf and decreases static stability, which favors convective precipitation, 3) a distinct signal precedes a heavy precipitation event (i.e., an increasing, positive moisture flux occurring across the northern Gulf Coast), potentially aiding in the forecasting of such events.

III. DATA, METHODOLOGY, AND ANALYSIS

This chapter highlights the data and methodology used to identify and analyze specific cases in which ARs were present. To ensure that all potential cases were consistently analyzed, reanalysis data was used for both identification and diagnostic analysis. Where appropriate, additional observational evidence was examined to verify the case selection using gridded analysis data.

A. DATA

For this study, the CFSR reanalysis model was used for case selection and analysis. The Climate Forecast System Reanalysis (CFSR) is a reanalysis model run at T382 horizontal resolution and a sigma-pressure hybrid vertical coordinate with 64 levels. Data assimilation depends on historical and operational archives of observations and makes use of raw observed radiance measures from satellite retrievals, with the bulk of the satellite instruments available during the 2008–2010 period. The CFSR model is considered "semicoupled." The land hydrology model is provided six variables from the atmospheric model, but the traditional model-generated precipitation is replaced with observed precipitation for added realism (Saha et al. 2010). In addition, a single 1 season (~123-day) hindcast run, initiated from every 00 UTC cycle over the 12-year period from 1999-2010, is required to calibrate the operational Climate Prediction Center (CPC) first season predictions for hydrological forecasts (precipitation, evaporation, runoff, streamflow, etc.) (Saha et al. 2010). Because our focus is on the Central U.S., this study used a CFSR data subset (Figure 3) with a domain of 341 x 141 grid points in the north-south and east-west directions, respectively, with a horizontal grid spacing of 0.5° and 38 vertical pressure levels. The data was re-gridded from the Mercator projection to a Lambert Conformal map projection (Figure 4) to aid in moisture flux and PV inversion calculations. Since the synoptic scale features were of primary interest,

the PV inversion used a degraded 150km horizontal resolution to aid in the numerical stability of the computations. The analysis time (F00) was not used in order to allow the model to spin up and produce precipitation; therefore, the 3-hr and 6-hr forecasts were used to cover the events in 3-hr increments.

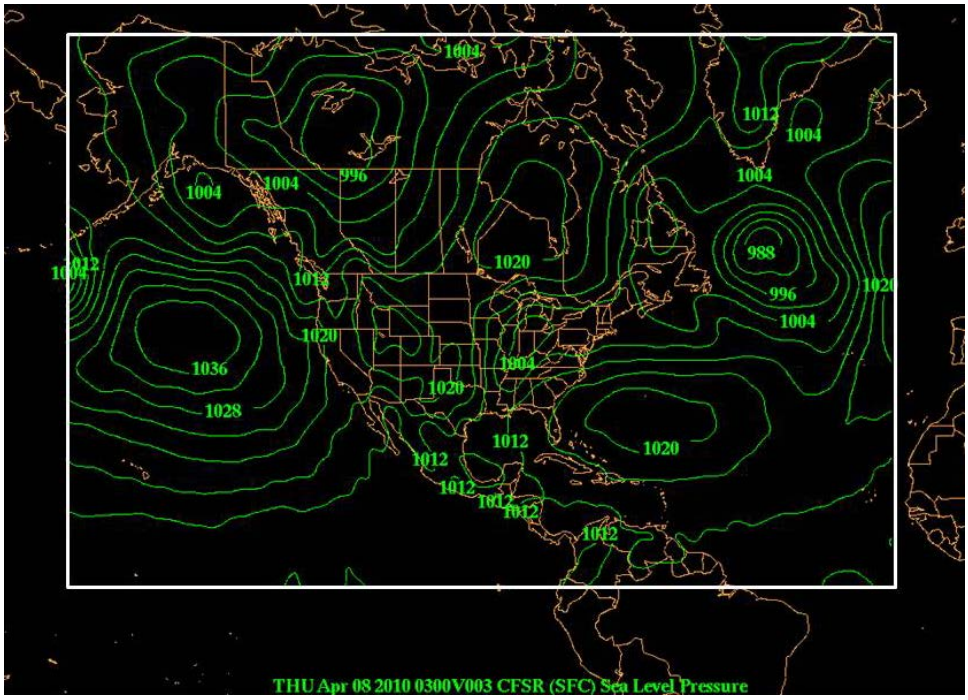

Figure 3. CFSR Data Subset Domain (White Box).

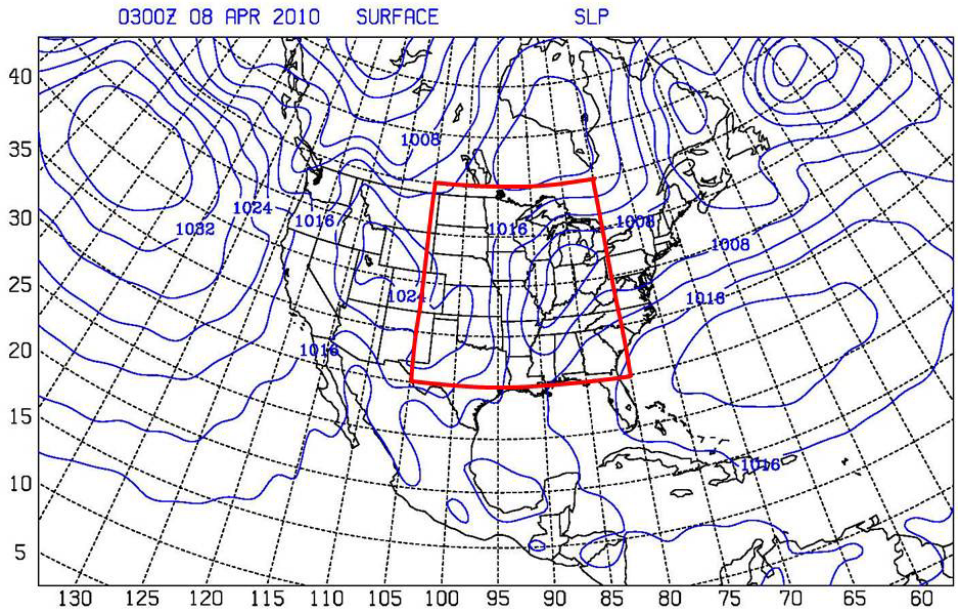

Figure 4. CFSR Data Subset Domain Re-gridded to Lambert Conformal map Projection. Inner Box (Red) is the Domain for Moisture Flux and Average Precipitation Calculations.

B. METHODOLOGY

1. Determining ARs

ARs were determined by first reviewing the animated loops generated by CFSR integrated precipitable water (IPW) every 12 hours for each year, 2008–2010. Subjective selection criteria included 1) plumes extending from the Caribbean/Gulf of Mexico into the central U.S., and 2) relatively narrow with respect to length. In fact to be consistent with previous definitions of ARs, the high PW air was required to originate south of 20°N in the region of tropical moisture based on the backward parcel trajectory analyses that will be described later in this section. Examples of the ARs that are subsequently examined in this study are shown in Figure 5. This resulted in 14 possible ARs. After the potential ARs were identified, event precipitation for each case was reviewed using the National Weather Service Advanced Hydrologic Prediction Service 24-hr precipitation archive data http://water.weather.gov/precip/). Cases of interest exhibited heavy (greater than 4” over event duration) and widespread

precipitation (approximately 50,000 square miles—about the size of Arkansas). Two cases captured the essence of different heavy precipitation modes and will be examined in detail for this study, 29 October 2009 and 19 March 2008. The October case appeared to exhibit primarily convectively driven precipitation (synoptic type as classified by Maddox et al. 1979), whereas the March case appeared to be strongly baroclinically driven (frontal type by Maddox et al. 1979). To add an element of comparison, the 7 April 2010 event was selected as a non-heavy precipitation AR event. This event exhibited precipitable water values similar to the March case and a synoptic pattern similar to the October case, but yielded only moderate precipitation.

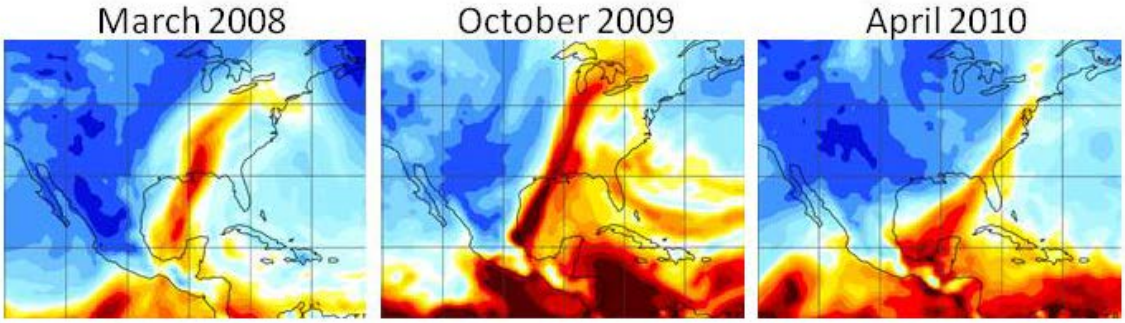

Figure 5. Example of ARs as Identified by IPW.

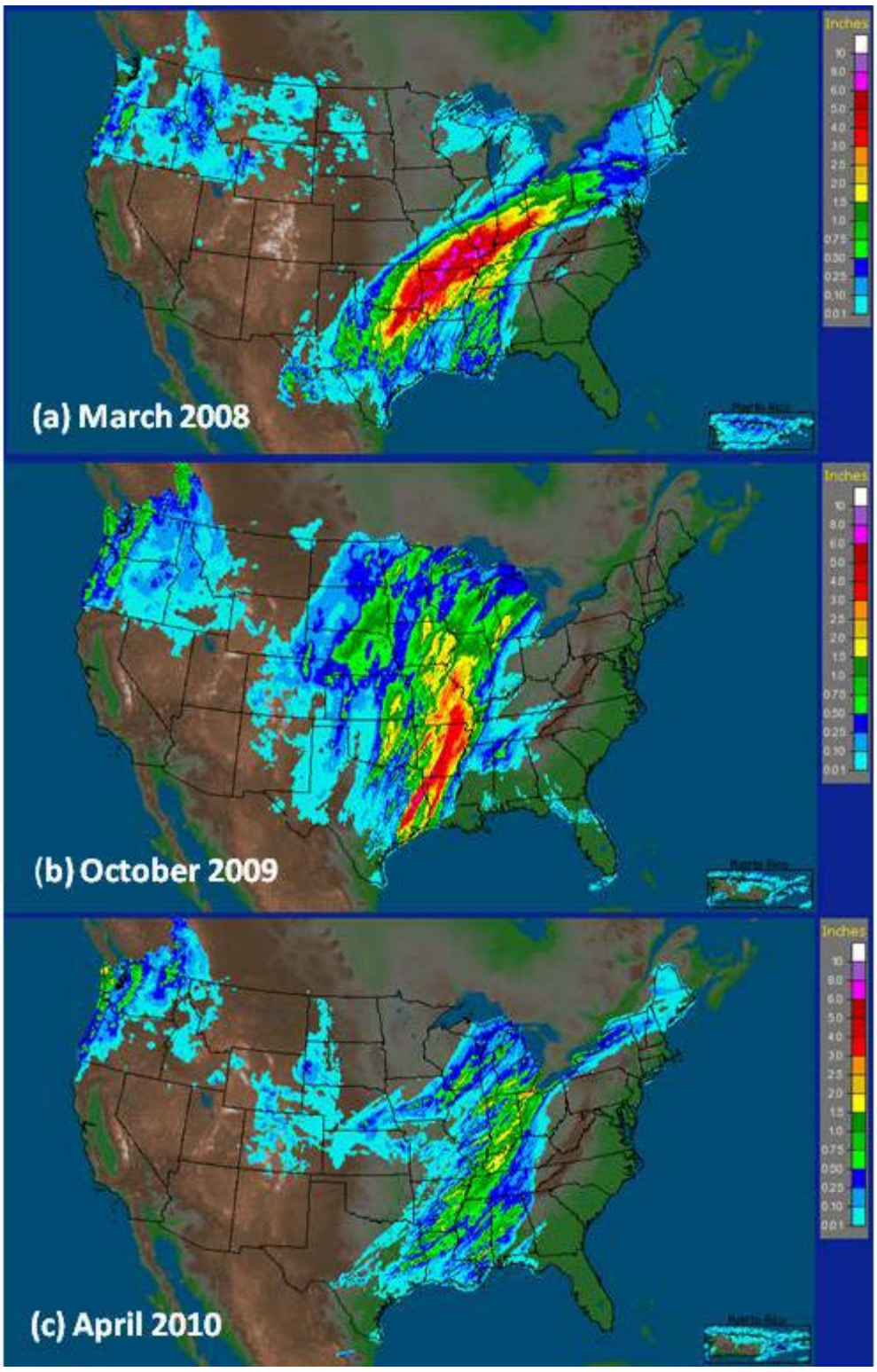

Figure 6. 24-hr Precipitation Ending at 12Z on (a) 19 Mar 08, (b) 30 Oct 09, and (c) 8 Apr 10.

To confirm the origination of the AR in the Gulf of Mexico or Caribbean, backward trajectories of parcels ending in the region of the most accumulated rainfall were computed using the NOAA HYSPLIT Model. The HYSPLIT (Hybrid Single-Particle Lagrangian Integrated Trajectory) model is a complete system for computing simple air parcel trajectories to complex dispersion and deposition simulations. The calculation method is a hybrid between the Lagrangian approach, which uses a moving frame of reference for the advection and diffusion calculations as the air parcels move from their initial location, and the Eulerian approach, which uses a fixed three-dimensional grid as a frame of reference to compute the pollutant air concentrations (Draxler and Rolph, 2012). The model uses existing meteorological forecast fields from regional or global models (in this case the GFS archive) to compute the advection, stability and subsequent dispersion. In the particle model, a fixed number of particles are advected about the model domain by the mean wind field and spread by a turbulent component. Since a different model was used for HYSPLIT trajectories compared to CFSR analysis, small differences may be possible.

The parcel trajectories were very similar for the March and October cases, with their origination in the central Caribbean Sea between 10-20°N, south of Haiti and the Dominican Republic. The parcels ending at 1500m (around 825hPa) over the regions of interest started in the layer near the surface (between 950hPa to 750hPa). The parcels then traveled NW over the central Gulf of Mexico into the Midwest U.S. For the majority of the travel northward, the parcels slowly descended, consistent with subsidence around the high pressure located to the east. (The unsteady trajectories near the beginning of the transport were likely due to ascent triggered by interaction with the terrain over the Yucatan Peninsula.) As they neared the region of interest, ascent was more drastic as expected based on the precipitation summaries.

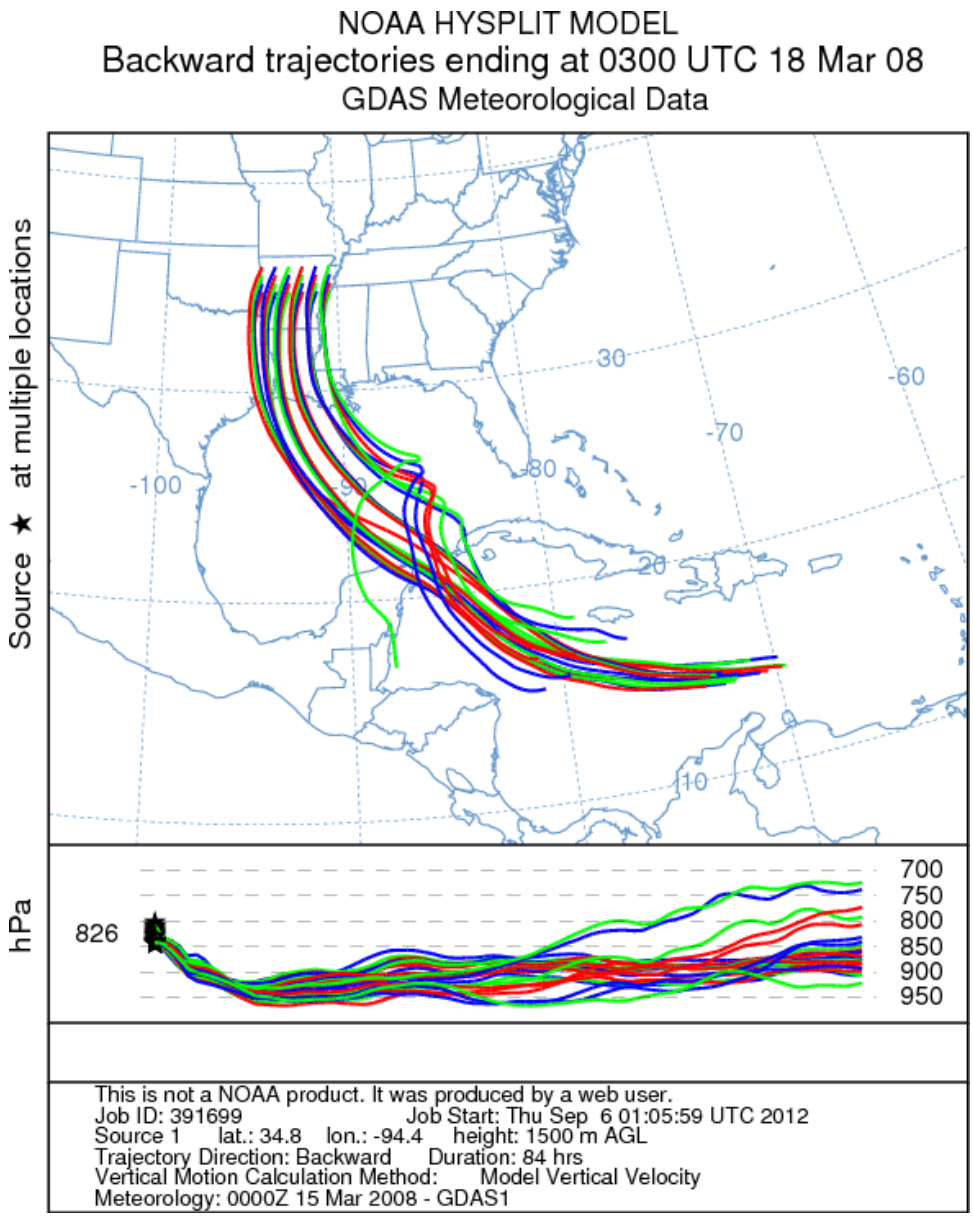

Figure 7. March 2008, 84-hr Backward Parcel Trajectories Ending at 03Z on 18 Mar 08.

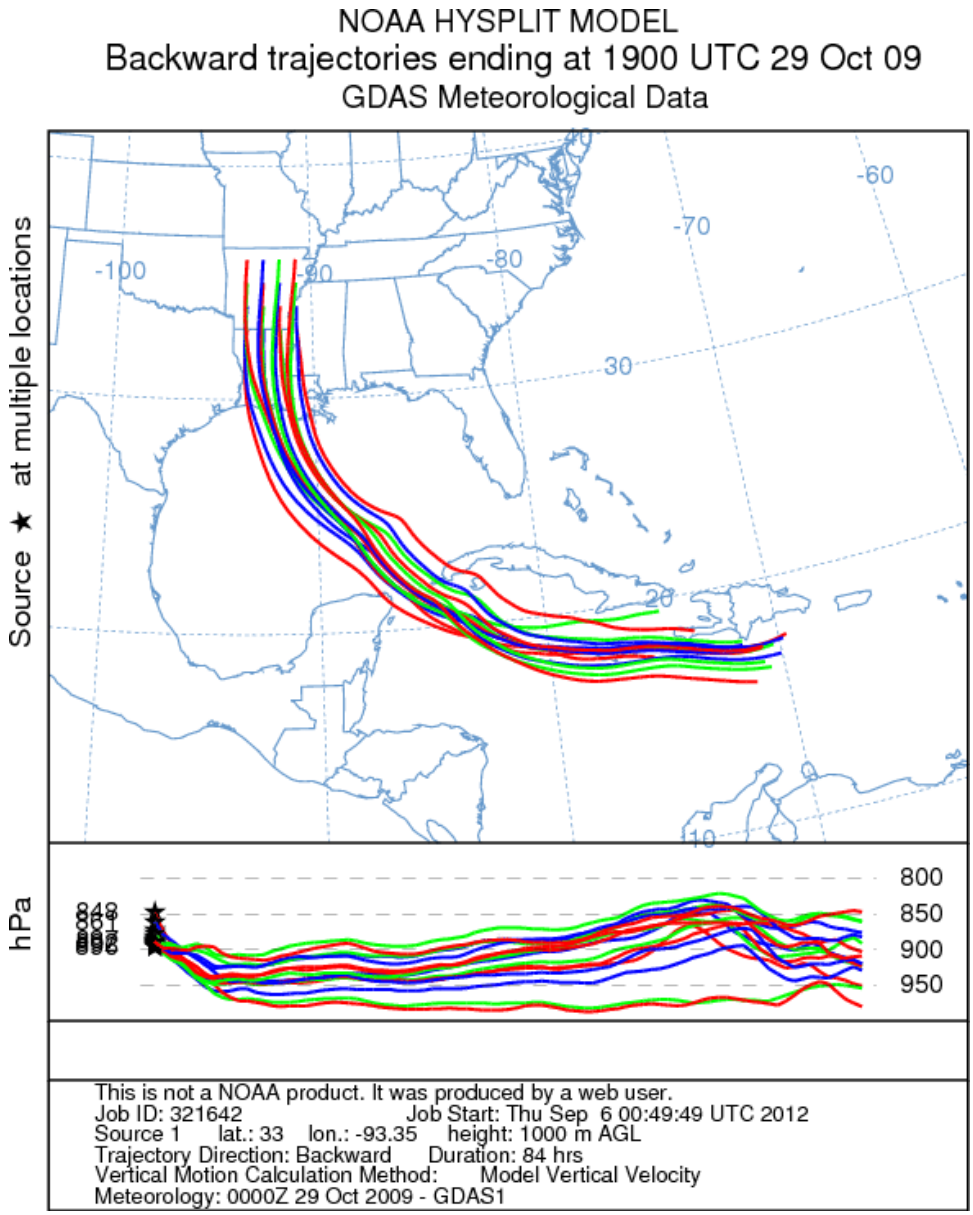

Figure 8. October 2009, 84-hr Backward Parcel Trajectories Ending at 19Z on 29 Oct 09.

The April case showed trajectories originating between the Gulf of Mexico and the Caribbean Sea around 20°N, slightly further north than the heavy precipitation cases. With the more northern source region, the April case only marginally qualified as an AR. They also originated near the surface. The path of the parcels took a more westerly path initially, and then curved drastically northward along the western coast of the Gulf of Mexico before entering the

Midwest with a northeastward flow orientation. Ascent near the end of the depicted trajectories was not as dramatic as the heavy precipitation cases.

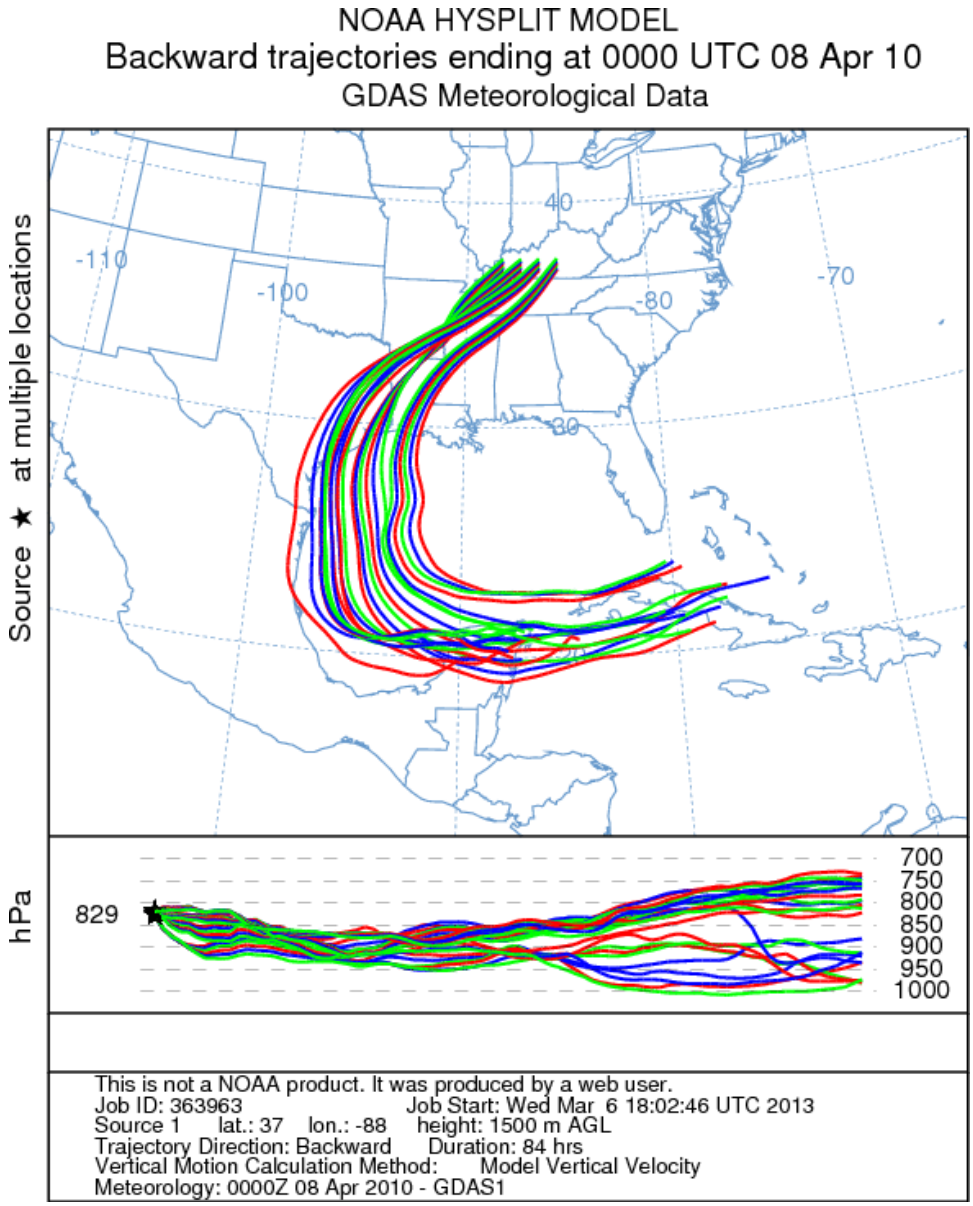

Figure 9. April 2010, 84-hr Backward Parcel Trajectories Ending at 00Z on 8 Apr 10.

Based on the precipitable water plumes shown in Figure 5 and the origination as confirmed by HYSPLIT, all three cases fit the definition of AR transporting moisture into the Midwest, a Maya Express. The April case was

somewhat marginal as an AR, but overall seemed to definitely fit even with its more northern source region.

2. Moisture Budget: Moisture Flux and Average Precipitation Calculations

To understand the relationship between heavy precipitation and an AR, moisture budgets were calculated. The moisture transport and precipitation can be combined in a balanced moisture budget to determine the extent of influence that ARs have on producing heavy precipitation. A balanced moisture budget is as follows:

$$\text{Inflow} - \text{Outflow} + \text{Source} - \text{Sink} = 0,$$

where the inflow and outflow are the moisture fluxes, the sink is precipitation and source is from evaporation within the domain. For this study, the source was assumed to be zero as the domain (Figure 4) was defined to be completely over land. Surface flux could also result from evapotranspiration, but this was also neglected.

The horizontal moisture flux was calculated using the moisture flux across the vertical planes of the domain. The box extended vertically from the surface to approximately 200hPa (this upper boundary is approximate as the calculation code used height as its vertical coordinate, but the approximation was deemed acceptable as the majority of the atmospheric moisture exists in the lower troposphere). The vertically integrated advection of specific humidity by the horizontal wind was calculated around the perimeter of the defined domain and summed to get the moisture contributed by advection. Total average precipitation in the defined domain was computed by adding the 3-hr precipitation at each grid point and dividing by the area of the domain.

3. Piecewise PV Inversion

To determine the influence that the upper-level PV anomaly and the low-level/surface temperature anomaly have in the moisture transport, a piecewise PV inversion technique was applied. The piecewise PV inversion was done on the upper-level and low-level/surface PV anomalies to separate their contribution to moisture transport from the south. A full PV inversion was first calculated on a 150km Lambert Conformal grid using a modified Davis-Emanuel PV inversion process (Davis and Emanuel, 1991). Perturbations were then defined as deviations from the east–west average (rather than a temporal filtering or time average), but were not strictly zonal due to the Lambert Conformal grid used. The mean state was defined as the east–west average, and the balanced mean flow was calculated from the mean PV and boundary potential temperature values. Perturbations were calculated by subtracting the mean fields (defining the total perturbation first).

The contributions from the upper-level PV anomaly on the low-level flow were calculated by setting the perturbation to zero below 600hPa. Conversely, the perturbation was set to zero above 600hPa to determine contributions from the low-level/surface temperature anomaly.

The cross section in Figure 10 shows the observed full-resolution vertical distribution of PV, potential temperature and meridional flow along the Gulf Coast (approximately 32°N). Comparing the meridional flow from the full PV inversion along a similar cross section (Figure 11), they appear similar. They do not exactly match due to the lower-resolution of the data set used in the PV inversion. Additionally, the cross section has a different length, slightly affecting the width of the features. Regardless of these differences, the inversion captures the synoptic features well. The eastern jet core is located higher in the atmosphere than the western core. Jet core speeds are also well-represented: 65kts in the inversion versus 65–70kts in the observed cross section. Even though the features are smoothed due to the lower-resolution data set, they capture the synoptic-scale features.

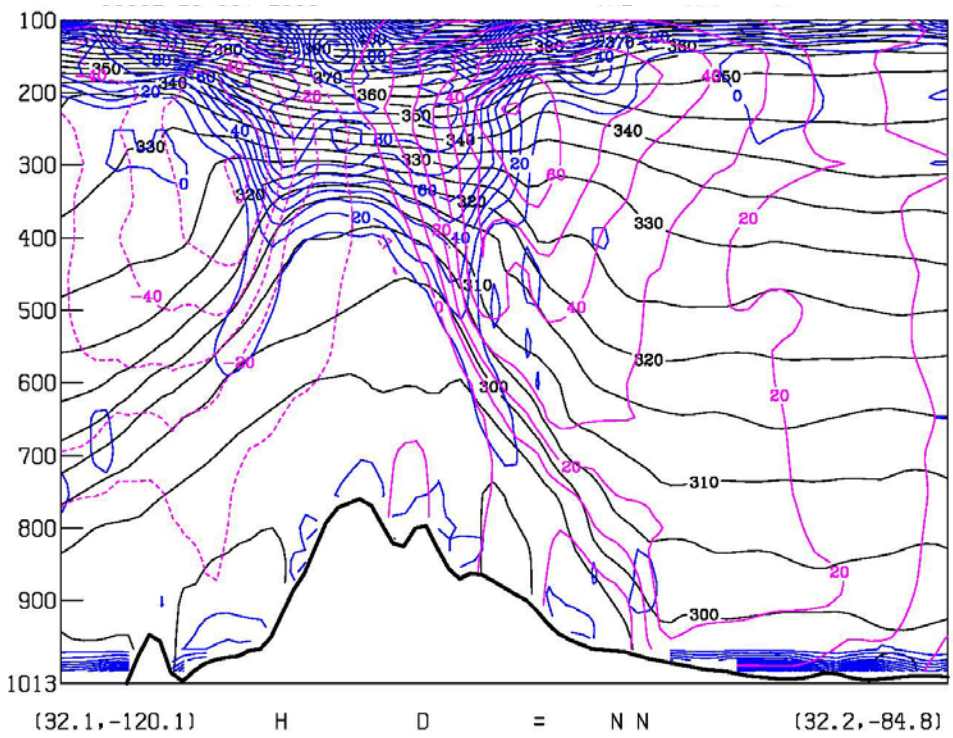

Figure 10. October 2009, Observed Vertical Cross Section, Midpoint 1 (29 Oct 09, 18Z). Potential Temperature (Kelvin) in Black Contours, Potential Vorticity with every 10 units equal to 1 PVU in Blue, and Wind (m/s) in Magenta.

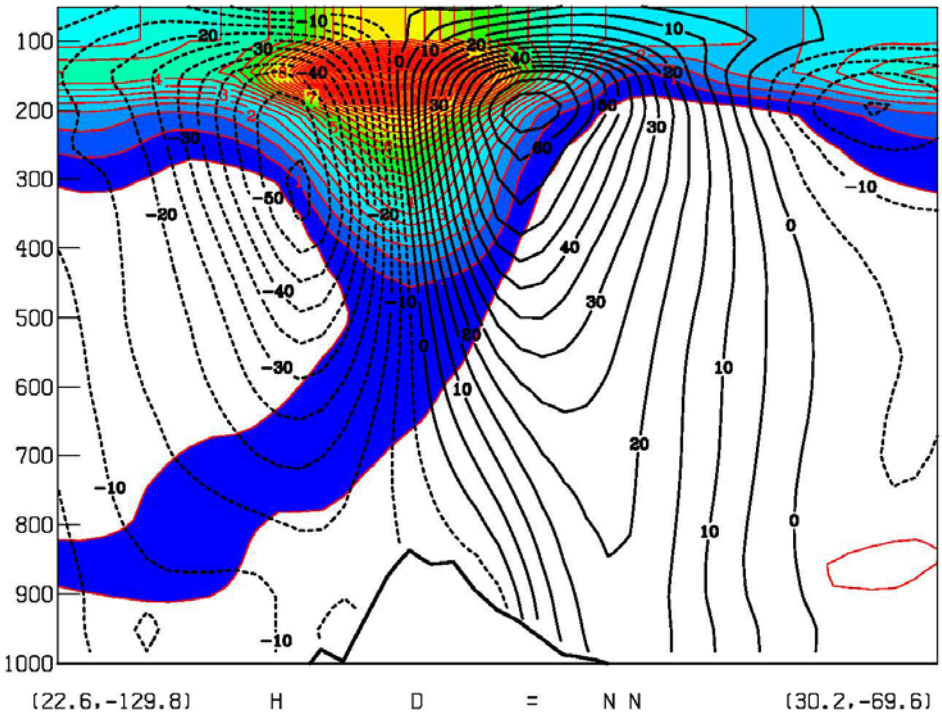

Figure 11. October 2009, Full PV Inversion, Vertical Cross Section, Midpoint 1 (29 Oct 09, 18Z). Potential Temperature (Kelvin) in Red Contours and Color-fill, and Wind (m/s) in Black.

C. ANALYSIS

1. Synoptic Overview of the Case Studies

Each of the cases were reviewed and compared to the other cases using comparative points in their evolution based on a predetermined "event onset." Event Onset is defined as the time at which the average precipitation began to increase significantly in the domain. Figure 12 shows the precipitable water at each of these times noted in Table 1.

Table 1. Dates/Times for Each Case at Specified Points in System Evolution.

	March 2008	October 2009	April 2010
9 Hours Prior to Event Onset	17Mar08 15Z	28Oct09 21Z	7Apr10 06Z
Event Onset	18Mar08 00Z	29Oct09 06Z	7Apr10 15Z
Midpoint 1	18Mar08 12Z	29Oct09 18Z	8Apr10 03Z
Midpoint 2	19Mar08 00Z	30Oct09 06Z	8Apr10 15Z
Event End	19Mar08 12Z	30Oct09 18Z	9Apr10 03Z

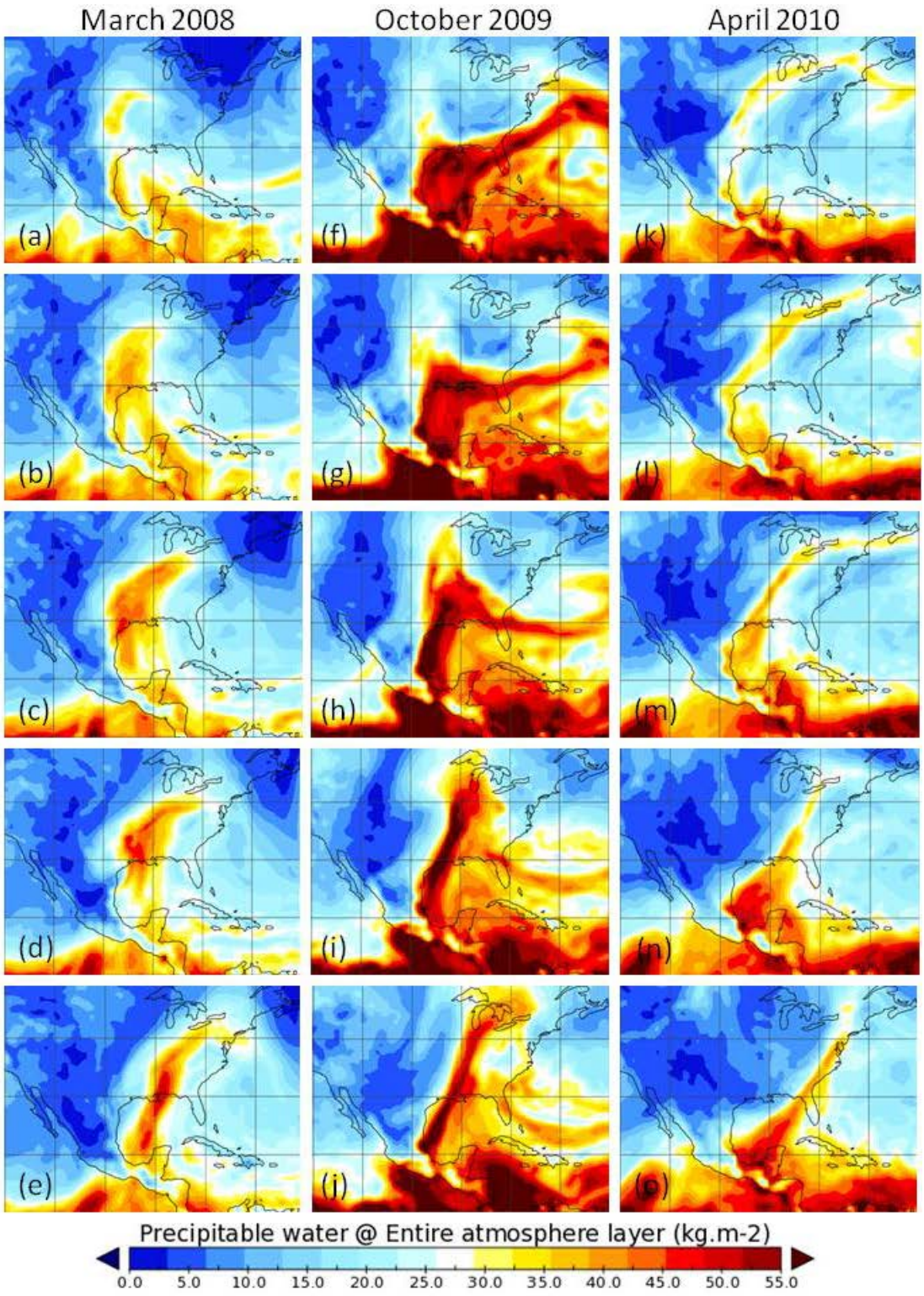

Figure 12. Precipitable Water Comparison for all Three Cases at Specified Points in the Evolution of the Systems (as Defined in the Analysis Section, Subsections (a) through (e) - see Table 1 for Dates/Times).

a. Prior to Event Onset

For all three cases (Figure 13), longwave troughing existed over the western U.S. (April's trough axis was slightly further east with a more neutral orientation) and longwave ridging covered the eastern U.S. The March case exhibited a narrower trough extending more southward than the other cases (Figure 13a). The amplitude of the October case was greatest, with the upstream ridge extending northward to the Gulf of Alaska (Figure 13b). Jet streaks were both entering and exiting the base of the trough at similar intensities during the March case; however, the October case had a stronger jet streak entering and the April case had a stronger jet streak exiting the base of the trough (Figure 13c). The anticyclonic jet associated with the warm front in the March case was very strong, which is indicative of strong baroclinic structure in the warm frontal region. The warm-frontal anticyclonic jet was nearly non-existent in the October case. April's anticyclonic jet showed a similar intensity to that of the jet streak exiting the base of the trough, with both being less intense than the other cases.

This upper-level pattern, even with the minor differences, produced surface features that favored moisture transport into the Midwest. In each case, low pressure at the surface occurred just downstream of the upper level trough. This surface low resulted in southerly flow across the Gulf Coast.

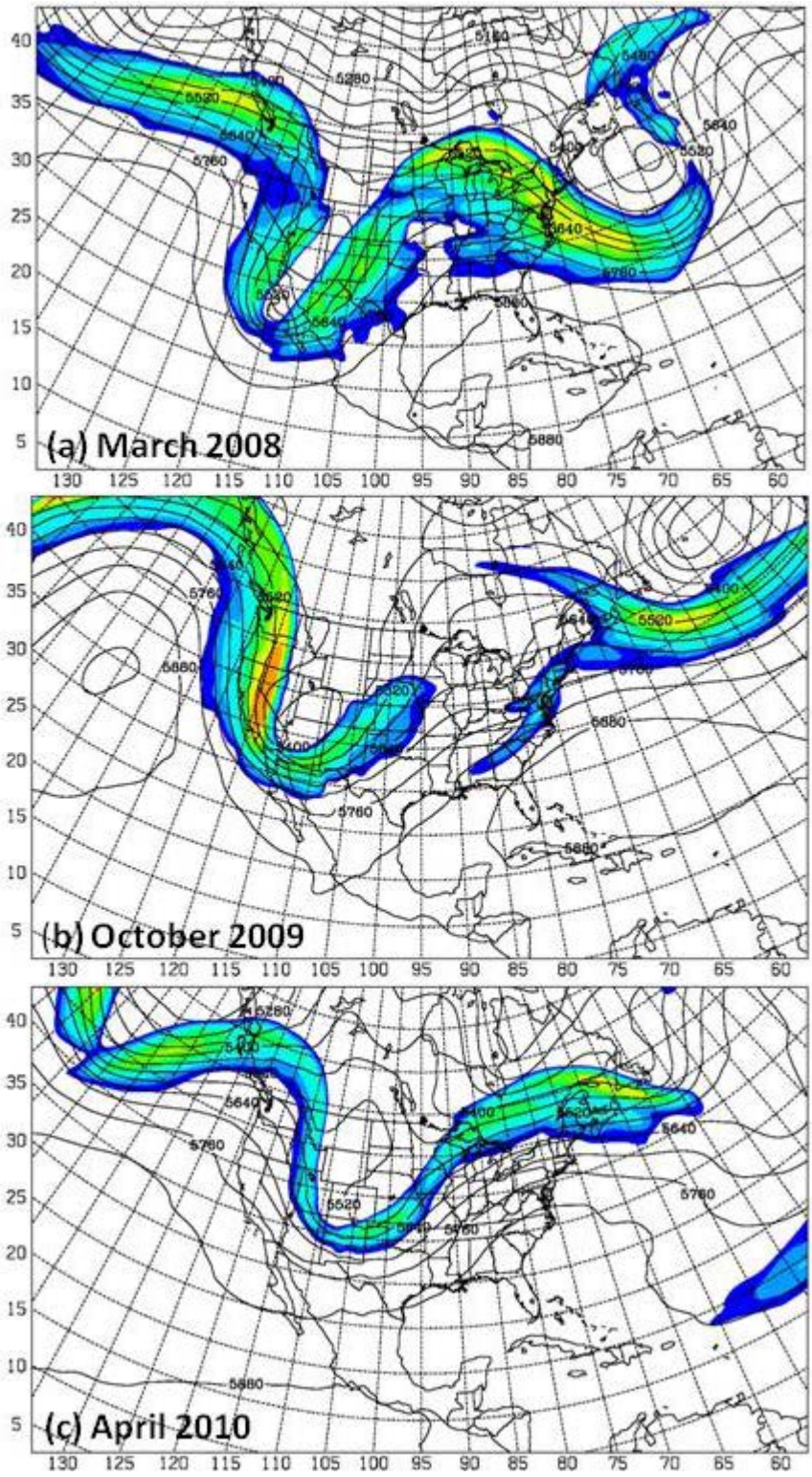

Figure 13. Upper-level Features, Prior to Event Onset. 300hPa Isotachs in Filled Contours Starting at 40 m/s (5 m/s Intervals). 500hPa Geopotential Height in Black Contours every 60 m.

Both the March and October cases had a low pressure center located over the panhandle of Texas with a cold front extending southwestward over western TX and a warm front extending southeastward toward the Gulf of Mexico. In the October case, a west–east stationary boundary extended from the low pressure system off the east coast and separated the moist air over the Gulf from the drier air over the southeast U.S. The delineation of this boundary was apparent in the isotherms along the northern Gulf Coast and in the mixing ratio plotted in Figure 15 (yellows and greens of the moist air and blues for the relatively drier air). This may have been why this case did not initially present as an AR located over the Midwest (Figure 12f). A similar boundary was present in the March case (Figure 14); however, the northwest–southeast feature was located further south and the difference in moisture was not as apparent at 925hPa as the October case. Due to the orientation of the boundary, an AR had started to develop, which is noticeable in the precipitable water plot in Figure 12a.

The surface features of the April case were located slightly further east, consistent with the slight position difference previously noted in the upper level pattern. Unlike the previous cases, a frontal train extended from Texas through Michigan, with a maritime tropical airmass extending into the southeast U.S. (Figure 16). With this configuration, flow across the Gulf of Mexico initially had a more southeasterly component, then traveling northward along the western Gulf Coast and along the frontal boundary as illustrated by the parcel trajectories in Figure 9. This AR was also apparent in the precipitable water plot (Figure 12k).

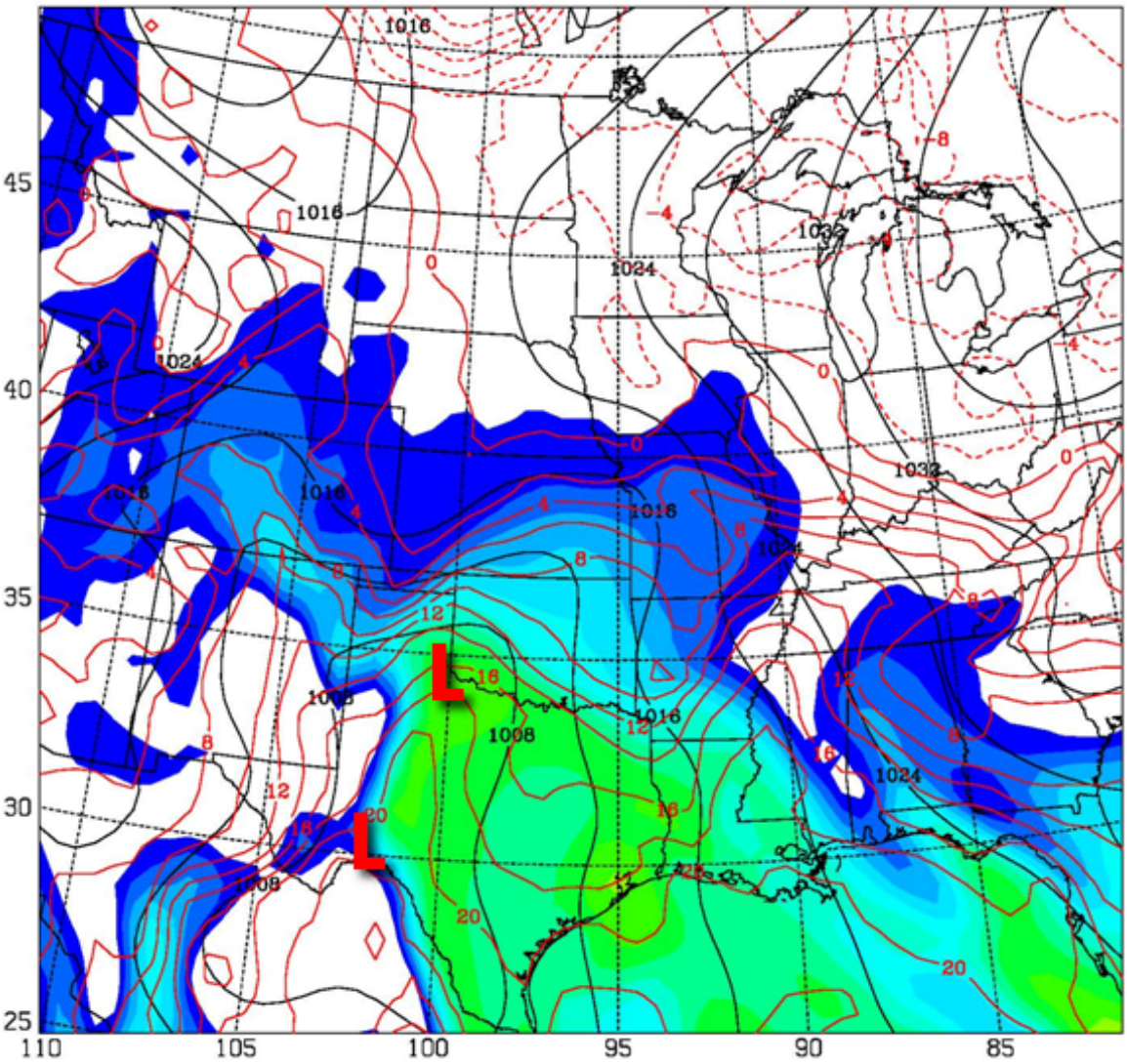

Figure 14. March 2008, Low-level Features, Prior to Event Onset (17 Mar 08, 15Z). MSLP (Black Contours, every 4hPa), 925hPa Temperature (Red Contours, every 2°C), Mixing Ratio (every 1 g/kg beginning at 4 g/kg).

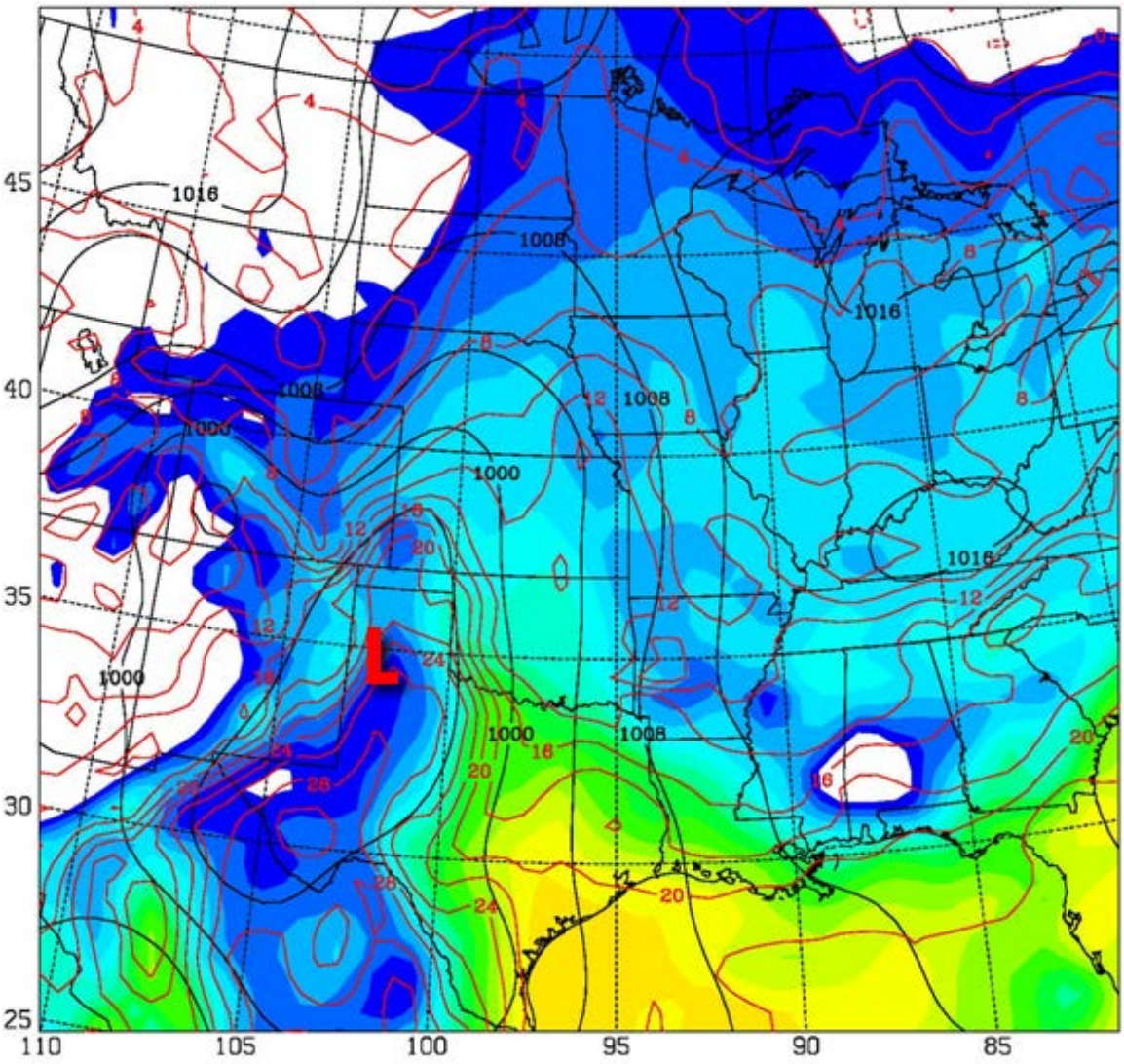

Figure 15. October 2009, Low-level Features, Prior to Event Onset (28 Oct 09, 21Z). Same as Previous Figure.

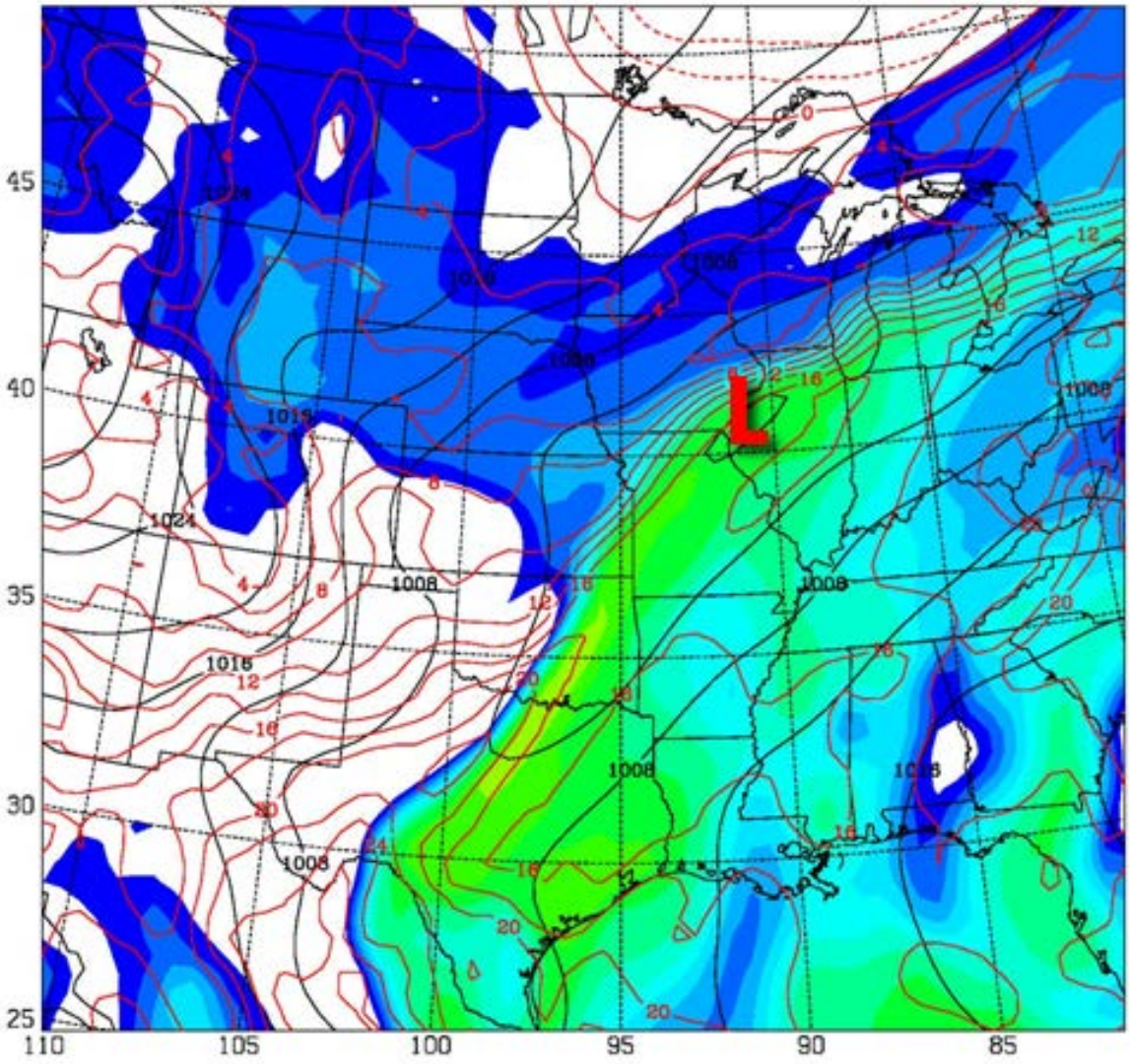

Figure 16. April 2010, Low-level Features, Prior to Event Onset (7 Apr 10, 06Z). Same as Previous Figure.

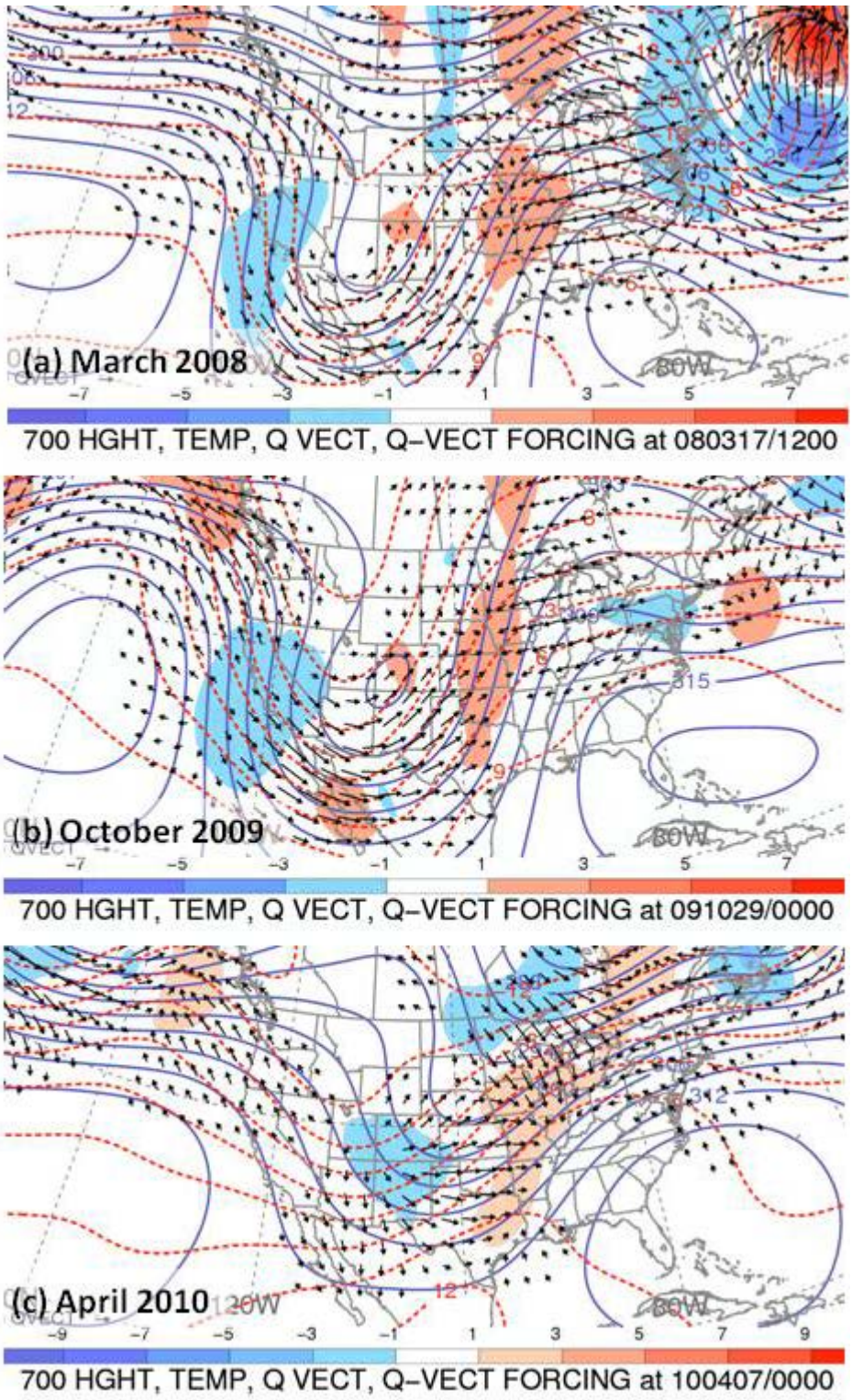

Figure 17. Q-Vector Convergence, Prior to Event Onset. 700 hPa. Geopotential Height (solid blue), Temperature (dashed red), Q-vectors (black arrow), Q-vector Forcing (blue-divergence, red-convergence).

The degree and character of baroclinic forcing is revealed through the Q-vectors at 700 hPa. Strong frontal forcing is revealed through Q-vectors that are perpendicular to the isotherms. Consistent with the intensity shown in the upper level jet, it is of no surprise that the frontal forcing for the March case (Figure 17a) is located in the warm frontal region, where the Q-vectors point across the isotherms over Kansas. The peak of the Q-vector convergence (red shading) indicating upward vertical motion was located at the peak in the thermal ridge, a signature of warm frontogenesis. For the October case, the Q-vectors cross the isotherms in a north-to-south line from Texas to South Dakota, along the cold front and inverted trough shown in Figure 15. Consequently, the area of Q-vector convergence and associated upward vertical motion in the October case (Figure 17b) was more elongated and extends further south than that seen in the March case. Overall, the upward vertical motion implied by the Q-vector convergence in the April case (Figure 17c) was weaker than that of the other two cases, but the Q-vectors show frontogenesis along the majority of the frontal train.

b. Event Onset

By event onset, the longwave trough in all cases had dug southward and shifted slightly eastward. Amplification in the trough/ridge couplet occurred in both the April (Figure 18c) and October cases (Figure 18b), but was greater for October. There was little change in the trough amplitude for the March case (Figure 18a).

The jet streak entering the base of the October trough weakened slightly, while the jet streak exiting the base of the trough intensified, signaling a strengthening temperature gradient in the low levels further to the south. Intensification of the anticyclonic jet streaks over the warm front occurred in the March and April cases, also indicative of an increasing thermal gradient in the low levels due to frontogenesis.

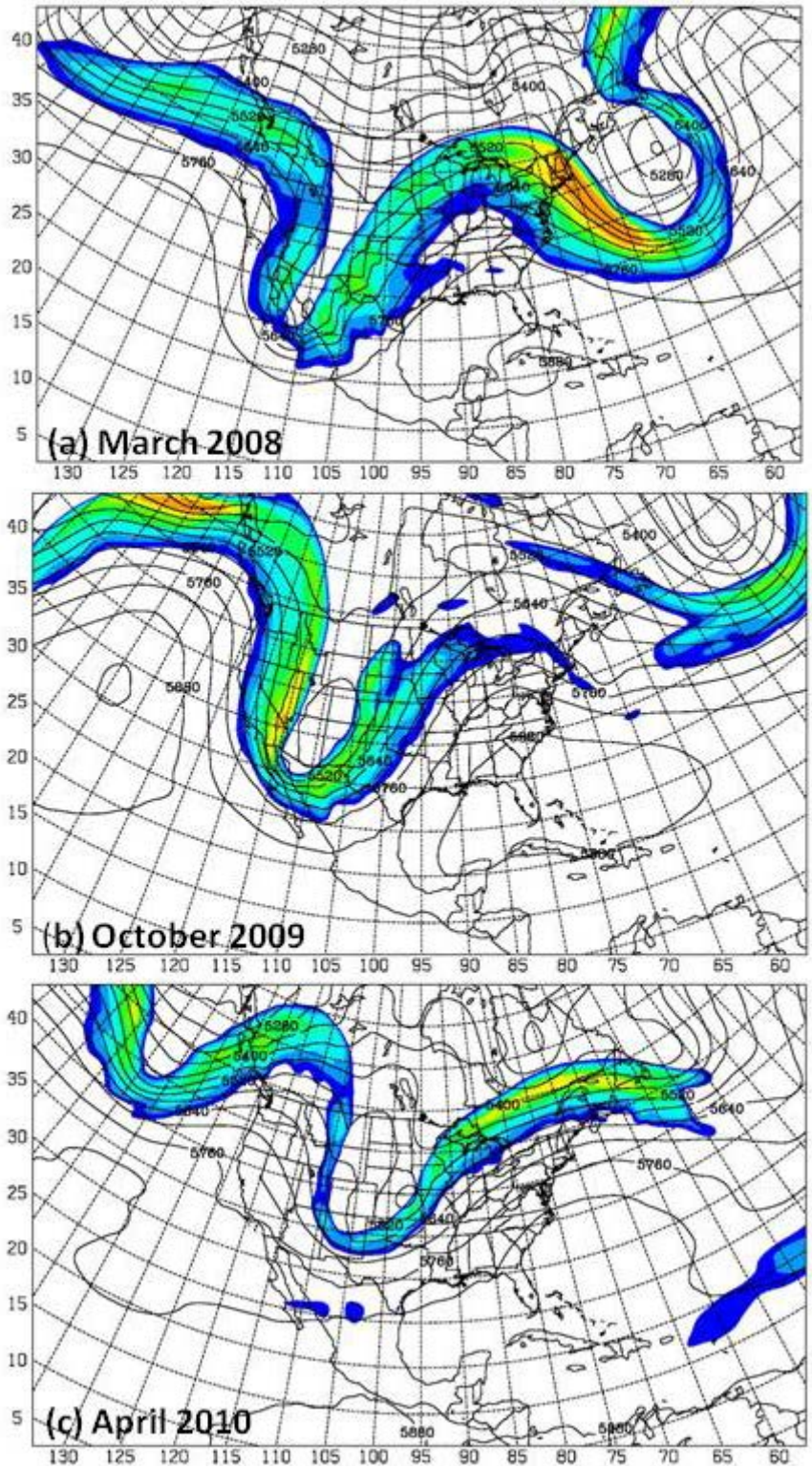

Figure 18. Upper-level Features, Event Onset. 300hPa Isotachs in Filled Contours Starting at 40 m/s (5 m/s Intervals). 500hPa Geopotential Height in Black Contours every 60 m.

As the overall pattern shifted eastward and the upper-level trough amplified, the pressure gradient in the warm sector tightened and the flow became more southerly for all cases. This occurred most notably in the March case (Figure 19), where surface cyclogenesis was occurring over the Rio Grande Valley. While there was very little eastward progression of the surface features, the strong baroclinic zone in place across Arkansas intensified and began to force upward motion of the moist air that was pumped in from south. The low pressure center located over extreme southern Texas began to deepen due to the eastward movement of the upper-level trough. This resulted in an increase of warm air advection over the southern plains.

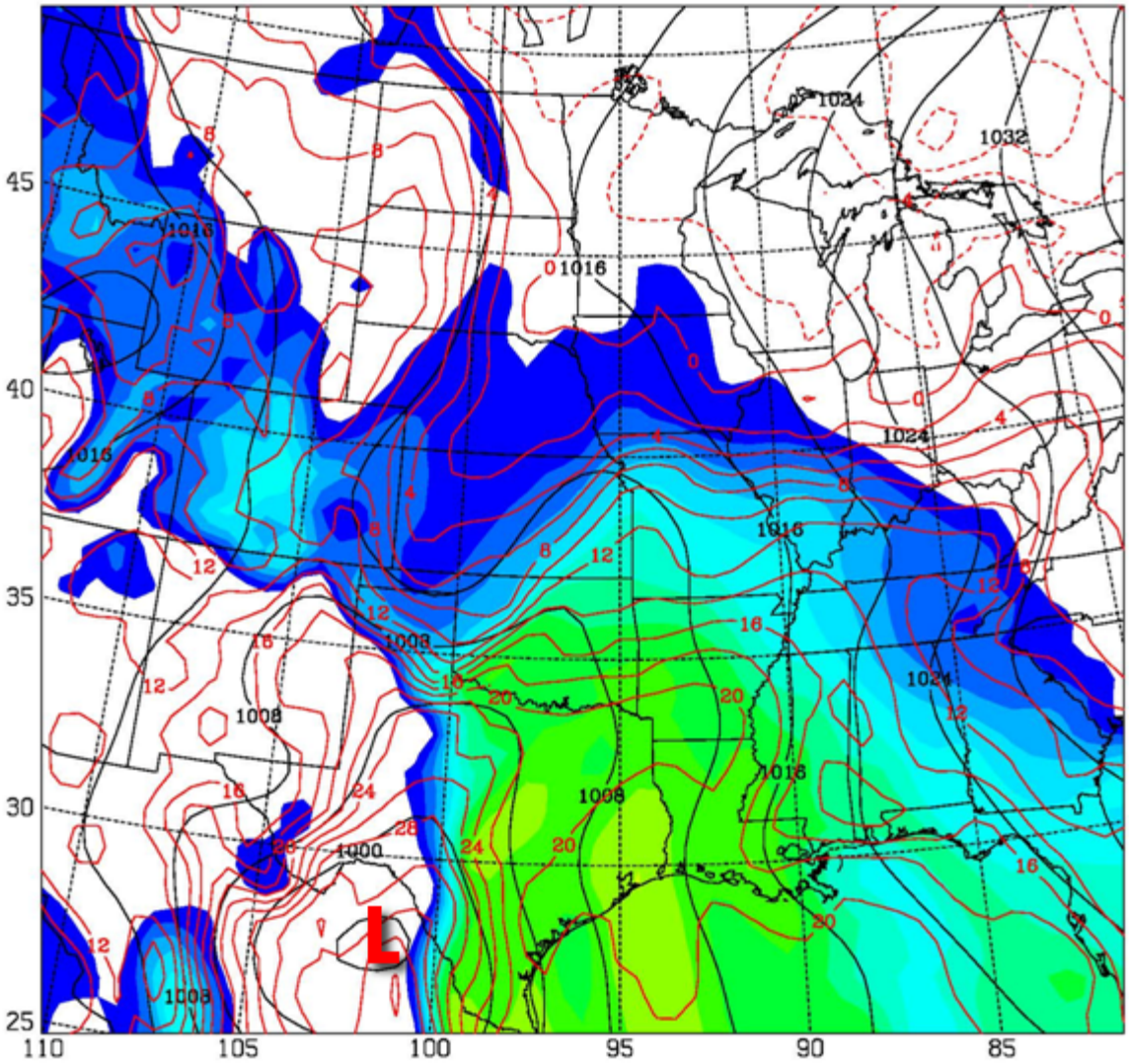

Figure 19. March 2008, Low-level Features, Event Onset (18 Mar 08, 00Z). MSLP (Black Contours, every 4hPa), 925hPa Temperature (Red Contours, every 2°C), Mixing Ratio (every 1 g/kg beginning at 4 g/kg).

In the October case, a further intrusion of moisture was evident in along the western Gulf Coast (Figure 20) in the warm sector of the frontal system. Radar revealed (not shown) that convection began to fire over eastern Texas associated with the warm frontal boundary and unstable, warm airmass. Moderate precipitation elsewhere in the domain was caused by the isentropic ascent as a strong low-level jet forced moist air over the warm front, which was

indicated by Q-vector convergence (Figure 22b) over a large extent of the Mississippi River.

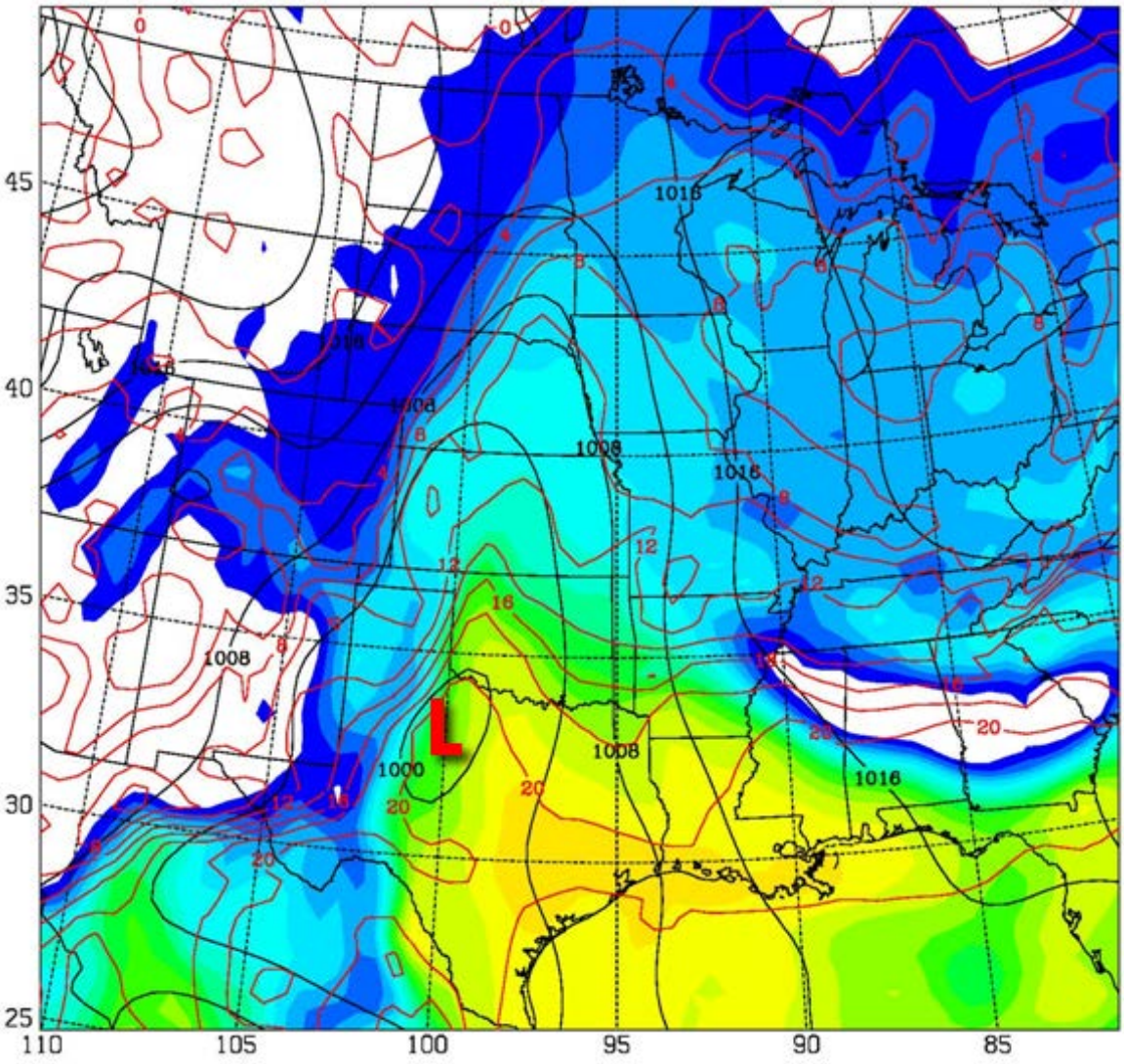

Figure 20. October 2009, Low-level features, Event Onset (29 Oct 09, 06Z). Same as Previous Figure.

The cold front in the April case progressed across Texas, which is apparent with the moisture content differences between the airmasses in Figure 21. Flow in the warm sector had a southwesterly trajectory that arched from the southwest to the northeast along the frontal train through the domain. Moisture content at 925 hPa was similar but slightly weaker than the March case.

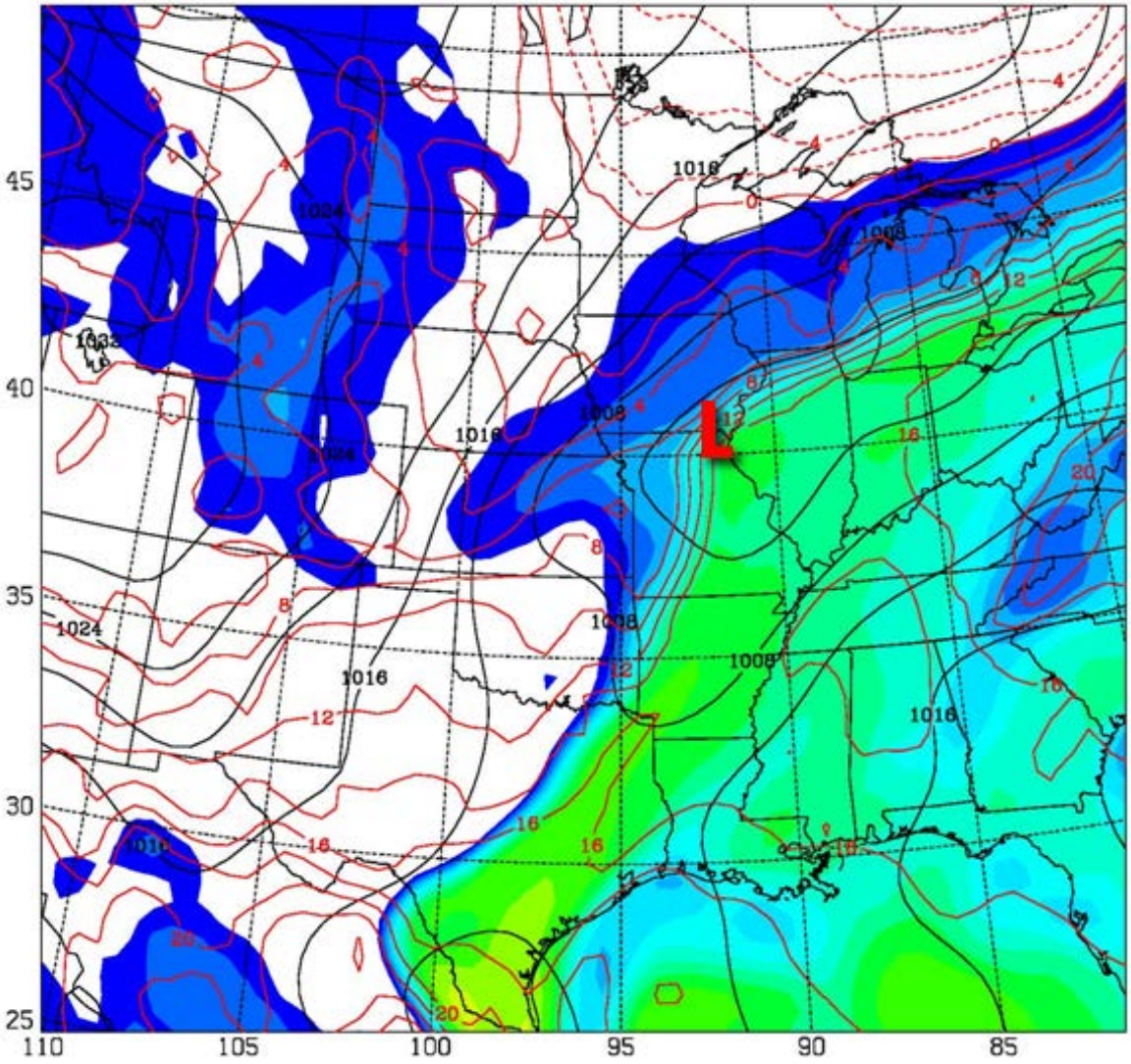

Figure 21. April 2010, Low-level features, Event Onset (07 Apr 10, 15Z). Same as Previous Figure.

The Q-vectors and Q-vector convergence confirms the intensifying frontal features as each case became more organized by event onset. The area of strong Q-vector convergence in the March case progressed along the ridge to the northeast (Figure 22a). The 700 hPa geostrophic confluence over Nebraska induced an ageostrophic circulation, indicated by the southward pointing Q-vectors. Additionally, the tightening thermal gradient associated with cold air advection over southwest Texas induced a secondary circulation with Q-vectors pointed toward the northeast. The Q-vectors converged with both speed and

direction in a west–east orientation across southern Texas, ahead of the deepening surface low and led to further strengthening of the warm front.

In the October case (Figure 22b), the Q-vector convergence region elongated further, extending southward. In addition, the length of the Q-vectors (representing the strength of the frontogenesis) increased substantially over eastern TX. This was also the situation for the April case (Figure 22c), but with weaker forcing indicated by lighter red shading.

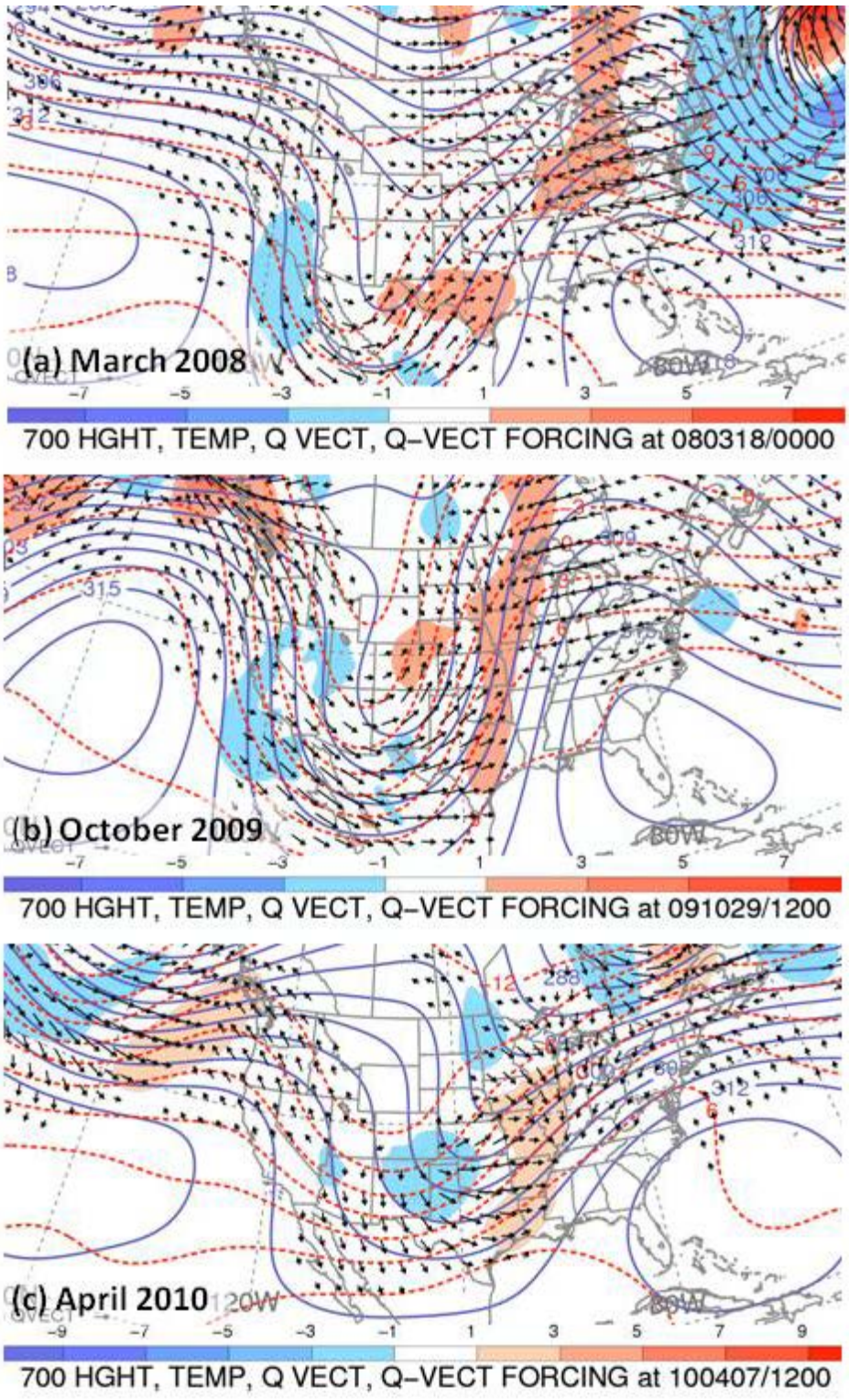

Figure 22. Q-Vector Convergence, Event Onset. 700 hPa. Geopotential Height (solid blue), Temperature (dashed red), Q-vectors (black arrow), Q-vector Forcing (blue-divergence, red-convergence).

c. Midpoint 1, 12 hours after Event Onset:

At twelve hours after event onset, each case exhibited a speed increase in the jet maxima at 300 hPa, indicating strengthening baroclinic zones (i.e., frontogenesis) (Figure 23) as the systems moved toward the Gulf Coast. For the March case (Figure 23a), 500 hPa geostrophic confluence continued downstream from the trough, further strengthening the ageostrophic circulation, which was evident by the increased speed in the anticyclonic jet. The longwave trough became more neutral in orientation. For the October case (Figure 23b), low-level cold frontogenesis (not shown) was indicated by the speed increase of the jet of the streak exiting the base of the trough. The trough and downstream ridge amplified further as the trough became more neutral in orientation. For the April case (Figure 23c), the jet intensified slightly over the Missouri and Illinois border as a result of the low-level cold frontogenesis (not shown). The right rear quadrant of the jet was located over eastern Missouri and western Kentucky/Tennessee.

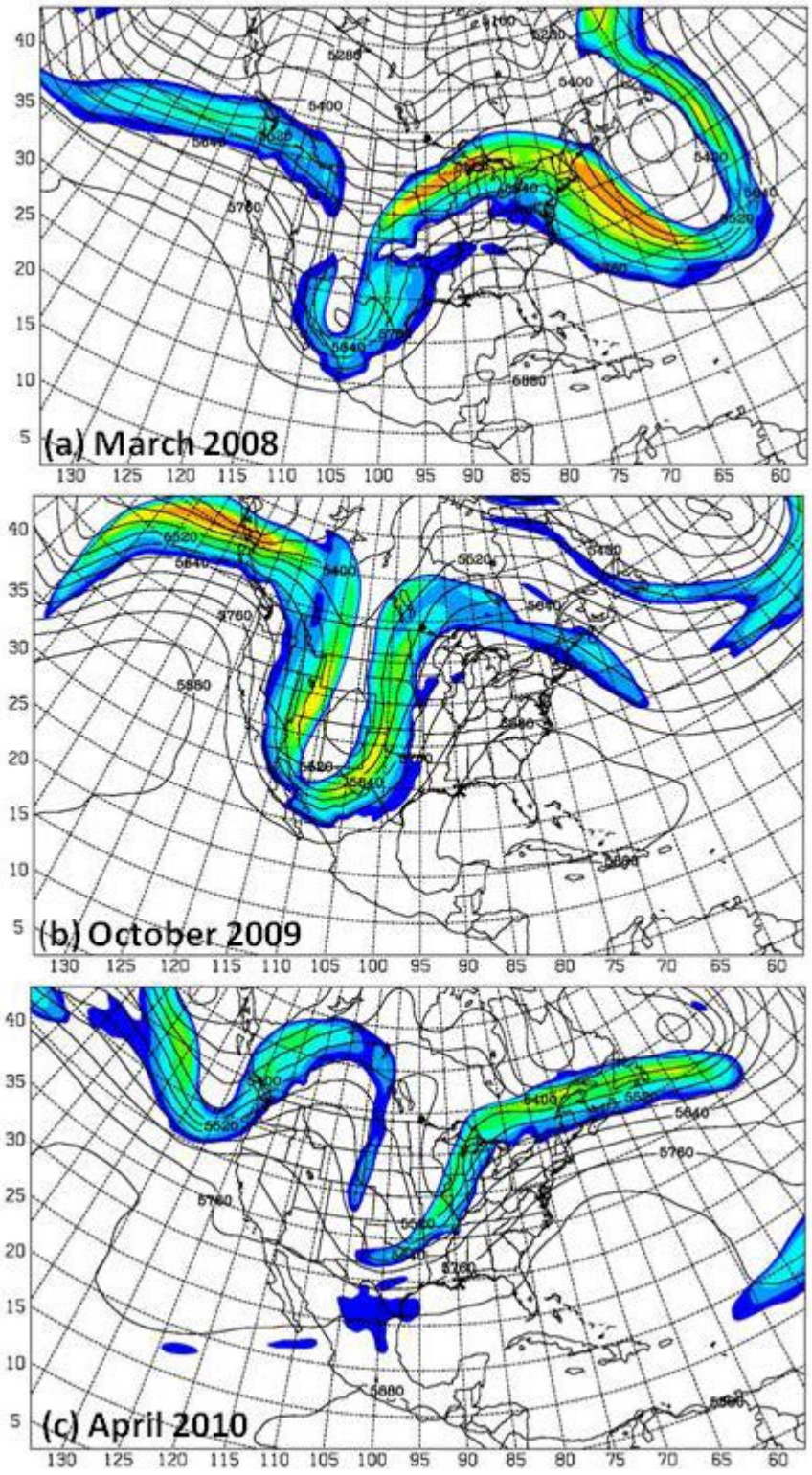

Figure 23. Upper-level Features, Midpoint 1. 300hPa Isotachs in Filled Contours Starting at 40 m/s (5 m/s Intervals). 500hPa Geopotential Height in Black Contours every 60 m.

In the March case, the warm frontal temperature gradient shown in Figure 24 tightened considerably compared to 12 hours earlier (Figure 19). This intensification was in response to the 500 hPa geostrophic confluence in the warm frontal region north of the low pressure center located over southern Texas. Although the low center had not deepened in the past 12 hours, the pressure gradient along the Gulf Coast increased and moisture (mixing ratios) increased south of the warm front with this stronger southerly flow. As will be shown later, ascent in the warm front region increased as well. Moisture that was transported from the south was further concentrated and the strong low-level jet forced ascent up the warm front. Warm air advection (with southerly flow implied by the pressure gradient across the isotherms in Figure 24) steepened the lapse rates and destabilized the air in the warm sector, resulting in isolated severe thunderstorms with strong wind. However, the heavy precipitation seen on radar (Figure 25) coincides with the warm front and is presumably a result of the interaction of the strong low-level jet with the warm front. Surface CAPE values (not shown) ranged from 400-600 J/kg over western Arkansas, which supported moderate frontal forced convection.

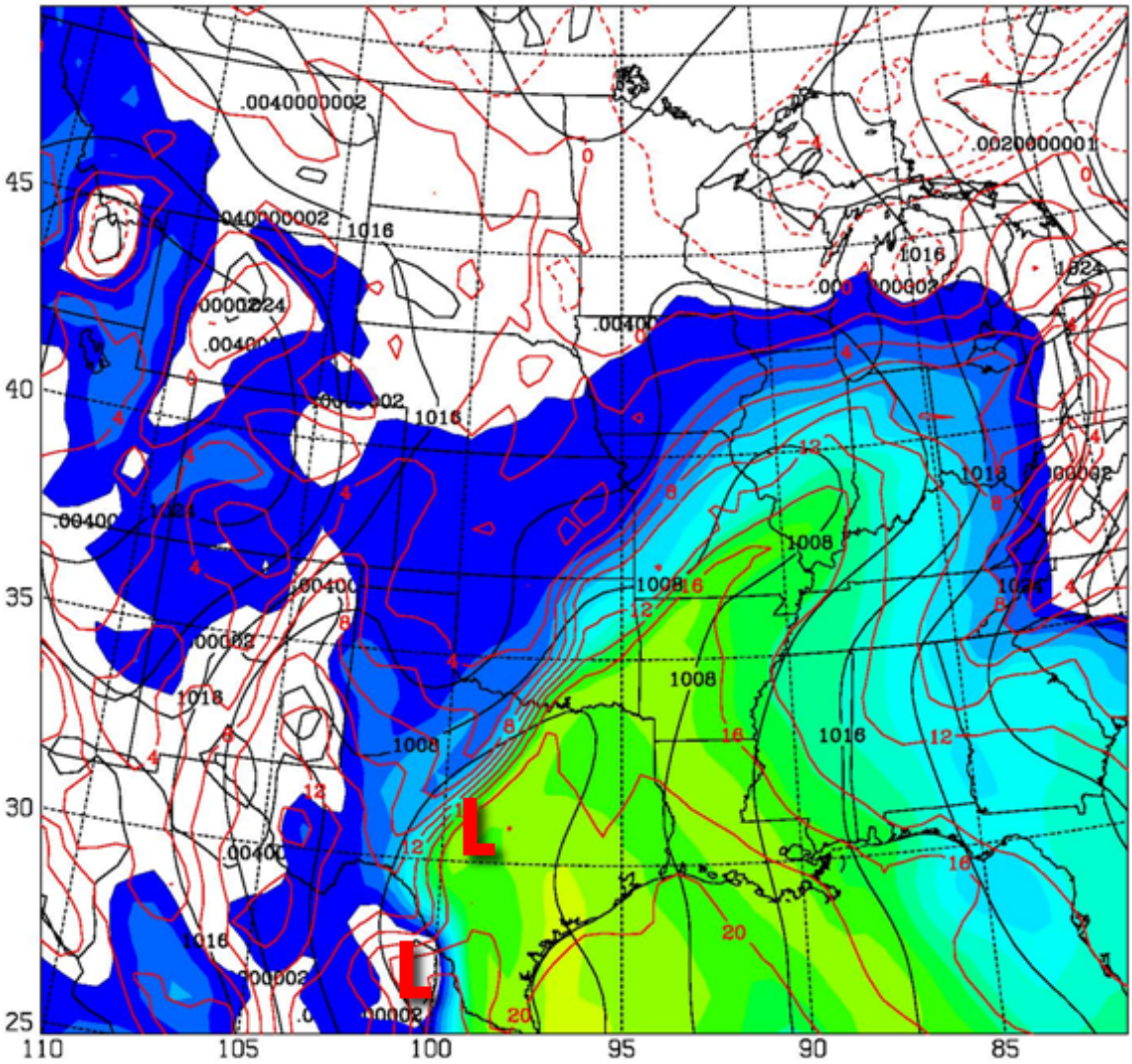

Figure 24. March 2008, Low-level Features, Midpoint 1 (18 Mar 08, 12Z). MSLP (Black Contours, every 4hPa), 925hPa Temperature (Red Contours, every 2°C), Mixing Ratio (every 1 g/kg beginning at 4 g/kg).

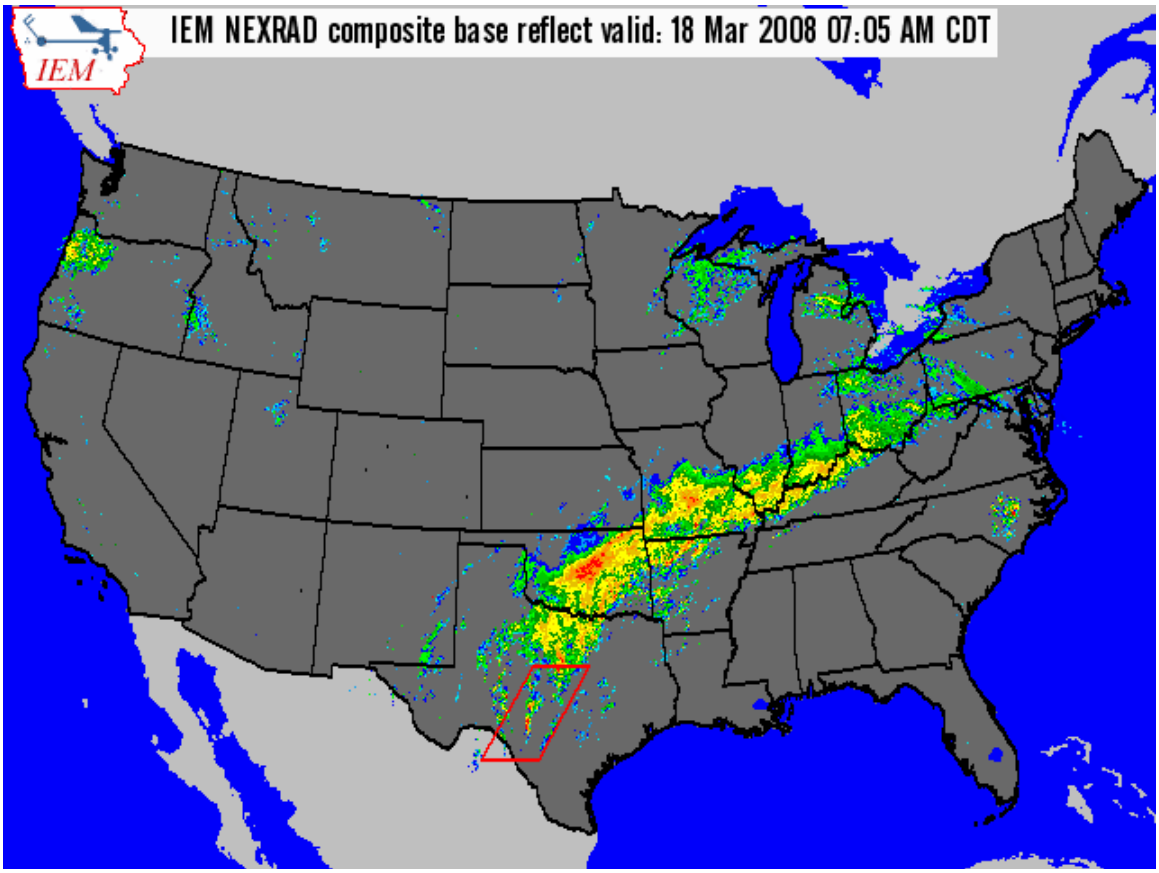

Figure 25. March 2008, National Radar Composite, Base Reflectivity, Midpoint 1 (18 Mar 08, 12Z).

The low-level vorticity strengthened considerably along the warm frontal region (Figure 26), which is consistent with an intensifying the warm front. In addition, vertical motion associated with the ascent through the frontal zone reached values around 10 microbars/second for this March case, shown by the red vectors in Figure 27. This warm frontal circulation coincides with the region of heaviest precipitation on the radar (Figure 25) as well as the CFSR rainfall analysis (not shown). Consequently, this case has been characterized as baroclinically forced rainfall (frontal type - Maddox et al. 1979).

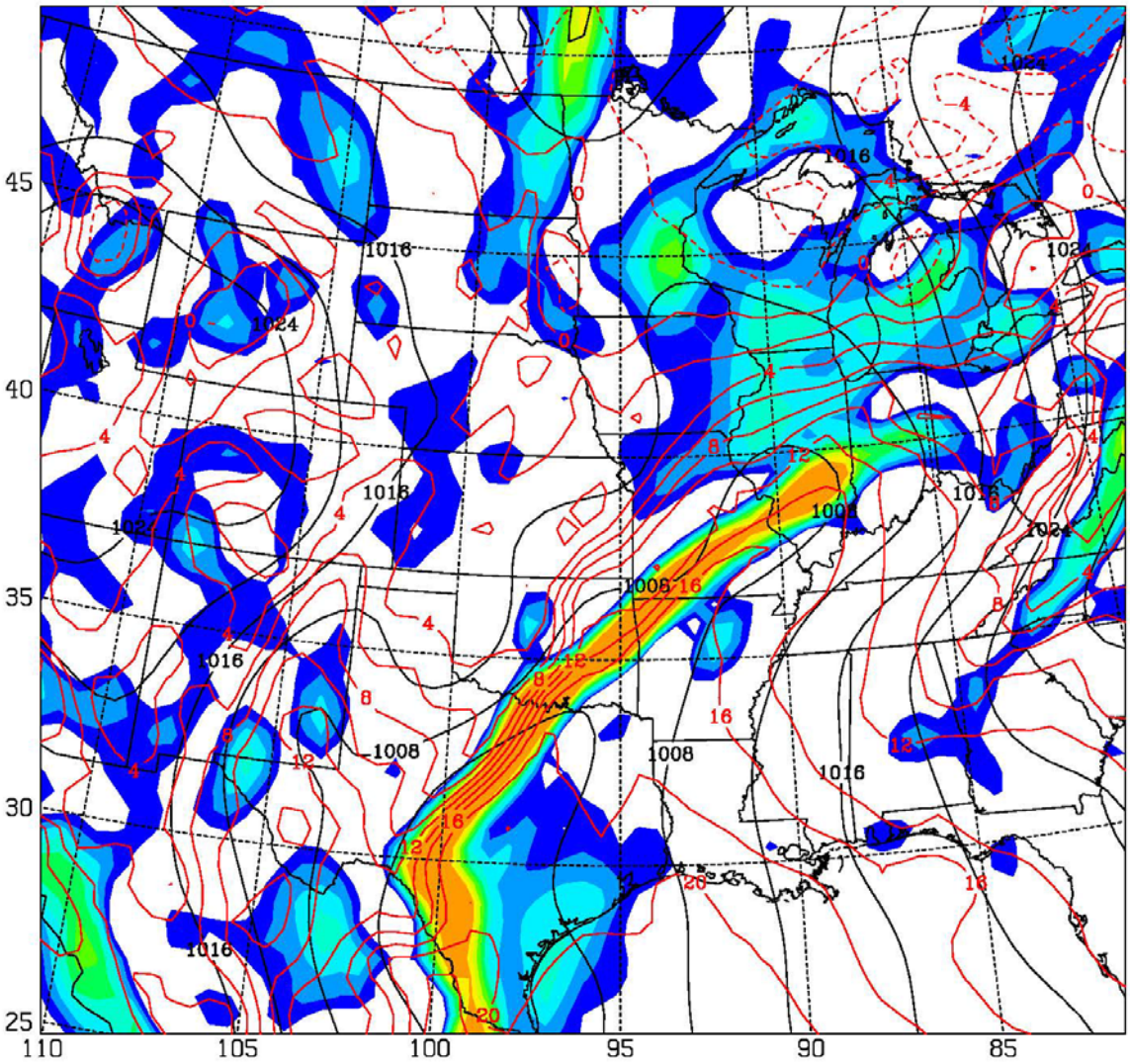

Figure 26. March 2008, Midpoint 1. MSLP (Black, every 4hPa), Positive Low-level Relative Vorticity (Shading in every 2) and Temperature at 925hPa (Red, every 2°C).

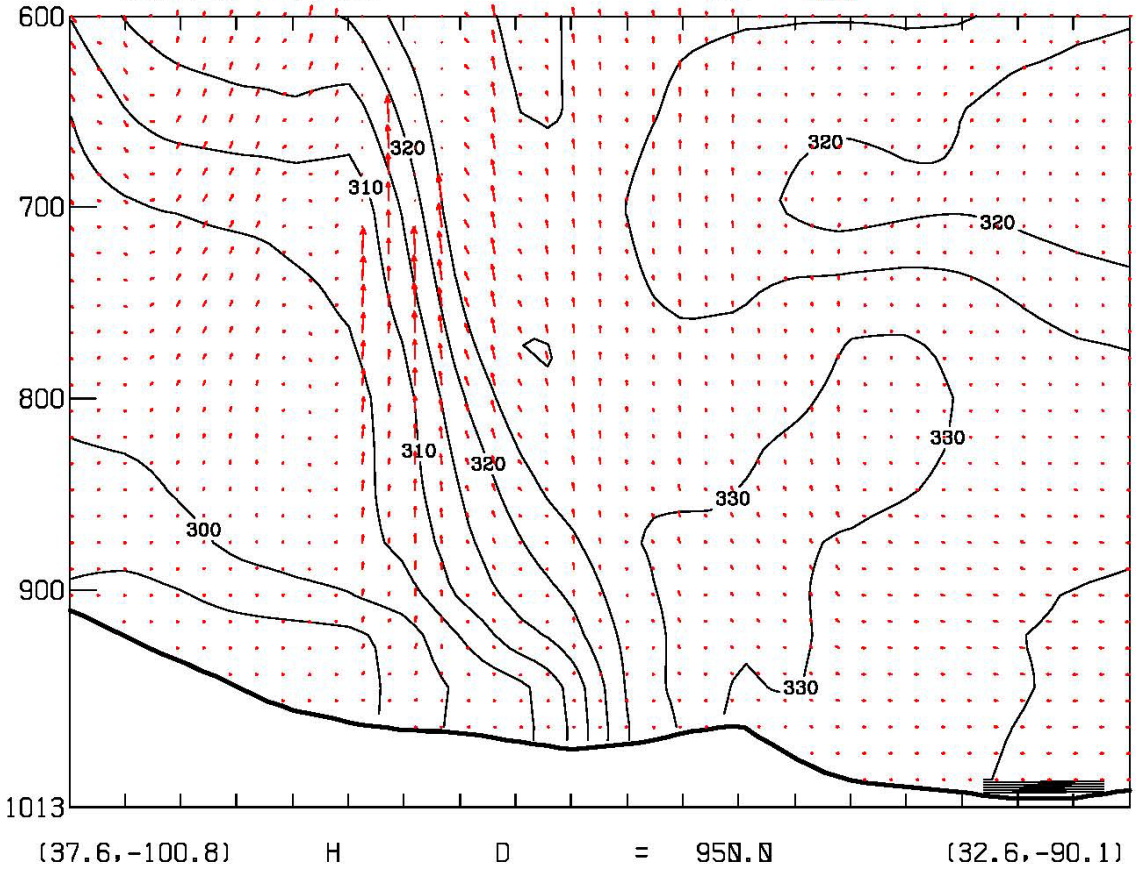

Figure 27. March 2008, Midpoint 1. Cross Section Perpendicular through the Warm Front. Equivalent Potential Temperature (Black Contours) and Observed Wind in the Plane of the Cross Section (Red Vectors).

For the October case, the cold front advanced eastward across Texas and the low center moved north along the axis of the inverted trough (Figure 28). The result was an increase in southerly flow ahead of the front, which helped to concentrate the moisture along the western Gulf Coast. The low-level moisture advection in the warm sector, combined with strong low-level shear ahead of the front, destabilized the atmosphere and set up conditions favorable for pre-frontal warm-sector thunderstorms (some became severe with damaging winds and tornadoes) (Figure 29). Surface CAPE values were as high as 1500-1800 J/kg over Louisiana.

Unlike the March case, this case had several regions of precipitation in the domain. The cold front began to trigger precipitation in the

region (southern Arkansas and Northern Louisiana) that received the heaviest precipitation by this point in the system's evolution. The warm front, located through Missouri (Figure 28), provided lift when the strong low-level jet brought moisture further north. To differentiate the importance of the frontal features to the precipitation, moisture and winds on the 300K isentropic surface are shown in Figure 30. On the 300K surface, the tight moisture gradients associated with both the cold and warm fronts are evident. In addition, the 40–50 knot low-level southerly jet is evident in the warm sector. Strong isentropic lift occurred in the warm frontal region as the flow goes up to low pressure on this surface. Precipitation efficiency, which is a ratio of the 3-hr precipitation and precipitable water, was highest along the western (cold front) and eastern (warm front) edges of the moisture tongue. This shows that the greatest (most efficient) extraction of precipitation occurred primarily in the frontal regions. Surface CAPE values were less than 300 J/kg, which was not very conducive to thunderstorms. The majority of the precipitation in the domain at this point was due to the precipitation that occurred over the Missouri/Illinois area associated with the strong isentropic ascent, which was not ultimately the region of heaviest precipitation.

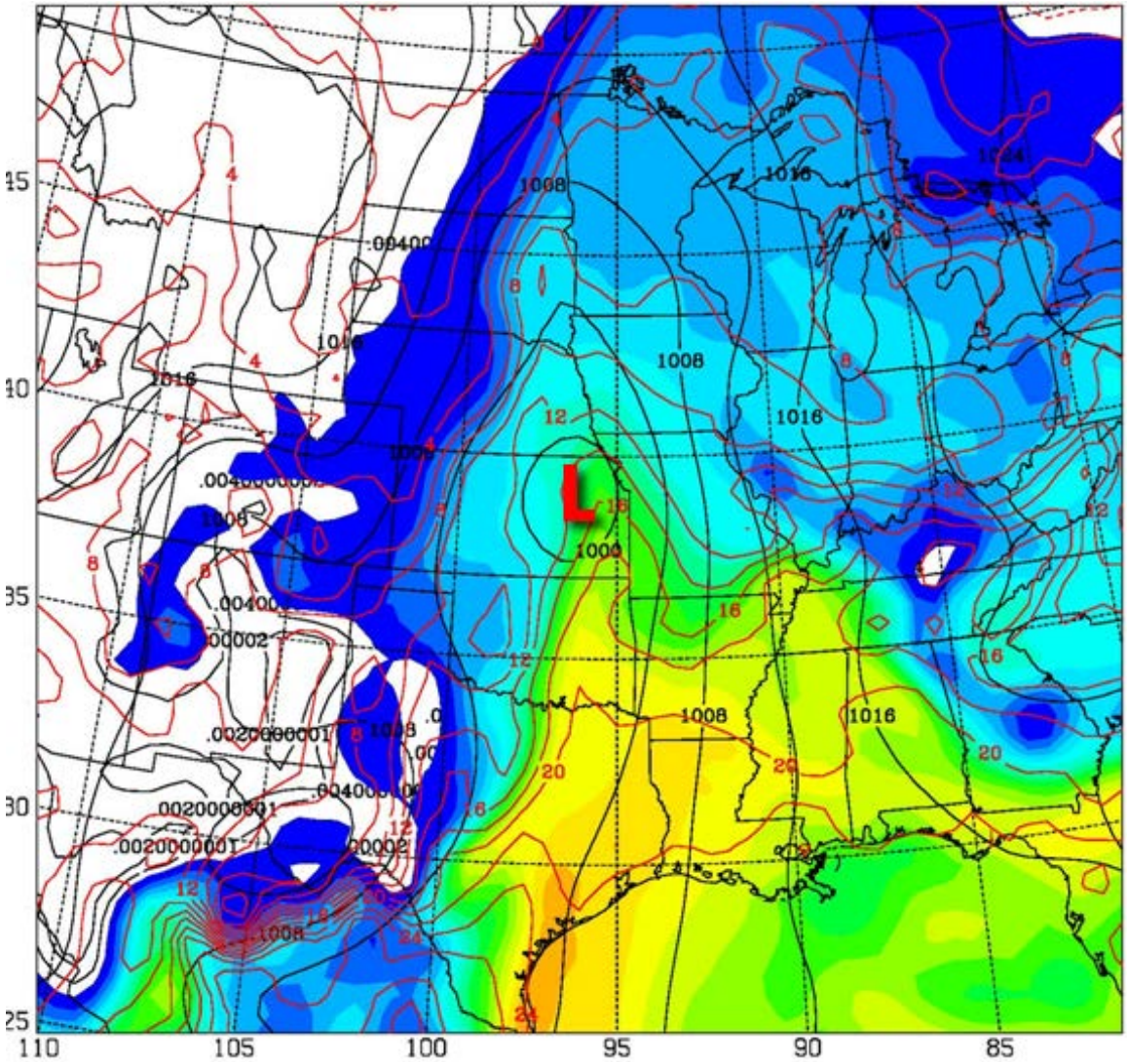

Figure 28. October 2009, Low-level Features, Midpoint 1 (29 Oct 09, 18Z). Same as Previous Figure.

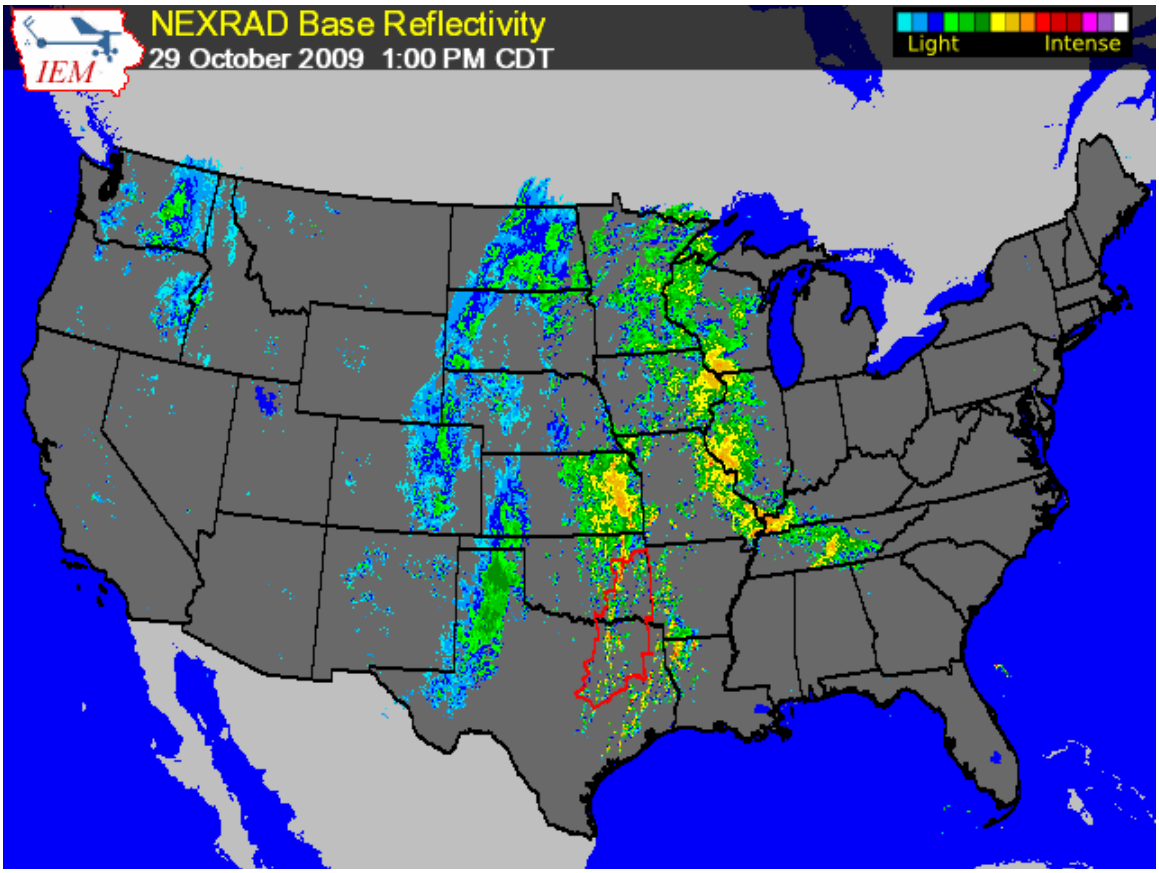

Figure 29. October 2009, National Radar Composite, Base Reflectivity, Midpoint 1 (29 Oct 09, 18Z).

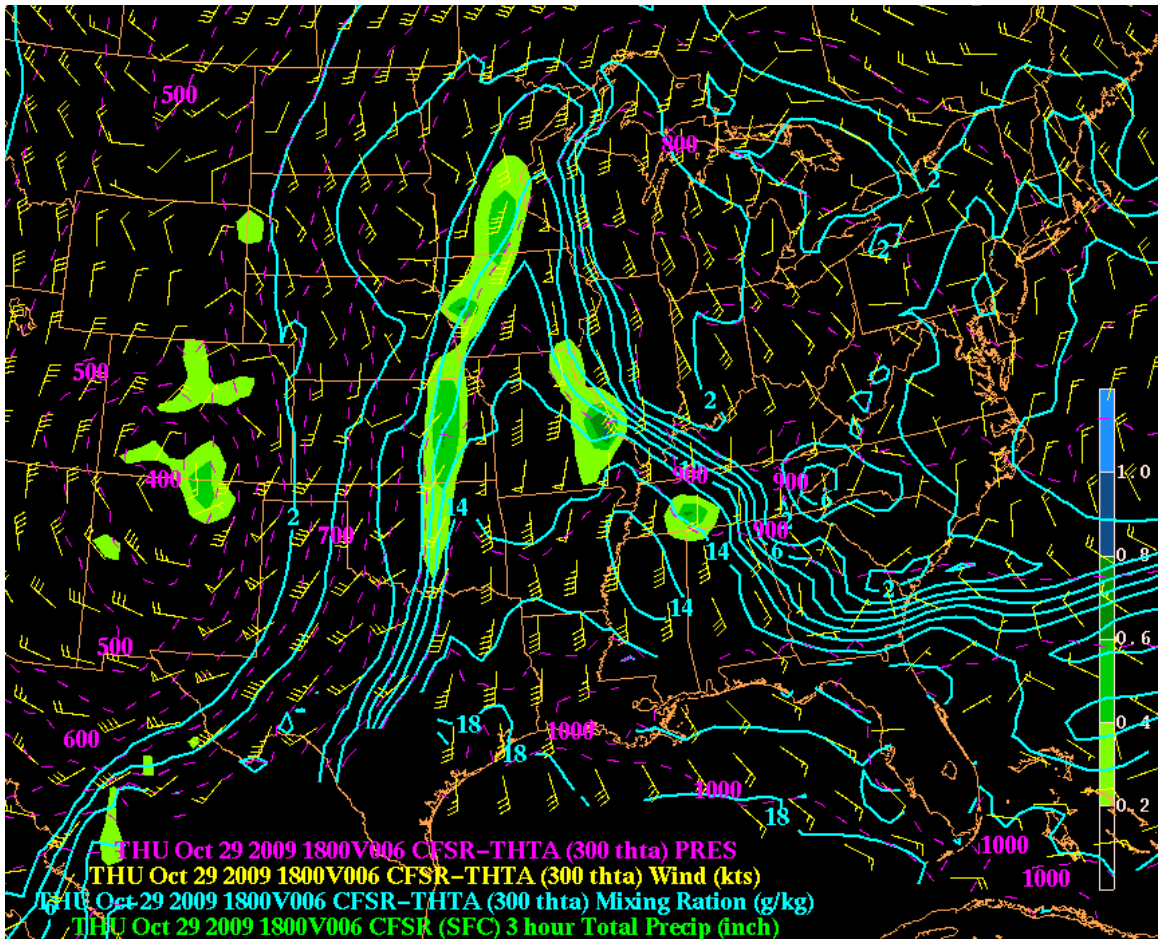

Figure 30. October 2009, 300K Theta Surface, Midpoint 1 (29 Oct 09, 18Z). Pressure Surfaces (Dashed Magenta), Mixing Ratio in g/kg (Solid Blue), Wind in Knots (Yellow Barbs), and Precipitation Efficiency (Fill).

For the April case, the low started to progress rapidly to the northeast following the falling pressure tendencies due to the vertical motions associated with the warm front. The moisture plume remained the most concentrated in the warm sector immediately ahead of the cold front (Figure 31) that extended from the Texas coast to Ohio. Precipitation stretched the entire length of the frontal system (Figure 32) within the core of the high PW air (the AR). Surface CAPE values ranged from 200-600 along the extent of the frontal train, which supported moderate frontal forced convection.

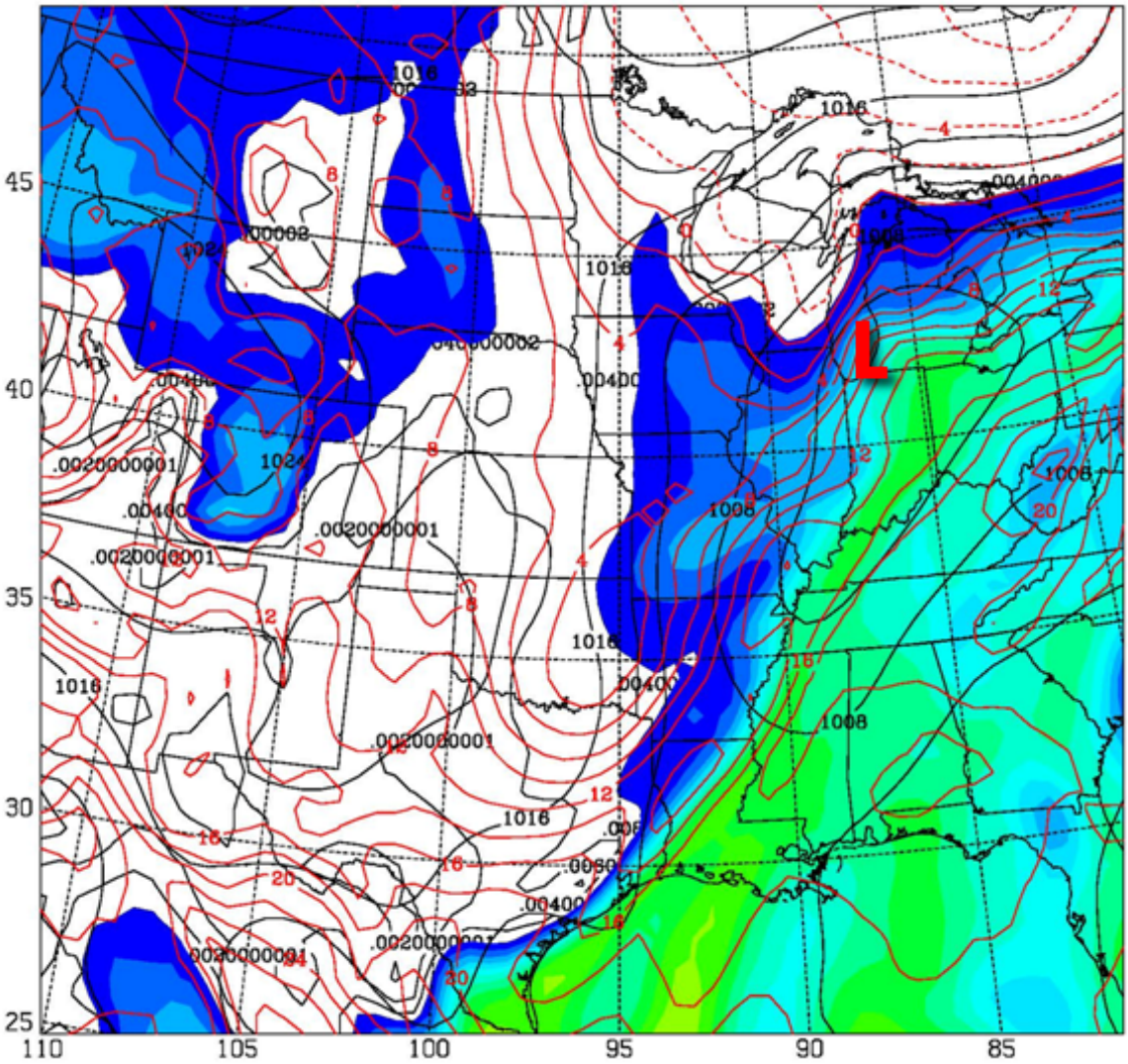

Figure 31. April 2010, Low-level Features, Midpoint 1 (8 Apr 10, 03Z). Same as Previous Figure.

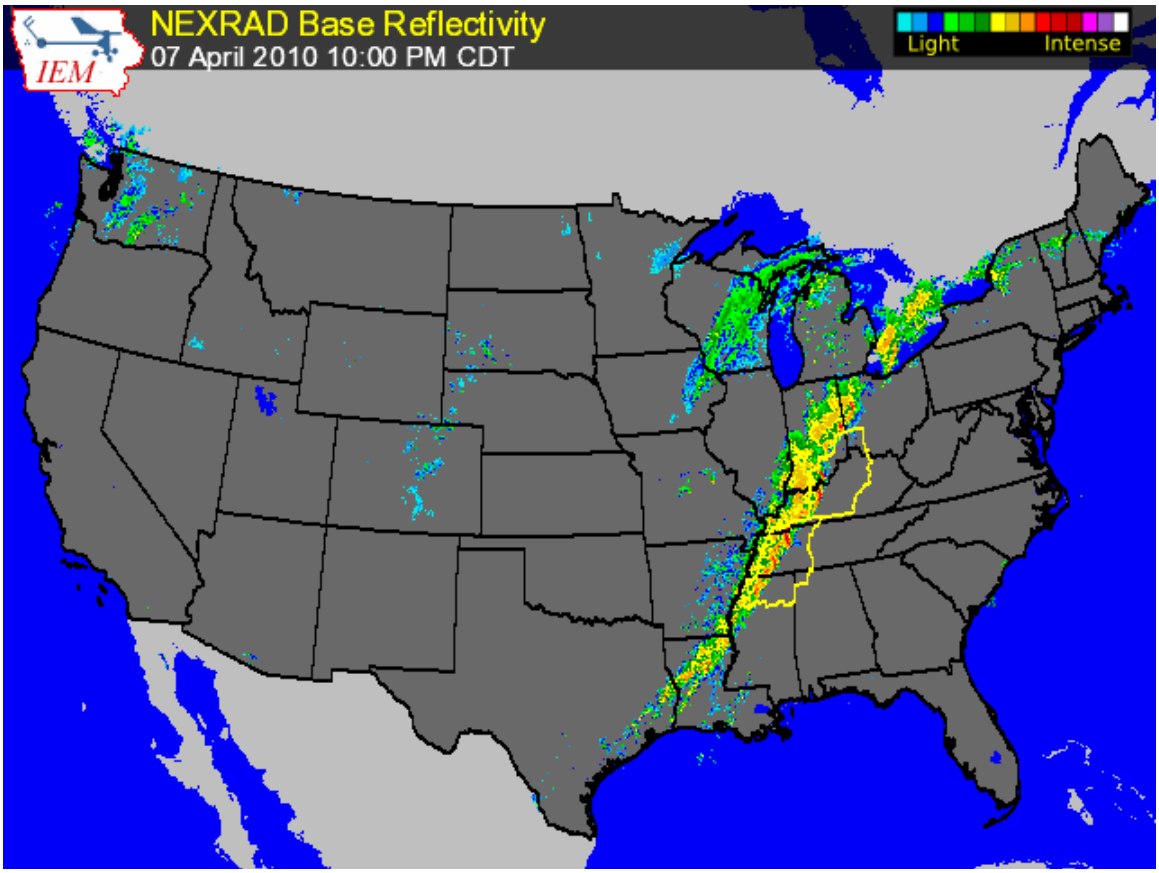

Figure 32. April 2010, National Radar Composite, Base Reflectivity, Midpoint 1, (8 Apr 10, 03Z).

To confirm the role of baroclinic frontogenesis in forcing the precipitation at this time, the Q-vector and Q-vector convergence were examined. In the March case, well-defined geostrophic confluence continued over Missouri area, as evident in the large Q-vectors that point across the isotherms. This frontogenesis supported increasing speed of the jet streak previously discussed (Figure 23a) and the region of Q-vector convergence over Texas and northward where precipitation was occurring (Figure 33a). The area of Q-vector convergence and associated frontal ascent for both the October and April cases split into two segments: one associated with the frontogenesis along the cold front to the south and the other with the low pressure center to the north (Figure 33b and 33c). Note the lack of Q-vector convergence in the October case over the Missouri/Illinois area where the moderate rainfall was occurring, contributing

to the majority of the precipitation in the domain. This suggests that although the frontogenesis was weak, the ascent that occurred was enough to initiate convection in this region.

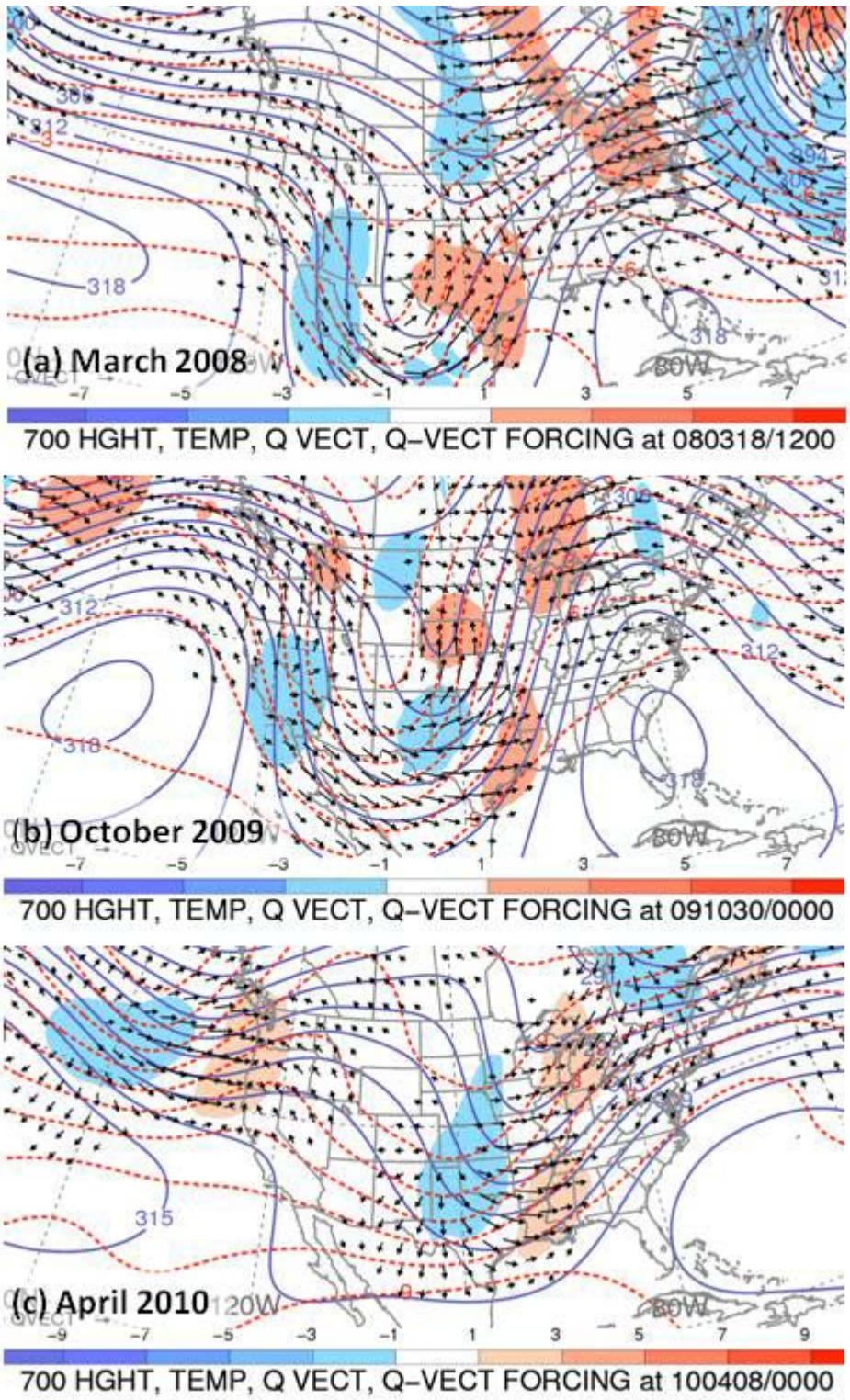

Figure 33. Q-Vector Convergence, Midpoint 1. 700 hPa. Geopotential Height (solid blue), Temperature (dashed red), Q-vectors (black arrow), Q-vector Forcing (blue-divergence, red-convergence).

d. Midpoint 2, 24 hours after Event Onset

By 24 hours after event onset, the upper-level features have progressed somewhat eastward, but have not substantially changed. In the March and October cases (Figures 34a and 34b), the jet speed maxima remained about as strong as 12 hours earlier, with some intensification in the October case. Both show very little progression in any direction that also resulted in slow-moving surface features.

April's trough became more neutrally tilted as the southern part moved eastward and the northern part stayed stationary over the Great Lakes. The downstream ridge amplified over the eastern U.S. as well to give a more north–south orientation of the trough and associated upper-level flow. The jet streak associated with the cold front progressed northward as the jet intensified over Michigan; however, the jet weakened to the south along the Gulf Coast, consistent with a weakening cold front.

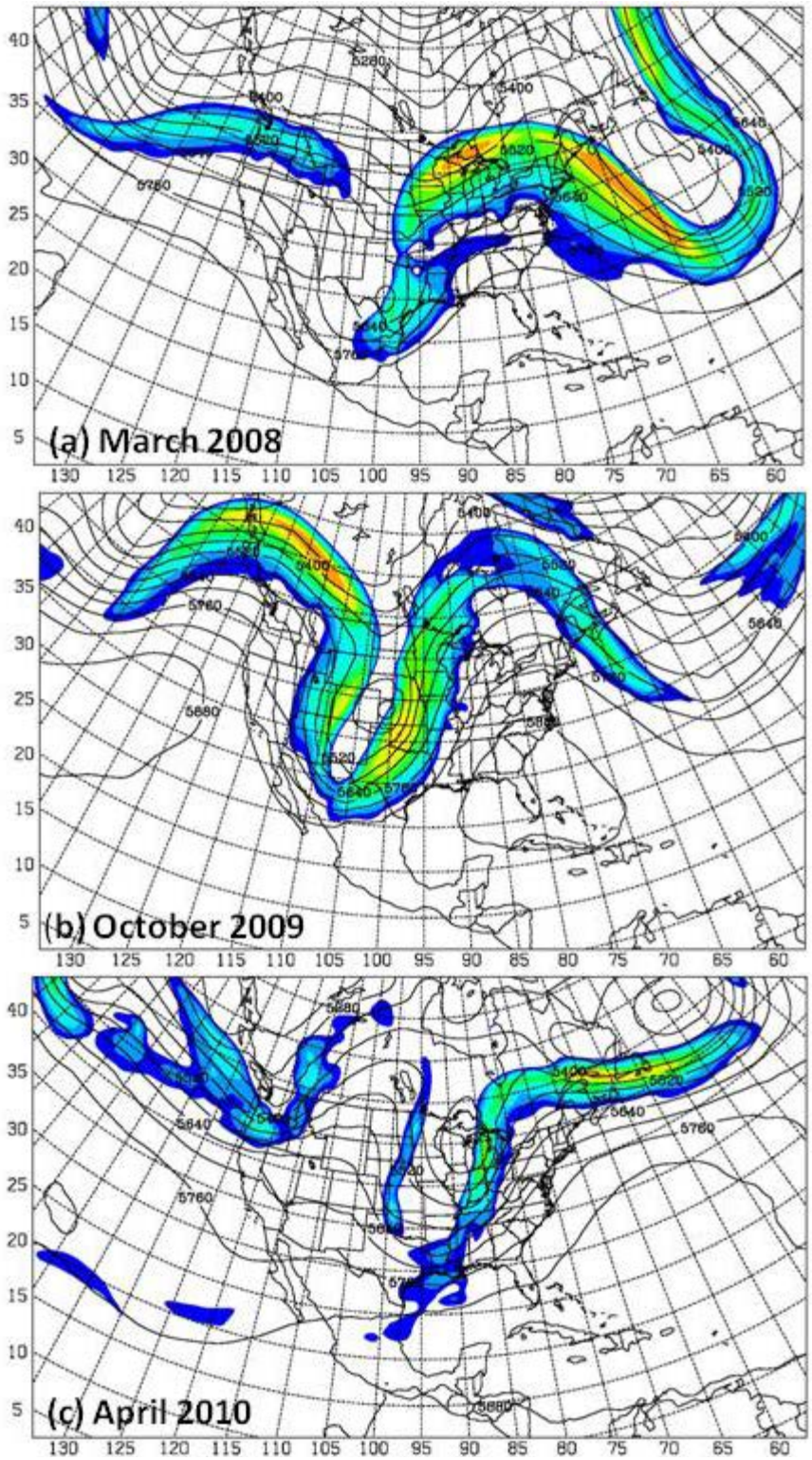

Figure 34. Upper-level Features, Midpoint 2 (19 Mar 08, 00Z). 300hPa Isotachs in Filled Contours Starting at 40 m/s (5 m/s Intervals). 500hPa Geopotential Height in Black Contours every 60 m.

The low pressure center of the March case tracked to the northeast along the warm front which remained relatively stationary over the Ohio Valley. The low also deepened further as pressure falls continued. With the slight eastward progression of the cold front through Texas, the moisture plume was concentrated further over the Mississippi River Valley. The pressure gradient tightened as well, leading to a low level jet of approximately 70kts (not shown), that was now feeding the precipitation region.

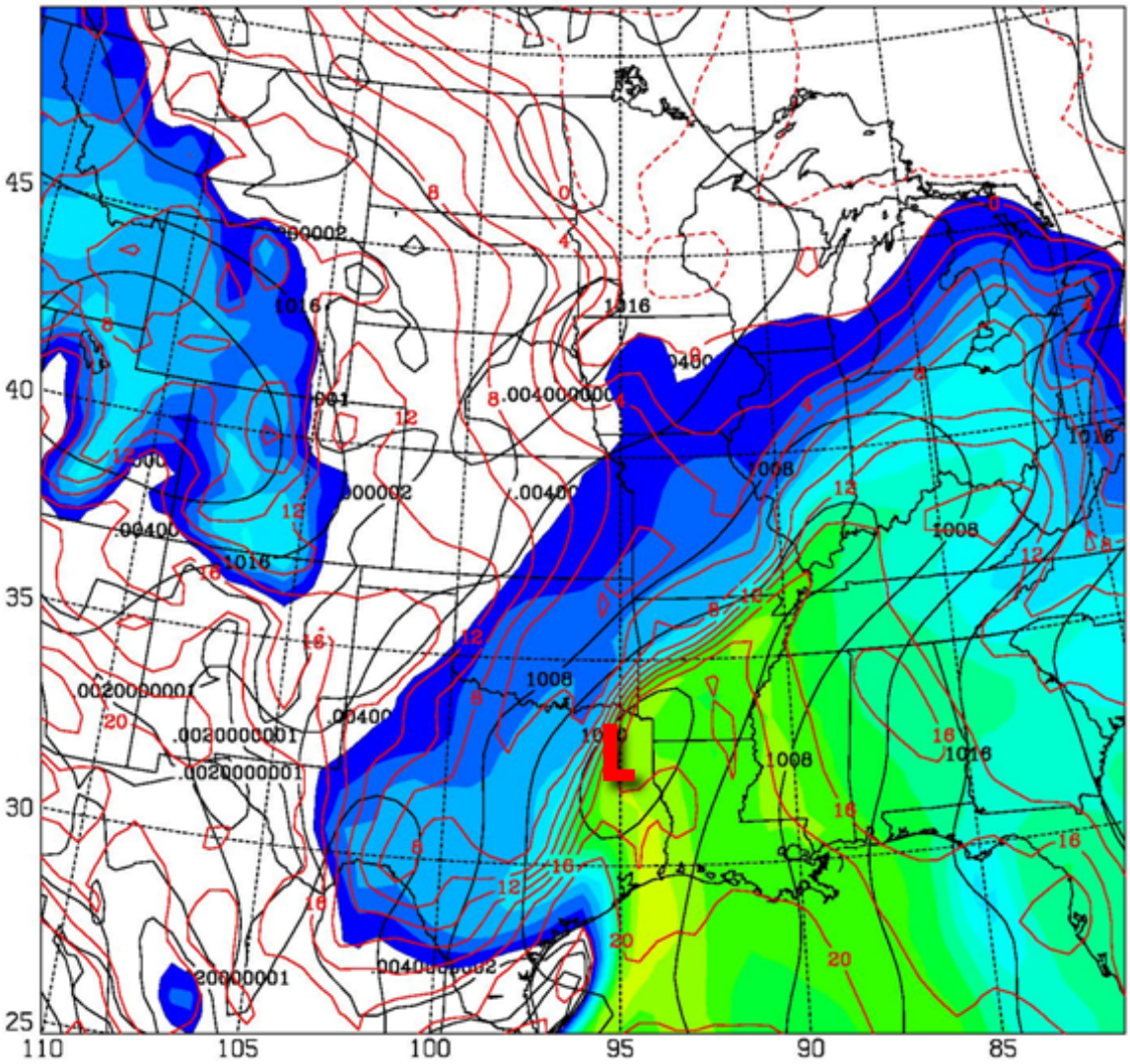

Figure 35. March 2008, Low-level Features, Midpoint 2 (19 Mar 08, 00Z). MSLP (Black Contours, every 4hPa), 925hPa Temperature (Red Contours, every 2°C), Mixing Ratio (every 1 g/kg beginning at 4 g/kg).

The surface low of the October case (Figure 36) began to occlude as the system progressed northeastward through the domain. Flow was southerly throughout the N–S extent of the domain, with moisture entering from the south and leaving through the northern boundary. However, the cold front intensified, resulting in a very strong moisture plume through the Mississippi River Valley. By this time, convection formed a line along the cold front. The northeastward cell movement on radar (not shown) was parallel to the slow-moving cold front, which caused rain to fall repeatedly over the same area.

The isentropic ascent associated with the warm front 12 hours earlier decreased due to the orientation of the flow (not as perpendicular to the pressure surfaces). Consequently, the precipitation in the Illinois region began to decrease in intensity. This region became less distinct as a separate precipitation area as the cold front advanced and became the dominant precipitation region.

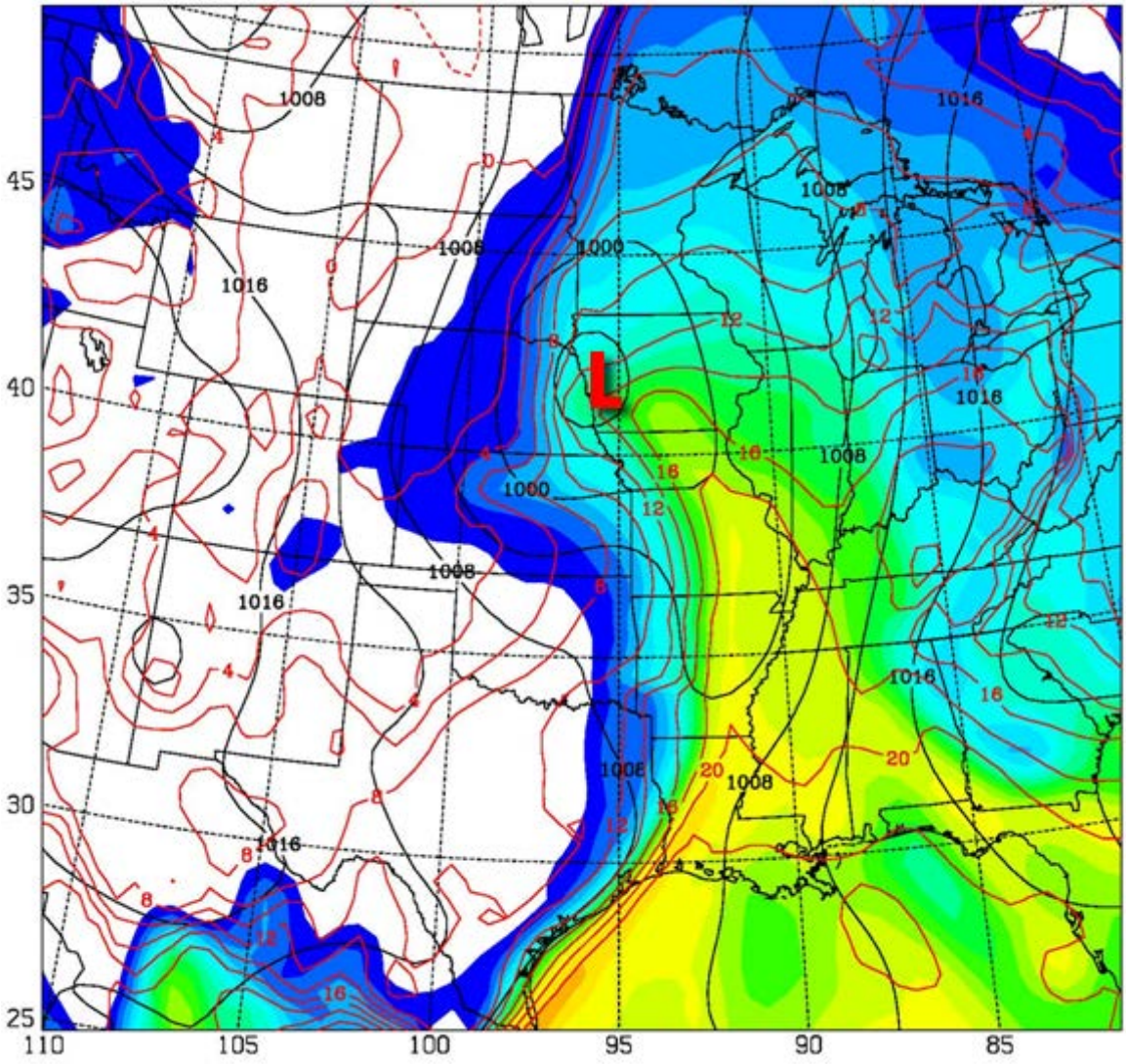

Figure 36. October 2009, Low-level Features, Midpoint 2 (30 Oct 09, 06Z). Same as Previous Figure.

Unlike the heavy precipitation cases in March and October, April's system continued to advance eastward through the domain. This eastward movement resulted in diminishing intensity and coverage of the rainfall along the front, and the location was well past western Tennessee/Kentucky where the highest rainfall previously occurred. Although there was still a plume of moisture extending out of the Gulf along the front, the progressive nature of this system prevented it from being a heavy precipitation event.

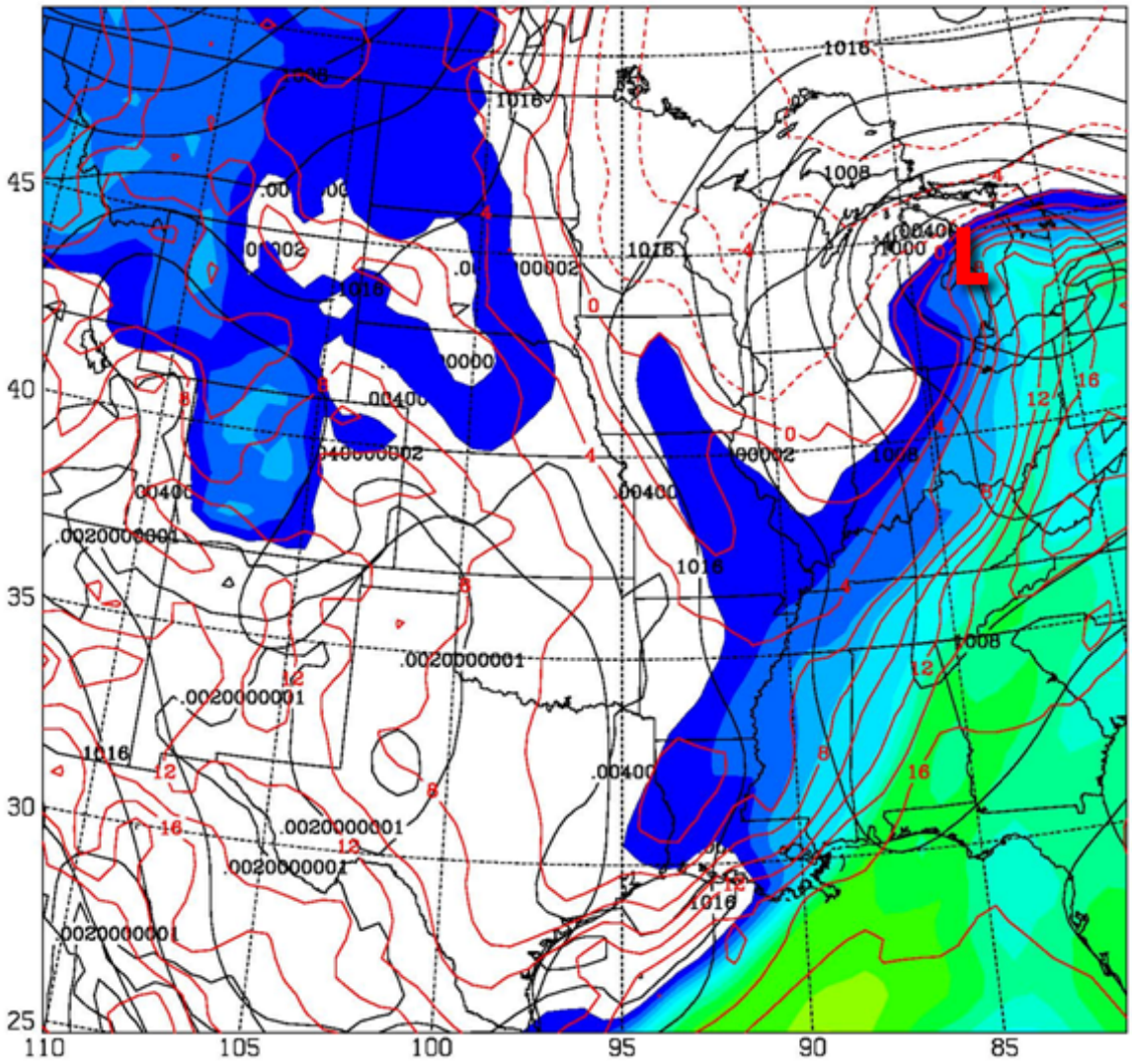

Figure 37. April 2010, Low-level Features, Midpoint 2 (8 Apr 10, 15Z). Same as Previous Figure.

The Q-vector plots shown in Figure 38 confirm the frontal and frontal forcing evolution noted on the surface plots. In the March case (Figure 38a), the area of Q-vector convergence became more north–south oriented over Arkansas and Louisiana as the longwave trough shifted eastward and the cold front became active as well as the warm front. The Q-vector orientation along the cold front changed to more westerly (compared to the southwesterly seen earlier in the evolution) as the trough ceased digging, indicative of active frontogenesis.

The warm frontogenesis was still active over Missouri and Indiana as seen by Q-vectors perpendicular to the isotherms in that region.

For the October case (Figure 38b), strong Q-vector convergence in the vicinity of the cold front indicated strong vertical motion. This was associated with very pronounced frontogenesis with Q-vectors that point across the isotherms. By this time, very little warm frontogenesis was evident with this case.

For the April case, the cold frontogenesis is evident in Figure 38c over the southeast. The magnitude of the Q-vectors and associated Q-vector convergence indicate that this system was weakening compared to 12 hours earlier.

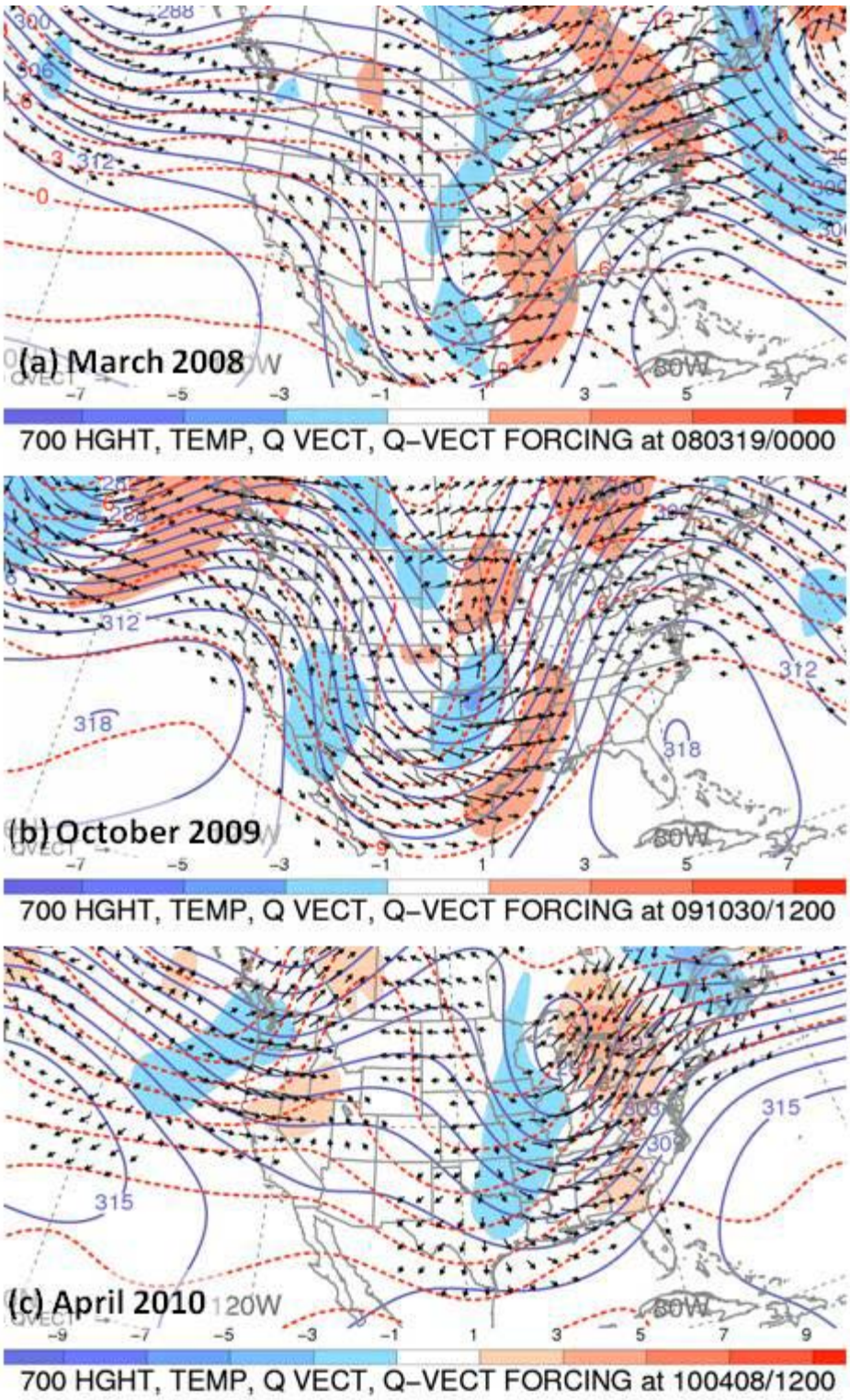

Figure 38. Q-Vector Convergence, Midpoint 2. 700 hPa. Geopotential Height (solid blue), Temperature (dashed red), Q-vectors (black arrow), Q-vector Forcing (blue-divergence, red-convergence).

e. Event End

Approximately 36 hours after Event Onset for the March and October cases, the features progressed eastward/northward enough to start the decrease of heavy precipitation over the central U.S. For the October case, the trough over the central United States shifted eastward but also weakened. The weakening may be due in part to the strong upstream amplification of the ridge over the West Coast. For the March case, the amplification of the downstream ridge due to the upward vertical motion associated with the warm front/warm air advection resulted in the northward progression of the feature. This also resulted in an overall weakening of the trough over the south central U.S. The longwave trough in the April case became neutrally oriented as it shifted eastward, ending precipitation over the area of interest as subsidence and cold air advection took over.

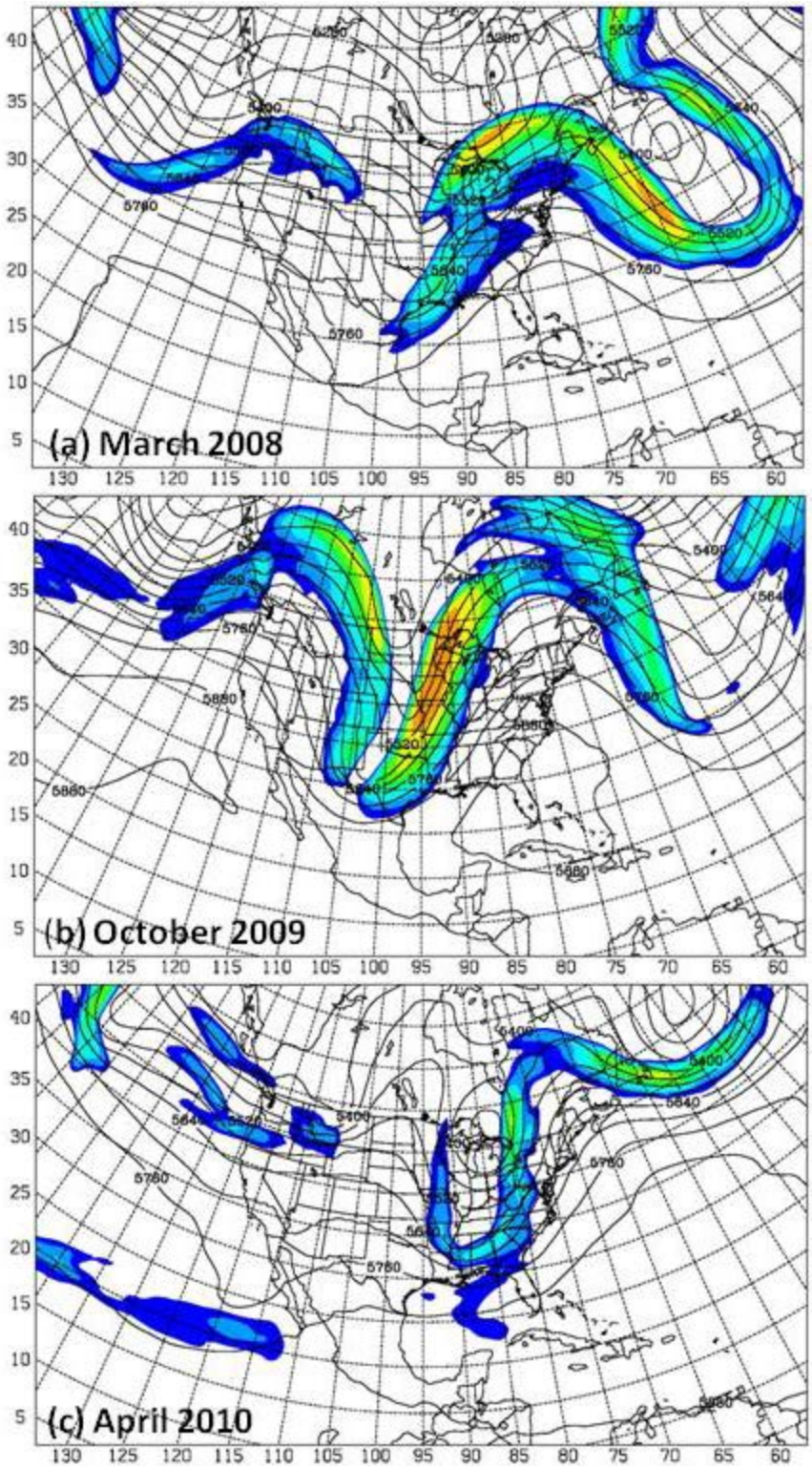

Figure 39. Upper-level Features, Event End. 300hPa Isotachs in Filled Contours Starting at 40 m/s (5 m/s Intervals). 500hPa Geopotential Height in Black Contours every 60 m.

The low-level features for the March case (Figure 40) confirmed the eastward shift of the warm front and low centers. Although warm frontal precipitation was still occurring, it moved eastward out of the area of heaviest precipitation. Precipitation falling on the backside of the low continued over the area of interest for approximately 6 hours after this time, but overall, precipitation decreased.

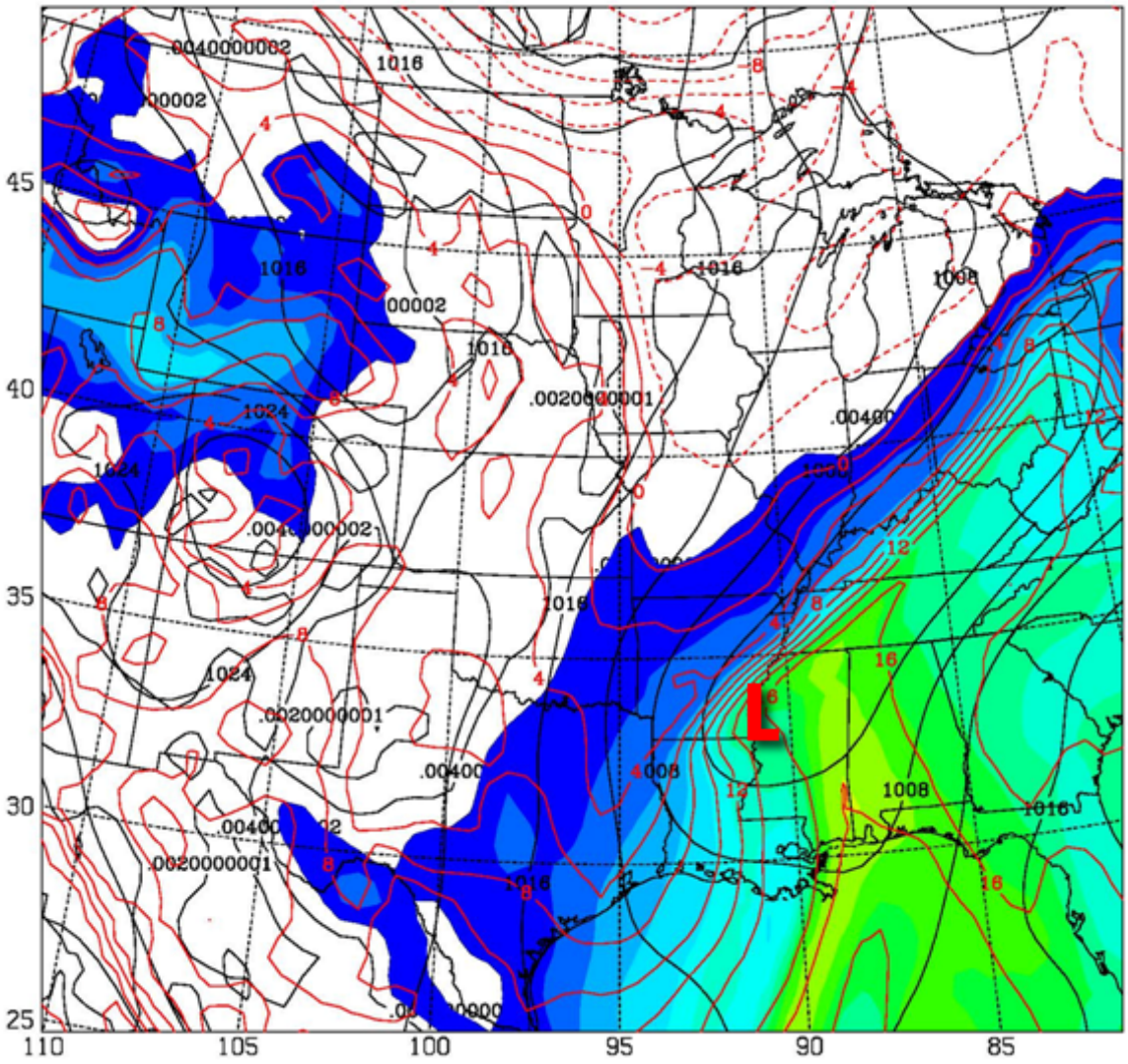

Figure 40. March 2008, Low-level Features, Event End (19 Mar 08, 12Z). MSLP (Black Contours, every 4hPa), 925hPa Temperature (Red Contours, every 2°C), Mixing Ratio (every 1 g/kg beginning at 4 g/kg).

For the October case, the event end identified based on the moisture flux across the Gulf Coast may not have been the true event end. The later onset of the rain in the region that experienced the heaviest precipitation and the slow movement of the surface cold front allowed precipitation to continue after this time. Precipitation was still occurring along the extent of the cold front, including Louisiana and eastern Arkansas. Over the course of the following 12 hours, the front did not move a considerable distance, but the precipitation decreased considerably as the forcing became less favorable for frontal convection.

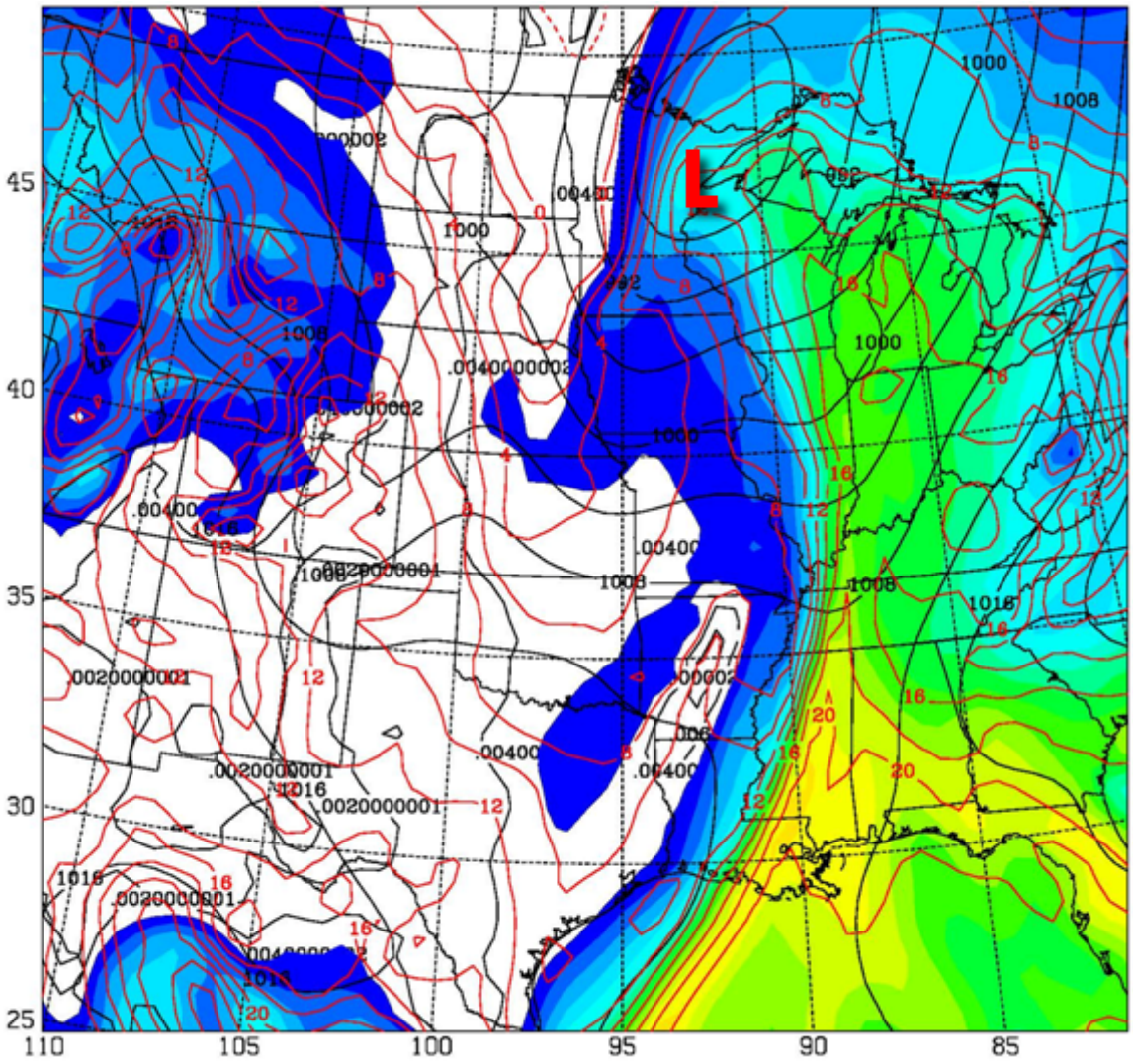

Figure 41. October 2009, Low-level Features, Event End (30 Oct 09, 18Z). Same as Previous Figure.

April's system was entirely out of the domain by this point. The tightest temperature gradient was located along the Appalachian Mountains, with relatively little moisture available for transport across the southern boundary of the domain. The speed of movement of this system suggests that the event end might be defined 12 hours earlier. However, this time has been included to provide a similar time window as the heavy precipitation events.

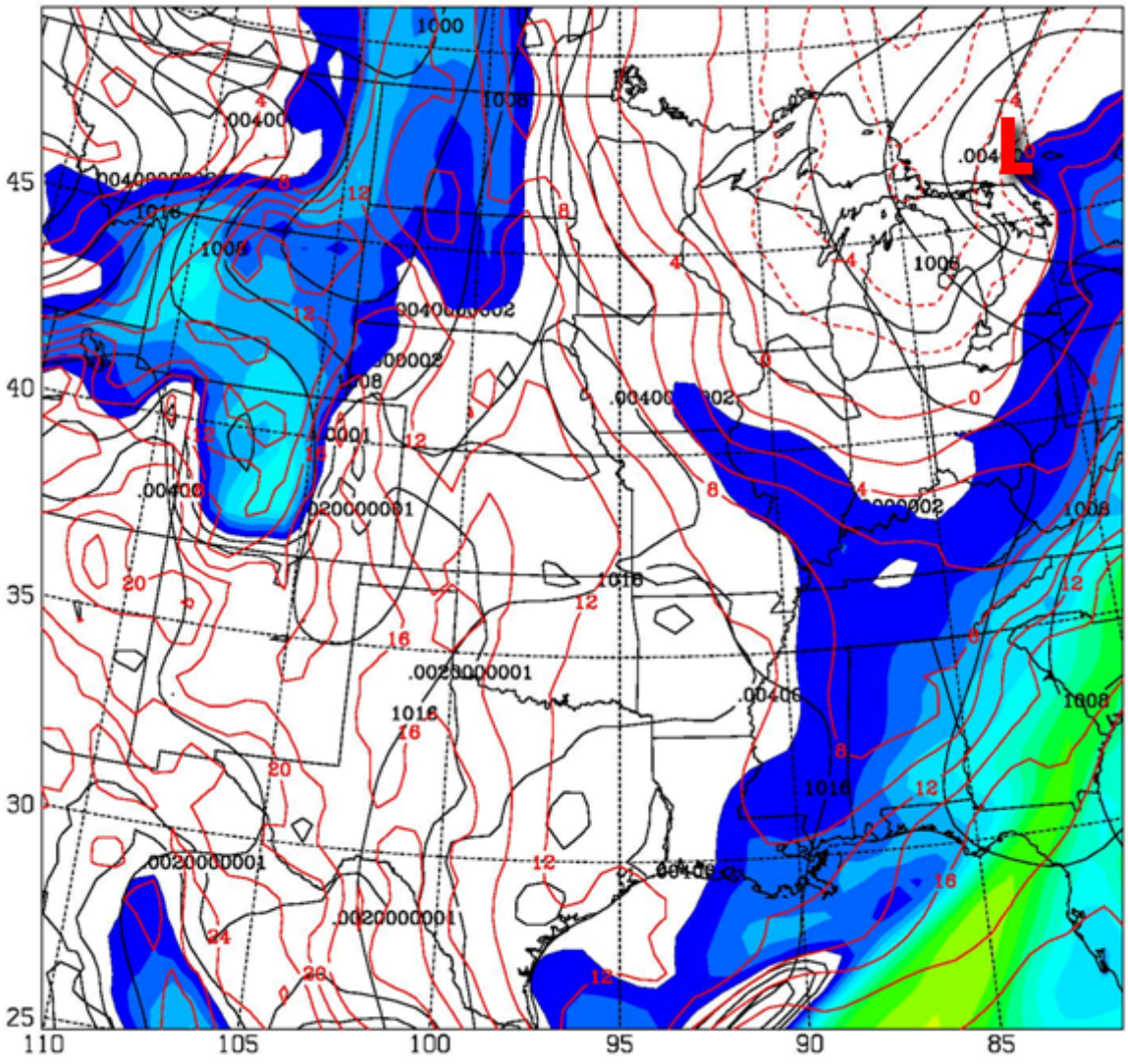

Figure 42. April 2010, Low-level Features, Event End (9 Apr 10, 03Z). Same as Previous Figure.

2. Cross-section Analysis

To get an initial view of the relationship between the upper-level PV anomaly, the low-level temperature anomaly and the moisture transport into the precipitation region, cross sections were constructed from west to east across the tip of the positive PV anomaly for each case at Midpoint 1. Figure 43 shows the locations of these cross sections for each case. Additional cross sections constructed from south to north through each moisture plume to view the vertical distribution of the moisture as it interacted with features (i.e., the warm front in the March case). The locations of the north–south cross sections are shown in Figure 44.

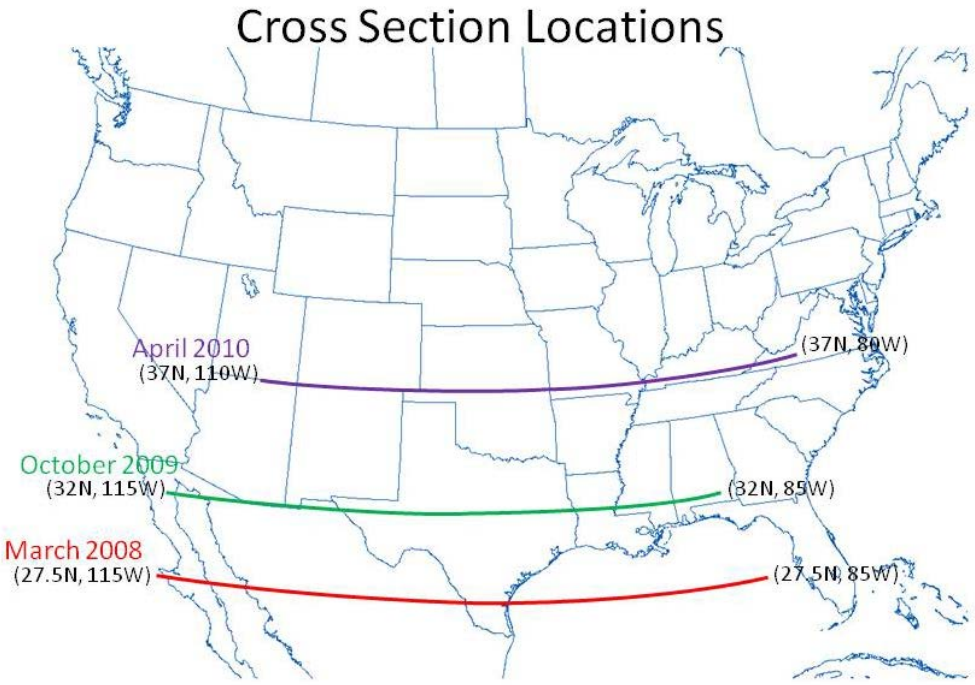

Figure 43. Cross-section Locations (West to East).

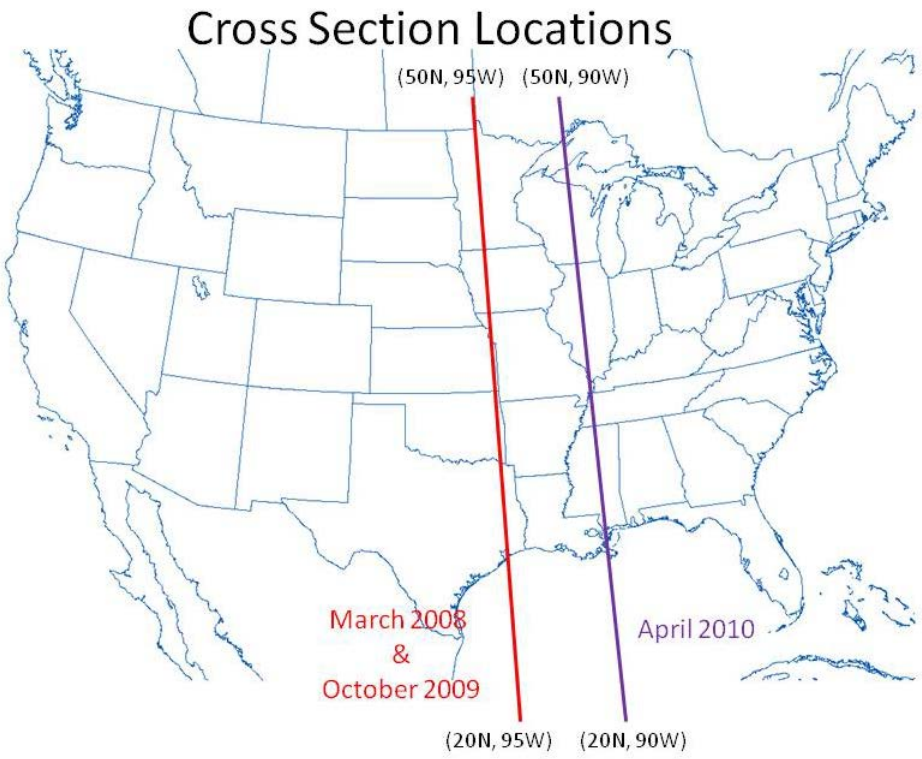

Figure 44. Cross-section Locations (South to North).

Analyses of the west–east cross sections showed marked differences in the breadth of the upper level PV anomaly and vertical moisture distribution. The March case (Figure 45) showed a narrower PV streamer compared to the October case (the minor difference in latitude notwithstanding) (Figure 46). The low-level jet in the warm sector in this case extended well to the east, which suggests that low-level structure associated with the high to the east may be important in setting up the moisture transport. The vertical extent of the moisture was limited and may be suppressed by the subsidence surrounding the anticyclone (Bermuda High) as the upper-level ridge axis was still over the southeast at this time (Figure 23a). The higher static stability in the low levels is consistent with subsidence over the region at and prior to this time.

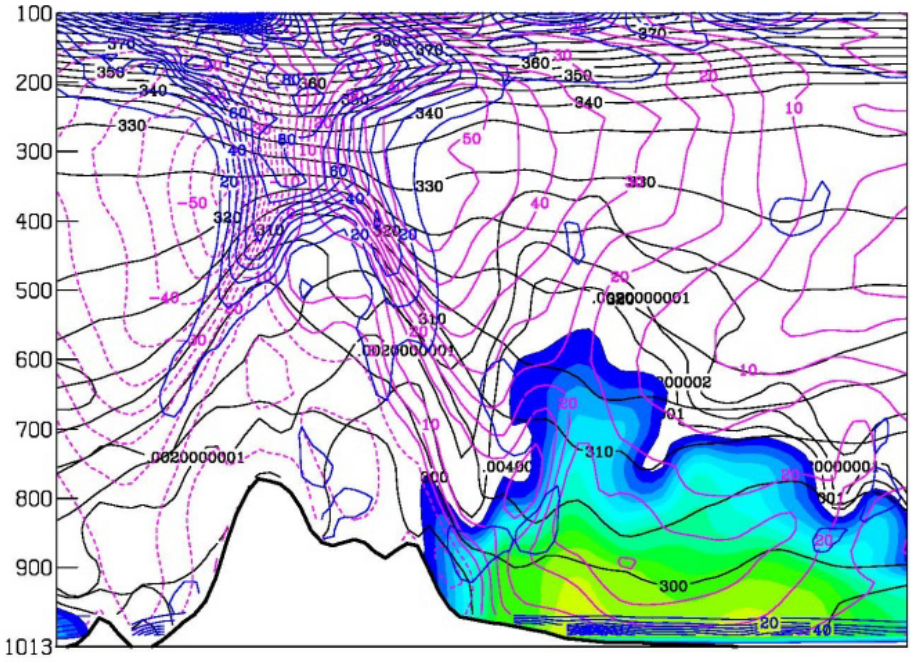

Figure 45. March 2008, West–East Cross Section, Midpoint 1 (18 Mar 08, 12Z). PV in blue (1 PVU= 10 units), meridional wind in magenta (m/s), mixing ratio in color fill at 1 g/kg intervals starting at 4 g/kg.

The PV streamer in the October case (Figure 46) appeared to penetrate the atmosphere more than the March case, and is considerably broader. The strong flow in the low levels in this case seems to be a direct extension of the upper-level jet as it does not extend to the east as much as the March case. The cross section is less statically stable than the March case, which is consistent with the upper-level ridge displaced more to the east (Figure 23b) and reduced subsidence.

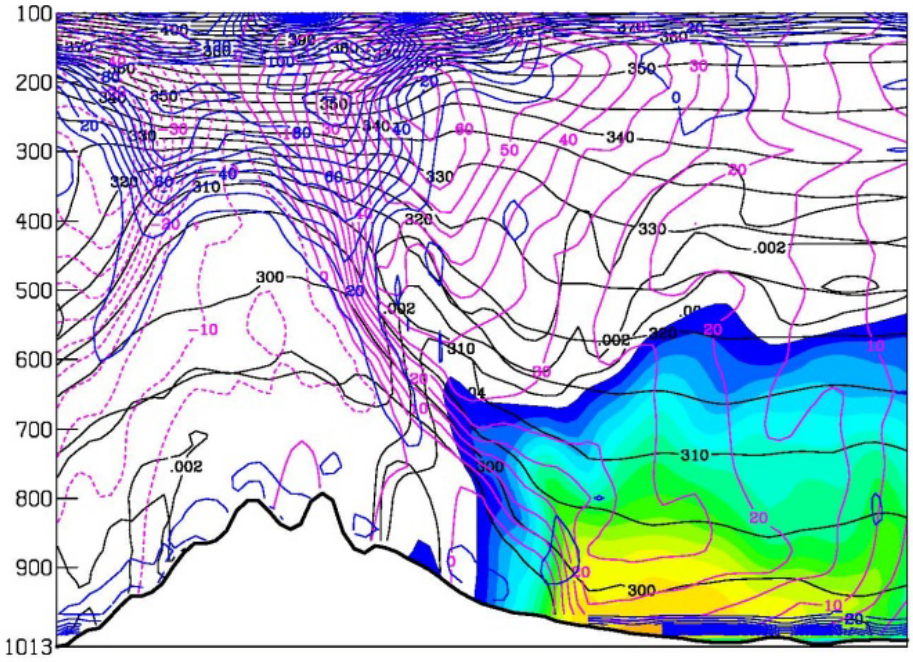

Figure 46. October 2009, West–East Cross Section, Midpoint 1 (29 Oct 09, 18Z). Same as Previous.

The PV distribution in the April case had the broadest streamer (Figure 47). However, the vertical penetration of the anomaly was not as great as that of the October case, consistent with weaker meridional flow. The moisture content in this case was less than the heavy precipitation cases and occurred well to the east compared to the other cases.

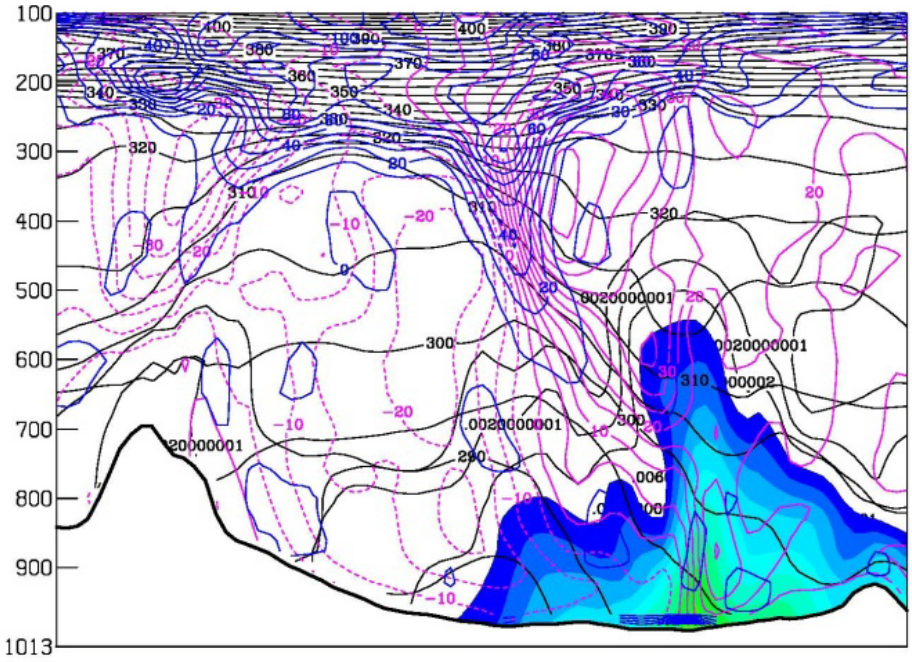

Figure 47. April 2010, West–East Cross Section, Midpoint 1 (8 Apr 10, 03Z). Same as Previous.

As noted previously, the March case was characterized by strong warm frontal forcing and ascent. In the south–north cross section for the March case (Figure 48), the warm front is clearly distinguishable with tightly packed mixing ratio contours near the center of the figure, where it divides the moist air in the warm sector from the dry air to the north. The vertical extent of the moisture at the warm frontal location is similar to the vertical extent of the moisture in the October case along the Gulf Coast (Figure 49). The moisture to the south, does not extend nearly as far upward in the atmosphere, perhaps due to less vertical mixing caused by increased static stability associated with the anticyclone as noted previously.

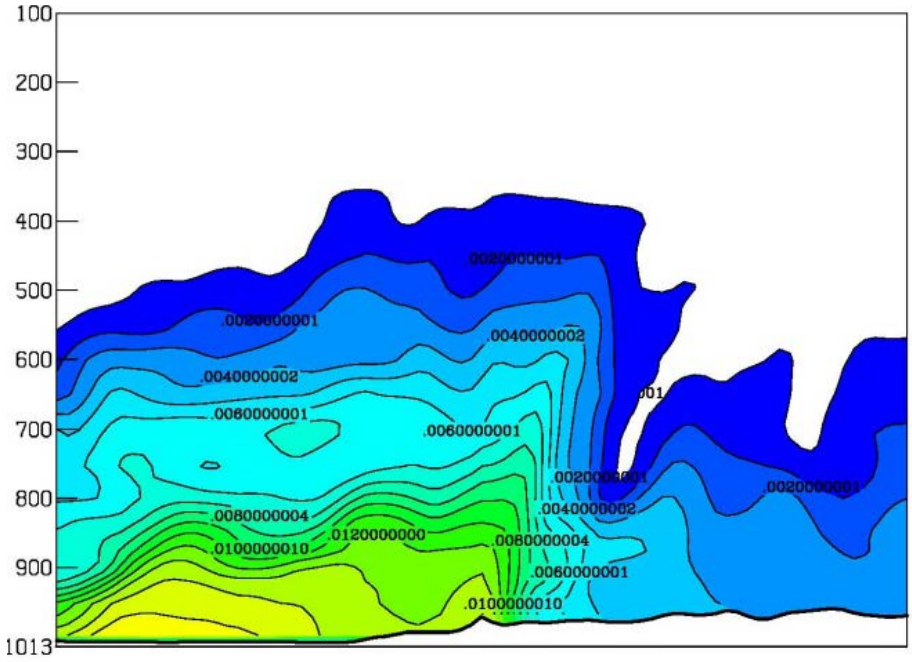

Figure 48. March 2008, South–North Cross Section, Midpoint 1 (18 Mar 08, 12Z). Mixing ratio in Colorfill at 1 g/kg Intervals Starting at 4 g/kg.

The warm front of the October case was not as intense as the March case, but is still visible on the cross section approximately one third in from the right side of the plot (Figure 49) where the strongest horizontal moisture gradient occurs. As previously noted, the precipitation at this time was occurring primarily along the warm front even though the frontal forcing was rather weak. Later convection within this deep moist layer became the primary precipitation mechanism.

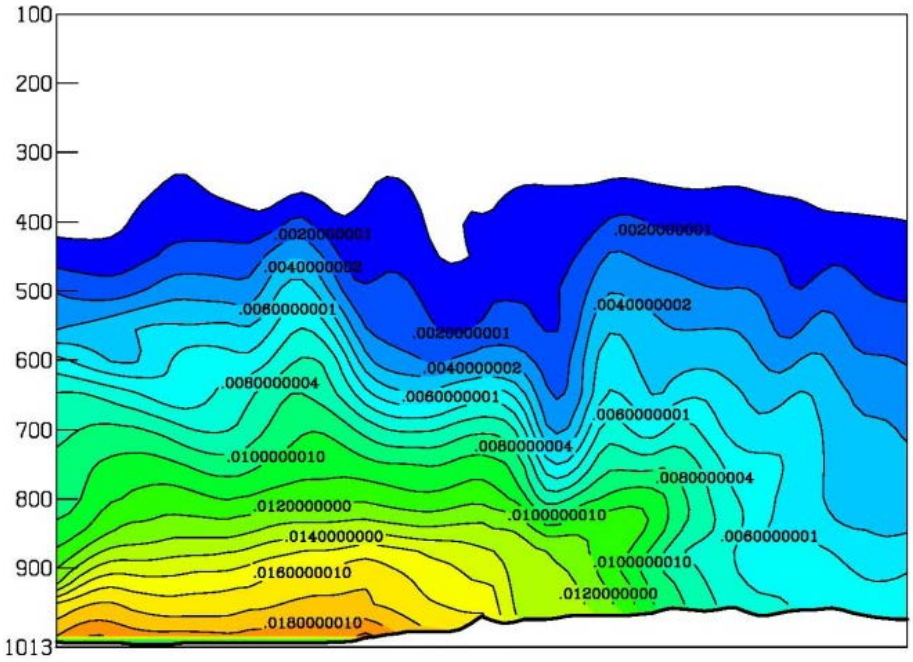

Figure 49. October 2009, South–North Cross Section, Midpoint 1 (29 Oct 09, 18Z). Same as Previous.

The south–north cross section for the April case shows a relative lack of moisture. This is due in part to the cross section cutting across the SW–NE oriented cold front. The frontal boundary is evident as the strong moisture gradient along the left side of Figure 50. The vertical extent of moisture within the warm sector reaches levels similar to the heavy precipitation cases. The shallower vertical moisture extent along the rest of the cross section is behind the front with the deeper moisture near the center of the plot being due to wrap around moisture near the low center (see Figure 31).

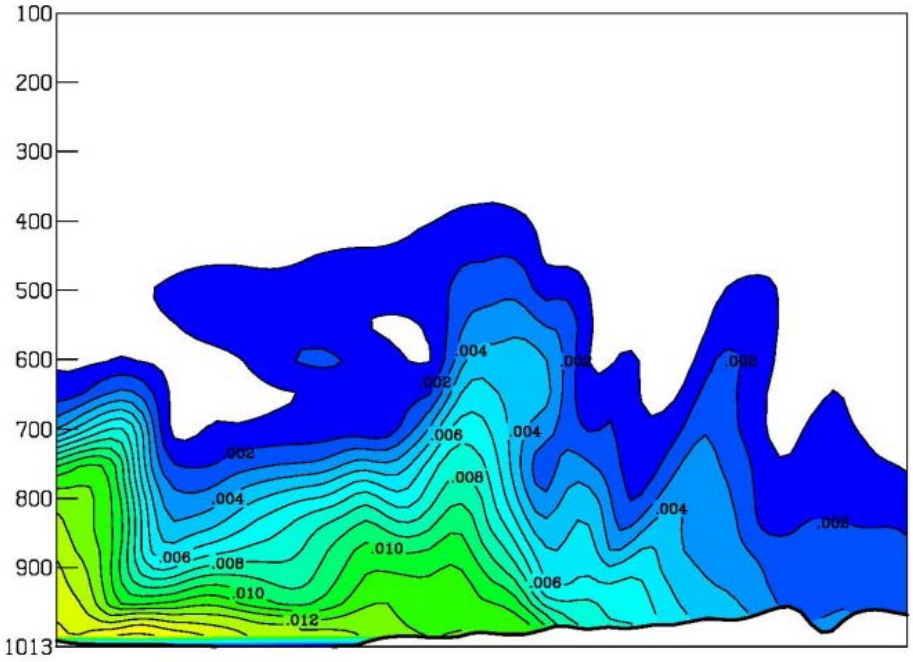

Figure 50. April 2010, South–North Cross Section, Midpoint 1 (8 Apr 10, 03Z). Same as Previous.

THIS PAGE INTENTIONALLY LEFT BLANK

IV. RESULTS

A. MOISTURE BUDGET

As noted in the previous chapter, a total moisture budget was calculated for each case over time to illustrate the relationship between moisture transport and precipitation. The total moisture flux (Figure 51) was greatest for the heavy precipitation cases, which increased significantly in the 9–12 hours preceding event onset. At event onset, the precipitation started to increase substantially, which was expected based on the definition of the system evolutions. Moisture flux (dashed lines) reached a peak approximately 3–6 hours before Midpoint 1. By Midpoint 2, all the systems showed a decrease in the total moisture flux. By the event end, the total moisture flux for the heavy precipitation cases approaches zero. April differed due to the quicker progression of the system through the domain as the moisture flux becomes negative just prior to Midpoint 1. As noted for this faster moving system, Midpoint 2 may be more indicative of event end.

The maximum in average precipitation (solid lines) occurred near Midpoint 1 for all three cases, with the moderate precipitation case (April) receiving only half the total rainfall as the heavy precipitation cases. Nearly all of the precipitation in the domain for the March and April cases was due to the frontal system as described in the last chapter. October, on the other hand, had several areas of precipitation, none of which were occurring in the region that received the most precipitation at that time (as previously mentioned in Chapter 3). The initial peak in precipitation occurred in a region on the eastern side of the moisture plume (moisture gradient) and the strong low level jet forced vertical motion isentropically. By Midpoint 2, nearly all of the precipitation in the domain for all cases was caused by the frontal forcing. The heavy precipitation cases exhibited dual peaks in the average precipitation. As previously mentioned, it appeared that the first peak in the October case was caused by the isentropic ascent on the eastern side of the moisture plume and the second peak was

caused by the strong cold frontal circulations and the slow moving cold front. The dual peaks for the March case may have been due to diurnal effects (Maddox et al. noted that the frontal events, like this March case, are distinctly nocturnal in nature). By event end, both of the heavy precipitation cases still had rain occurring in the domain, but the regions that received the heaviest precipitation were seeing a decrease.

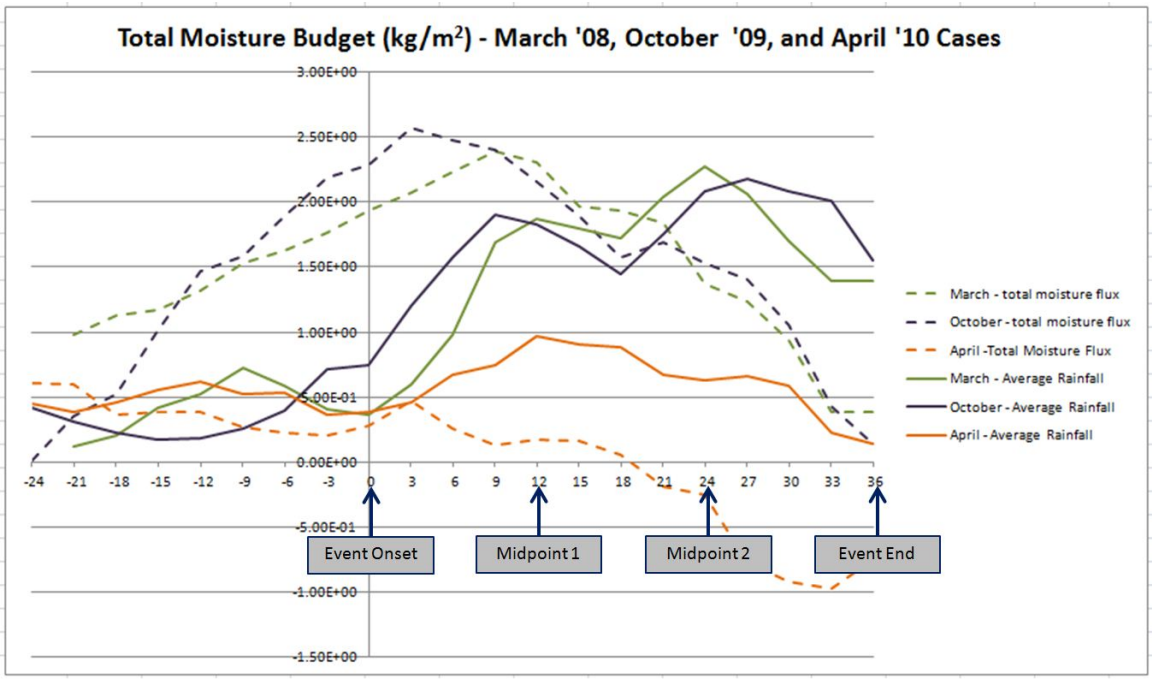

Figure 51. Total Moisture Budget, All Three Cases.

Since both the October and April cases were of the same classification (synoptic), their event duration can be compared more directly by shifting the evolution of the October case to the left 12 hours: Midpoint 1 is shifted to be Event Onset (Figure 52). As mentioned in Chapter 3, the precipitation in the region that received the heaviest precipitation began later in the October case (around Midpoint 1). Assuming that the first peak in the average precipitation is primarily due to the precipitation caused by the isentropic ascent in the vicinity of the warm front and that the ramp up in precipitation due to the forcing associated with the cold front is masked by the overlap, the graphs

have a similar event duration and moisture flux pattern. The main differences are the leading moisture flux, which is much greater for the heavy precipitation case. Therefore, the October case compares with the March case in that it is a heavy precipitation event. It also compares with the April case in that the event duration was relatively short when the warm frontal precipitation away from the heavy precipitation region is ignored.

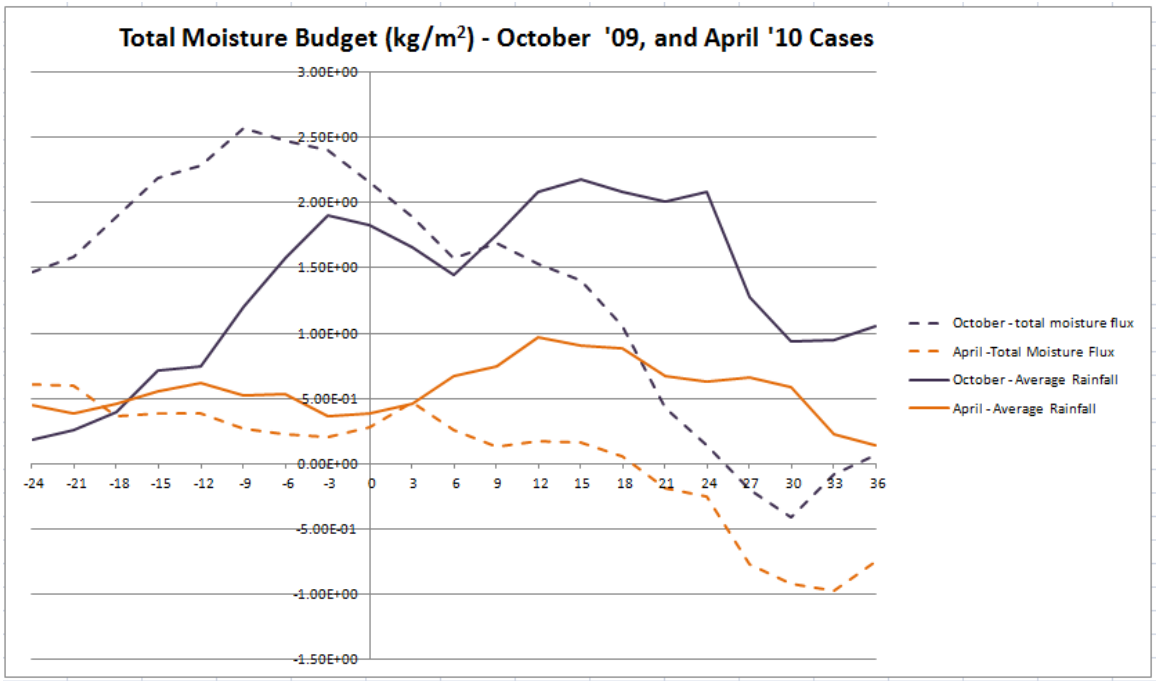

Figure 52. Total Moisture Budget, October and April Cases. October's Event Onset Shifted for more Direct Comparison.

Using the system evolution designated in Chapter 3 once again, Figures 53–55 further detail the moisture flux across each of the boundaries for each case. The main contribution to the total moisture flux came across the southern boundary for all three cases (blue dashed line in Figures 53–55). The other feature common to all three cases was the increasing flux out of the eastern boundary (more negative eastern flux) around Midpoint 2 (24 hour point in the plots), signaling the progression of the systems out of the domain.

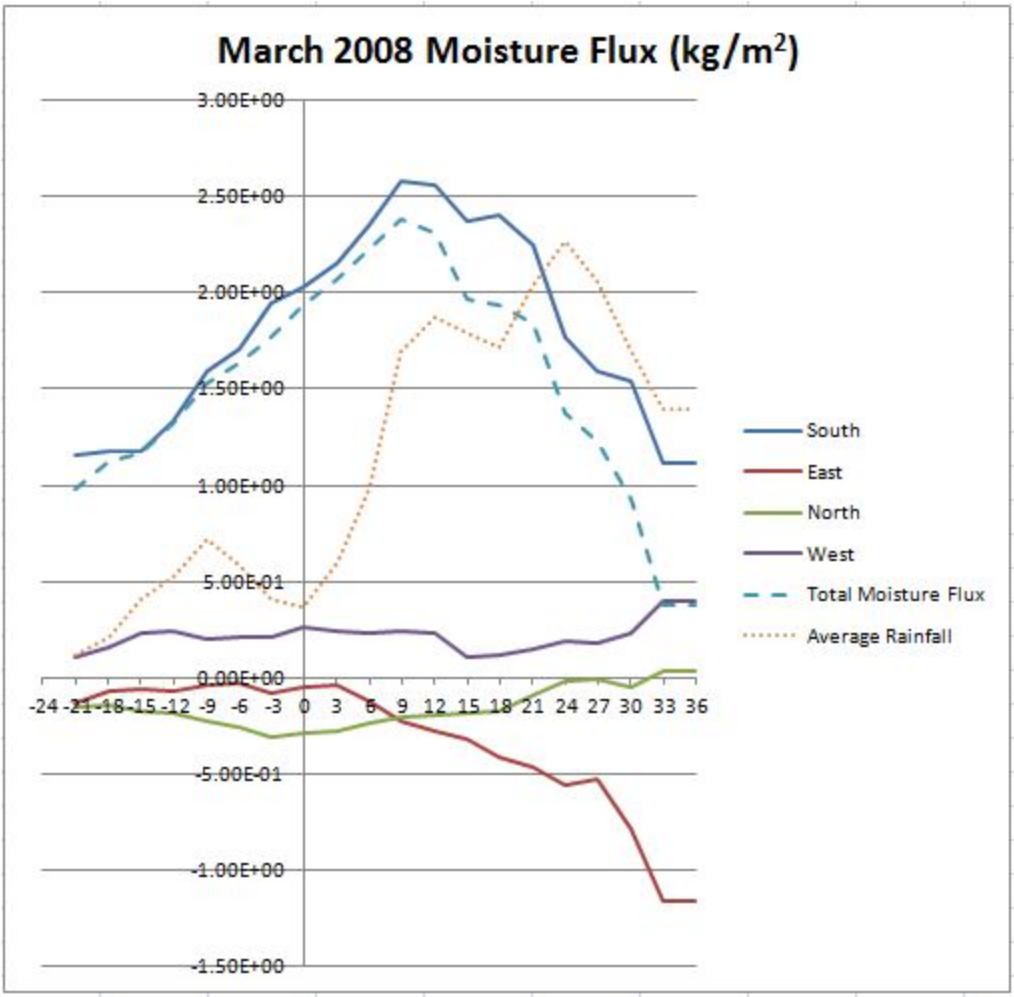

Figure 53. March 2008, Moisture Flux and Average Rainfall.

For the March case, the western, northern, and eastern boundaries exhibited fairly constant flux prior to event onset. Shortly after onset, the flux out of the eastern boundary started to increase gradually (become more negative). This occurred as a result of a shift in the position of the system with respect to the defined domain and the anticyclonic nature of the low level jet. Flow that had been leaving via the northern boundary was now leaving via the eastern boundary (thus the simultaneous decrease in flux out of the northern boundary – flux becoming more positive).

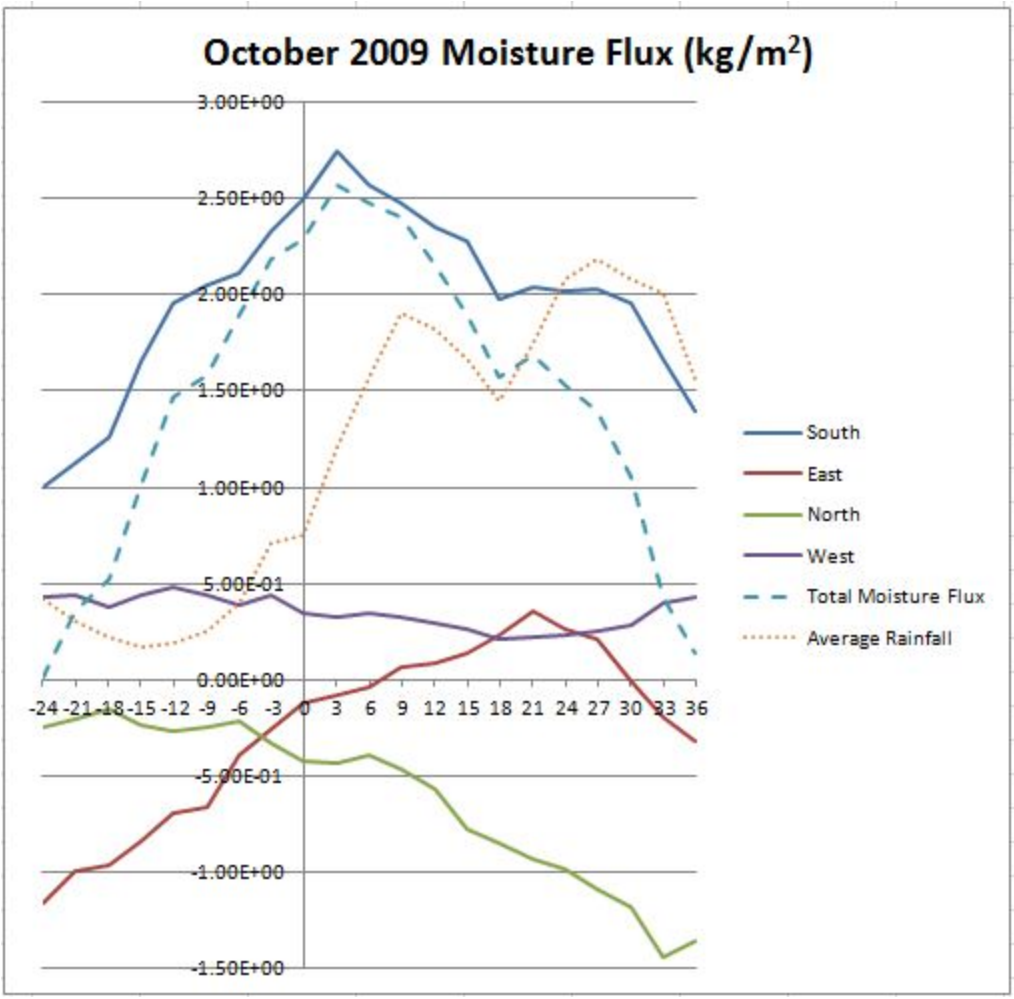

Figure 54. October 2009, Moisture Flux and Average Rainfall.

During the October case, the total moisture flux increased much more significantly compared to the March case, rising from near zero to the 2.5 kg/m^2 in the 24 hours prior to event onset. This dramatic increase in the total moisture flux was due to the increasing moisture flux across the southern boundary. As the low level flow shifted to a more southerly direction, the moisture-rich air located over the Gulf of Mexico (Figure 12f) began to reach the domain, thus causing the drastic increase in total moisture flux. The flux across the eastern boundary exhibited an increasing trend (starting out with a loss out of the eastern boundary, progressing to a gain in moisture through the eastern boundary). This was due to the trough/ridge amplification causing the system to stall in its

eastward progression. An additional result of this amplification was the increasing loss of moisture out of the northern boundary; the meridional flow brought moisture in from the southern boundary and out through the northern boundary.

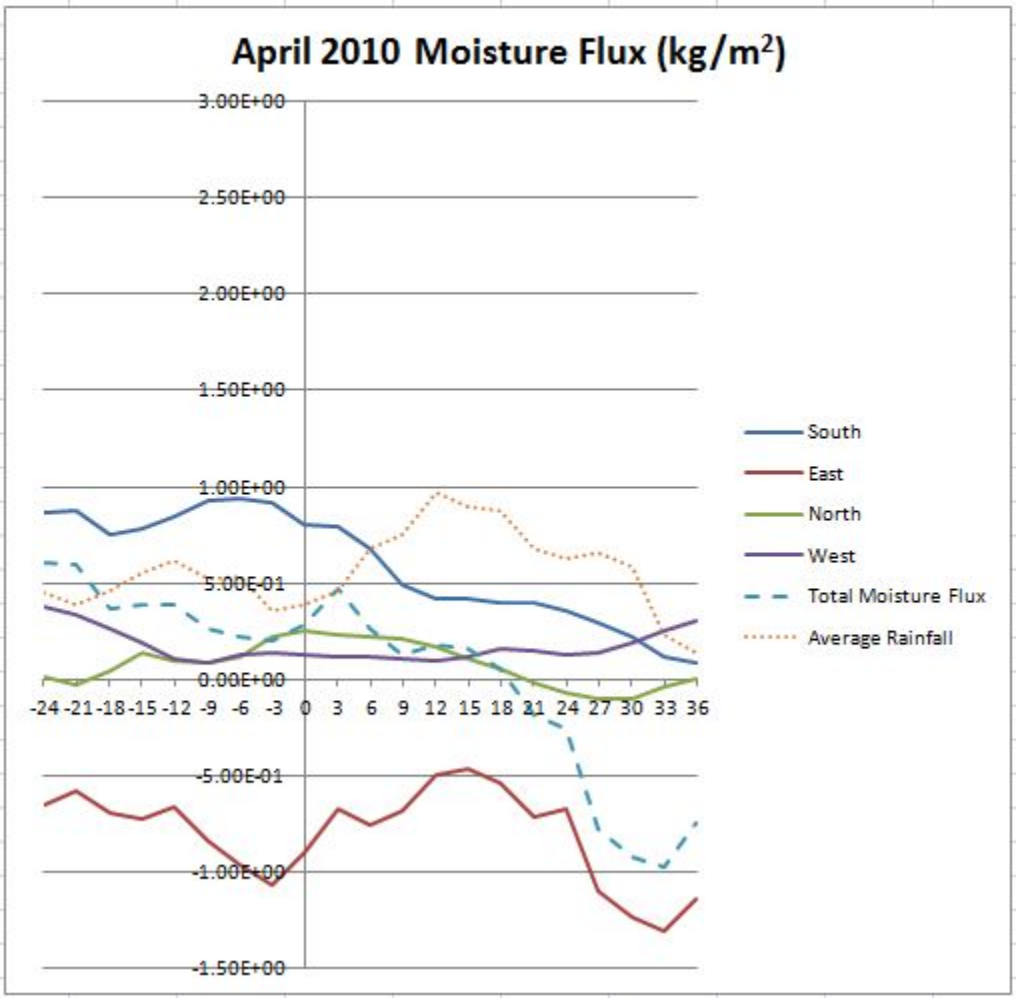

Figure 55. April 2010, Moisture Flux and Average Rainfall.

The April case had relatively constant moisture flux values early in the system's evolution. Moisture flux across the southern boundary did not increase like what was seen for the heavy precipitation cases. Shortly after event onset, the moisture flux across the southern boundary decreased as a result of the cold front advancing and limiting the greatest moisture flux to the far eastern side of the southern boundary. The loss of moisture through the eastern boundary is

consistent with eastward progression of the system. The size of the domain may have dampened the results for this case due to the faster progression of the system and the overall strength of the flow, yet the moisture flux across the southern boundary was greater than the other boundaries, consistent with an atmospheric river.

B. PIECEWISE PV INVERSION

The moisture budget analysis clearly shows that the moisture flux across the southern boundary was important for the heavy precipitation cases. As seen on the cross sections in Chapter 3, the low-level flow on the eastern side of the upper-level trough or PV anomaly is in the warm sector experiencing southerly flow and transporting moisture into the region. The piecewise PV inversion technique was applied to determine the contribution of the upper-level PV anomaly and the low-level/surface temperature anomaly to the low-level flow and associated moisture transport. The contribution from the upper-level PV anomaly on the low-level flow was calculated by setting the perturbations to zero below 600hPa. The perturbations were set to zero above 600hPa for the low-level/surface temperature anomaly calculations.

The full PV inversion shown in Figure 56 for the March case shows 15-20 m/s of meridional flow in the low levels that transport moisture northward east of the mountains. Considering the contribution from the upper-level PV anomaly alone, the low-level flow was relatively weak (5 m/s or less) in the region of moisture transport (Figure 57). However, the low-level/surface PV anomaly, when inverted, resulted in induced low-level flow approximately 15 m/s in the region east of the mountains where moisture transport was occurring (Figure 58). For this case, it appeared that the surface temperature anomaly was the primary contributing factor in setting up the southerly flow and the low-level moisture transport.

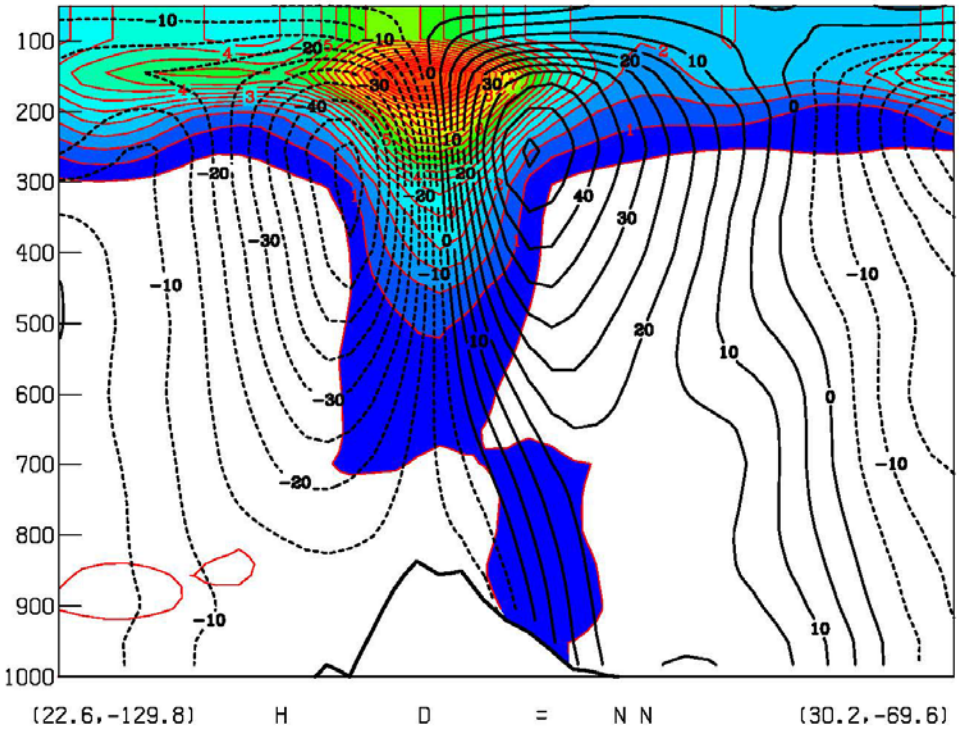

Figure 56. March 2008, Full PV Inversion, Midpoint 1 (18 Mar 08, 12Z). PV in Colorfill, Meridional Wind (m/s) in Black Contours.

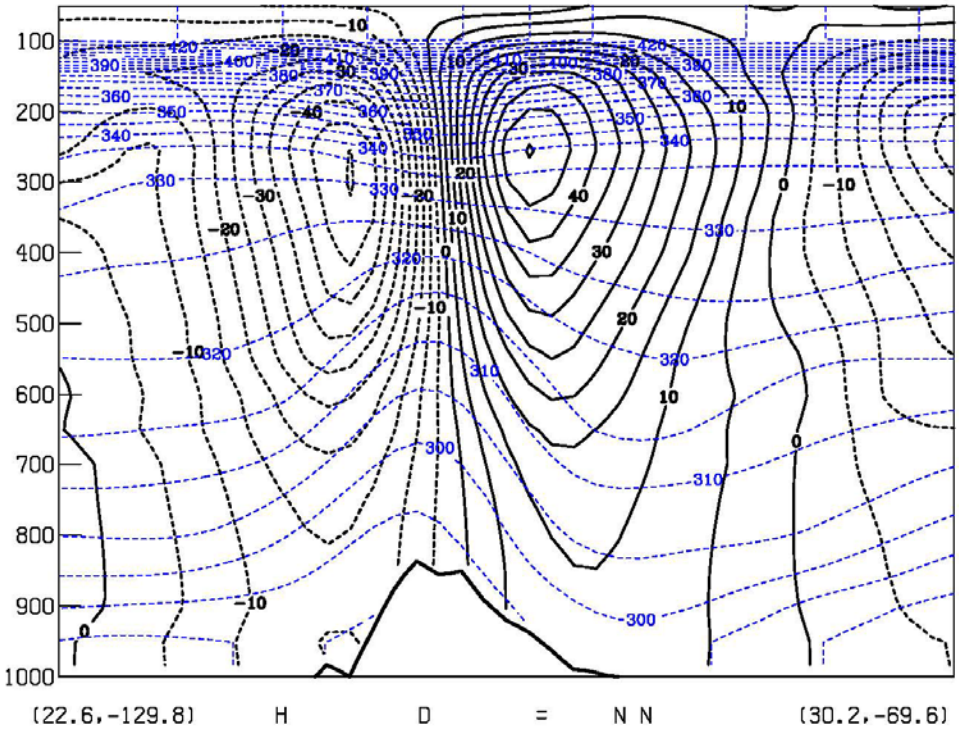

Figure 57. March 2008, Upper PV Inversion Only, Midpoint 1 (18 Mar 08, 12Z). Meridional Wind (m/s) in Black Contours. Potential Temperature (K) in Dashed Blue Contours.

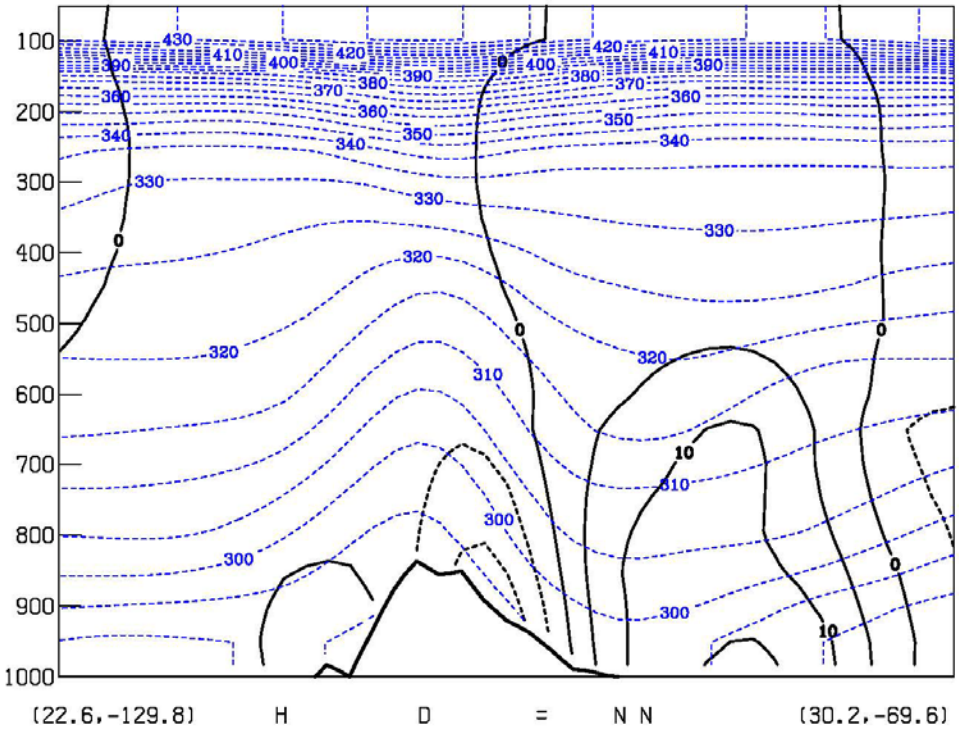

Figure 58. March 2008, Lower PV Inversion Only, Midpoint 1 (18 Mar 08, 12Z). Same as Previous.

The full PV inversion shown in Figure 59 for the October case shows 10-15 m/s of meridional flow in the low levels that transport moisture northward east of the mountains. Considering the contribution from the upper-level PV anomaly alone, the low-level flow was relative strong (10-15 m/s) in the region of moisture transport (Figure 60). However, the low-level/surface PV anomaly, when inverted, resulted in induced low-level flow that was much weaker (less than 5 m/s) in the region east of the mountains where the moisture transport was occurring (Figure 61). For this case, it appeared that the upper-level PV anomaly was the primary contributing factor in setting up the southerly flow and the low-level moisture transport.

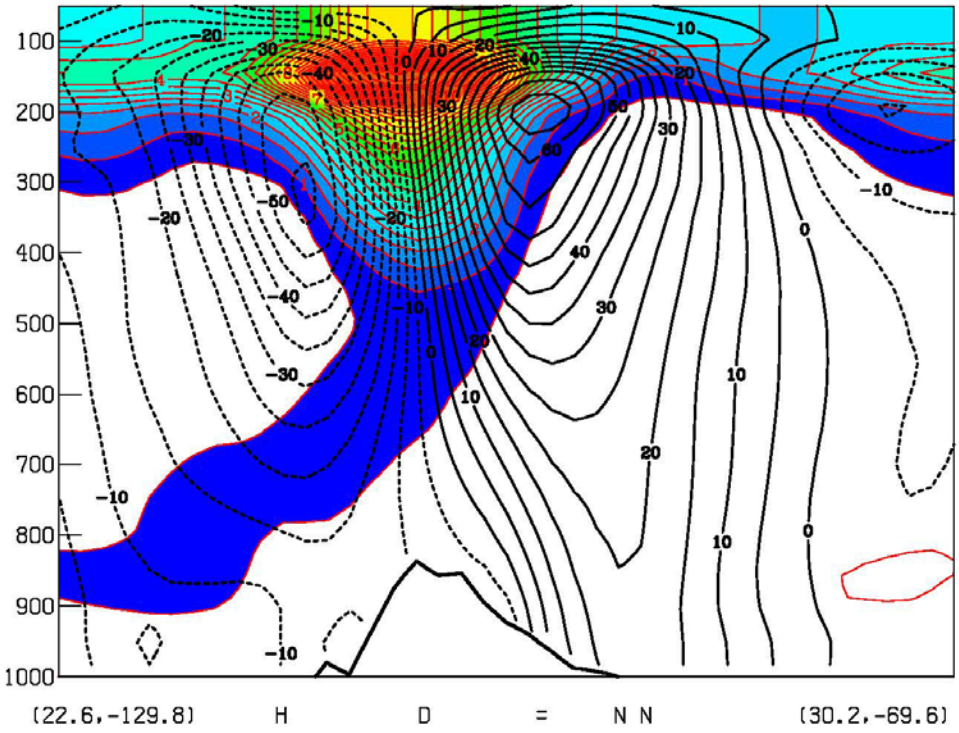

Figure 59. October 2009, Full PV Inversion, Midpoint 1 (29 Oct 09, 18Z). Same as Figure 56.

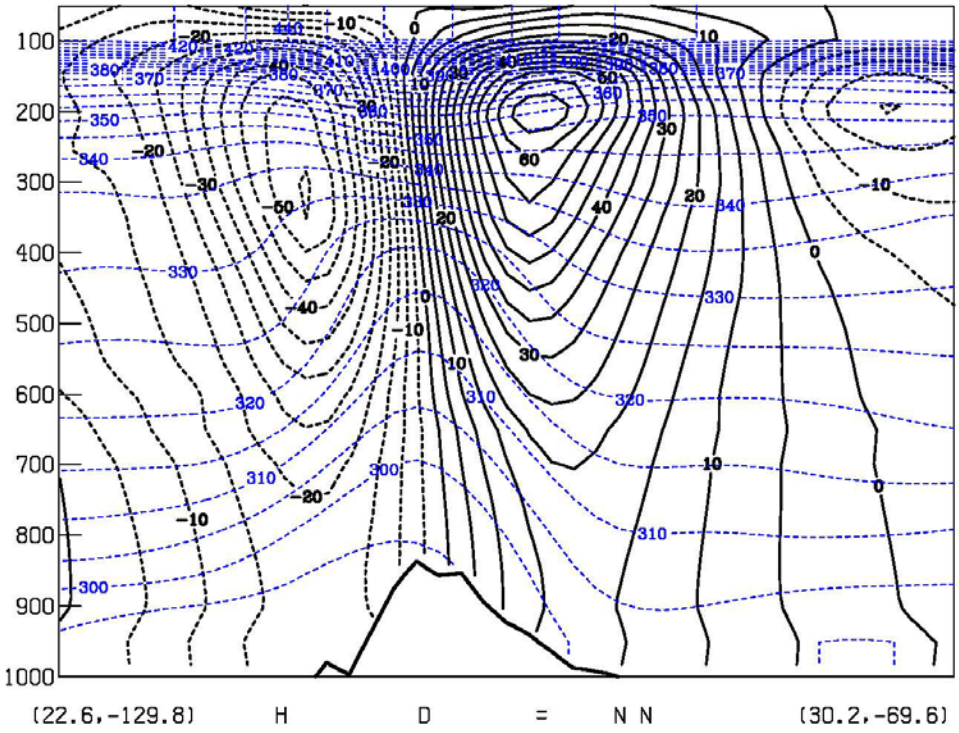

Figure 60. October 2009, Upper PV Inversion Only, Midpoint 1 (29 Oct 09, 18Z). Same as Figure 57.

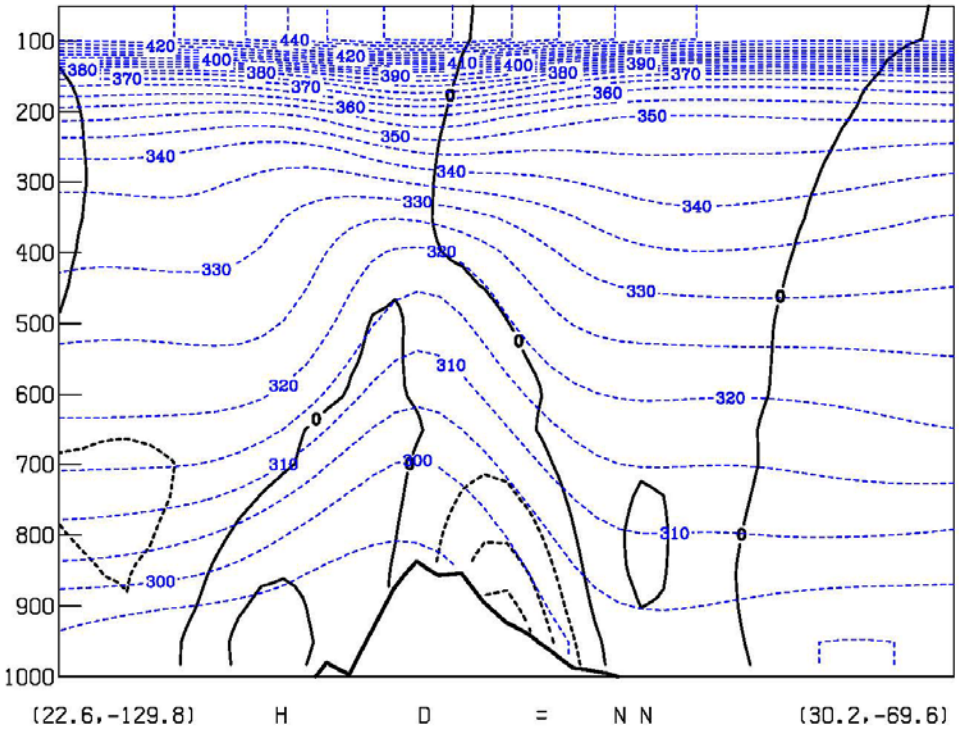

Figure 61. October 2009, Lower PV Inversion Only, Midpoint 1 (29 Oct 09, 18Z). Same as Figure 57.

The full PV inversion shown in Figure 62 for the April case shows 10 m/s of meridional flow in the low levels that transport moisture northward east of the mountains. Considering the contribution from the upper-level PV anomaly alone, the low-level flow was approximately 10 m/s in the region of moisture transport (Figure 63). However, the low-level/surface PV anomaly, when inverted, resulted in induced low-level flow near 0 m/s in the region east of the mountains where moisture transport was occurring (Figure 64). For this case, it appeared that the upper-level PV anomaly was the primary contributing factor in setting up the southerly flow and the low-level moisture transport. This case is similar to the October case, but with weaker southerly flow. This is not surprising since the upper-level southerly jet was nearly half the speed of the October case (35 m/s versus 65 m/s) as seen in Figures 59 and 62.

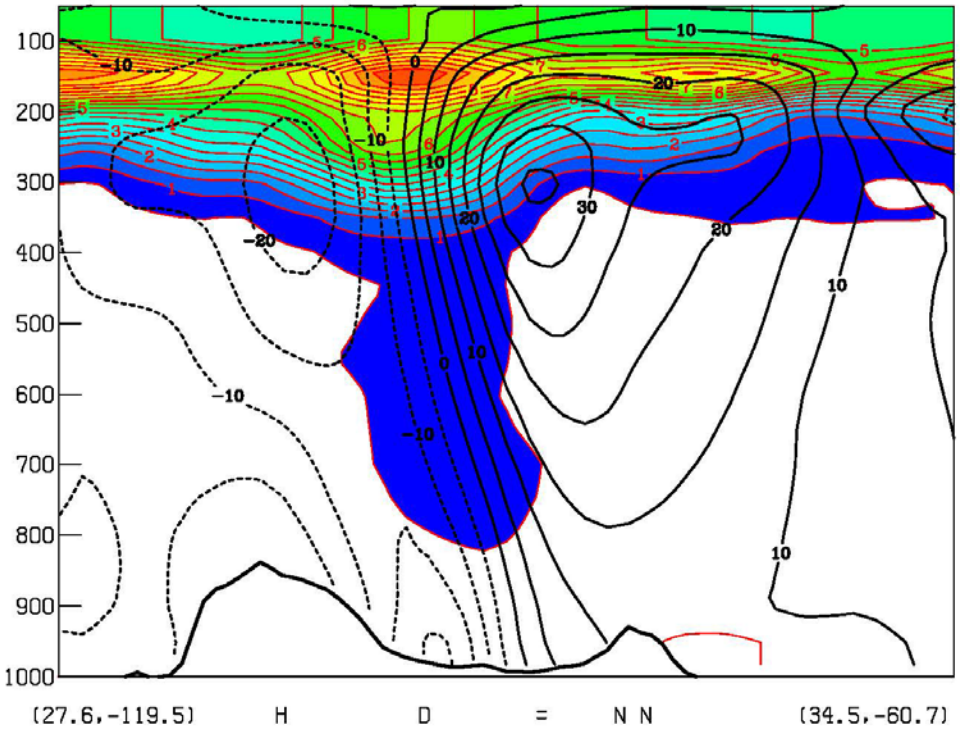

Figure 62. April 2010, Full PV Inversion, Midpoint 1 (8 Apr 10, 03Z). Same as Figure 56.

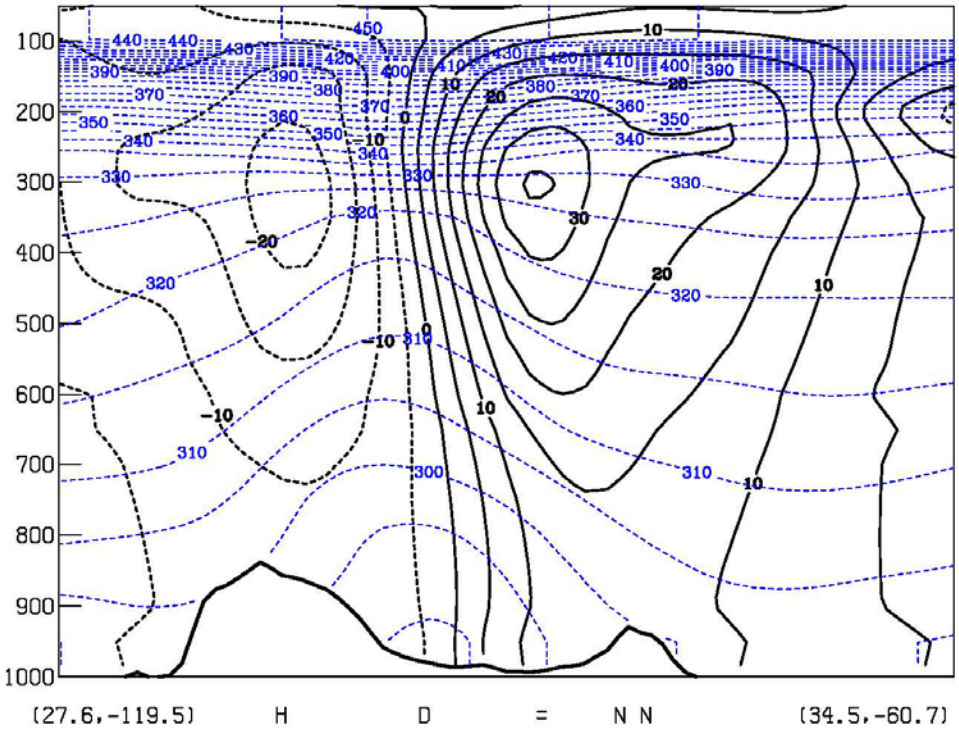

Figure 63. April 2010, Upper PV Inversion Only, Midpoint 1 (8 Apr 10, 03Z). Same as Figure 57.

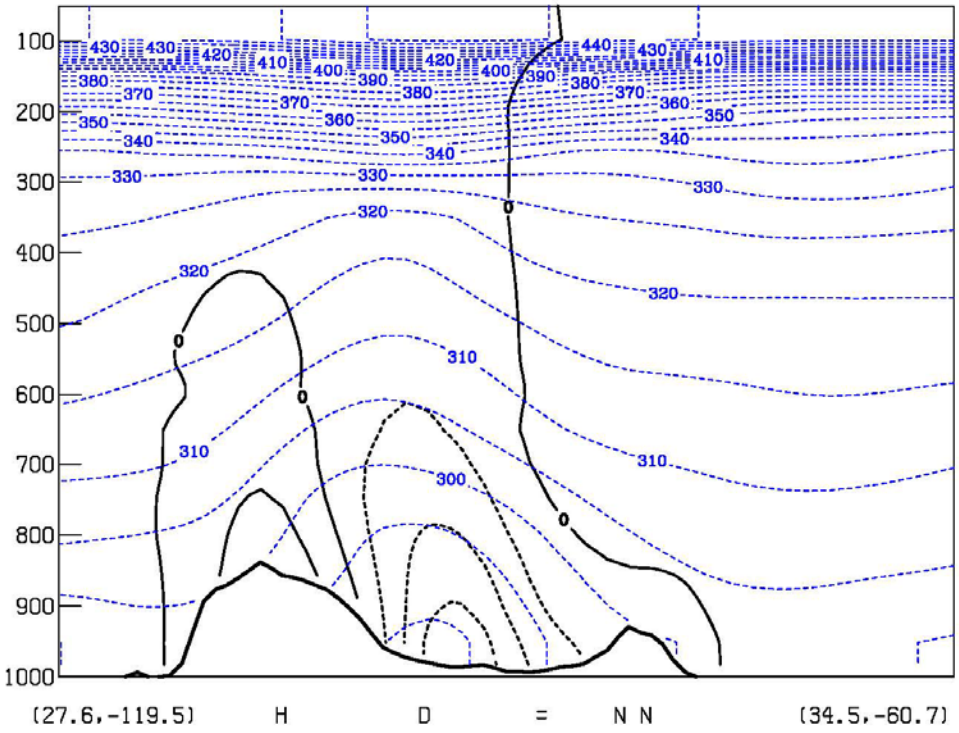

Figure 64. April 2010, Lower PV Inversion Only, Midpoint 1 (8 Apr 10, 03Z). Same as Figure 57.

V. CONCLUSION & RECOMMENDATIONS

A. CONCLUSION

Three cases exhibiting ARs originating from the Caribbean and Gulf of Mexico were chosen for comparison. Two of the cases were chosen due to the heavy precipitation that occurred. They represented two types of systems (as defined by Maddox et al. 1979): frontal and synoptic. The third case was chosen for having only a moderate amount of precipitation and a flow pattern similar to one of the heavy precipitation cases (synoptic). A comparison of the key features for these three cases is summarized in Table 2 below.

Table 2. Comparison of Key Features of All Cases

	March	**October**	**April**
Amount of Precipitation	Heavy	Heavy	Moderate
System Classification	Frontal	Synoptic	Synoptic
Precipitation Type	Stratiform	Convective	Convective
Evolution Point of Precipitation Starting in HP region	Event Onset	Midpoint 1	Event Onset
Duration of Precipitation in HP region	>36hrs	30hrs	30hrs
PW Range of AR (kg/m^2)	42-48	48-55	35-42
Moisture Transport Influence - Upper PV Anomaly	5 m/s	10-15 m/s	10 m/s
Moisture Transport Influence - Lower Temp Anomaly	15 m/s	< 5 m/s	0 m/s
Peak Value of Average Precipitation (kg/m^2)	2.27E+00	2.18E+00	9.65E-01
Peak in Moisture Flux Preceding Event Onset?	Yes	Yes	No
Vertical Depth of Moisture > 4 g/kg	650hPa	500hPa	750hPa

The March case represented a frontal-type system (as classified by Maddox et al. 1979) and resulted in heavy precipitation throughout Arkansas and Missouri. The precipitation was forced by isentropic ascent and enhanced by strong frontal circulations associated with frontogenesis of the warm front. The slow-moving nature of the longwave pattern caused approximately 36 hours of moderate to heavy precipitation to fall over the same region. Vertical moisture

distributions did not reach as high in the atmosphere as the October case, possibly due to greater static stability. Moisture transport in the low levels from the Caribbean and Gulf of Mexico was largely driven by the surface temperature anomaly, as indicated by the piecewise PV inversion in Figure 58. The moisture flux was greatest across the southern boundary, with the flux increasing dramatically in the 24hrs preceding event onset. At this point, precipitation began in the region that received the heaviest precipitation. Average precipitation peaked near Midpoint 1 and again near Midpoint 2, with this dual peak signature possibly due to diurnal variations. The moisture flux began to decrease shortly after Midpoint 1 as the AR became narrower. After Midpoint 2, the moisture flux decreased dramatically as the system began to exit the domain. By event end, the moisture flux was near zero, and precipitation was decreasing, but not yet halted over the region of interest.

The October case represented a synoptic-type system with the precipitation occurring in the warm sector ahead of the advancing cold front. While there was other precipitation in the domain caused by the same system (associated with the isentropic ascent in the vicinity of the warm front), the largest accumulation of precipitation was associated with the convection ahead of the cold front. Precipitable water values for this case were the highest, with a broad area of high moisture content located over the Gulf of Mexico. The vertical extent of this case was the highest of all three cases, with values of at least 4 g/kg extending to 500hPa. As the system developed, the moisture was concentrated more horizontally into an AR and pumped into the Midwest. Frontogenetical forcing was associated with the cold frontal region as indicated by the Q-vector convergence in Figure 33b and appears to have aided the construction of the AR. Moisture transport in the low levels was largely driven by the upper level positive PV anomaly, as indicated by the piecewise PV inversion in Figure 60. Again, moisture flux was greatest across the southern boundary, with the flux increasing dramatically prior to event onset. Precipitation occurring in the domain around event onset was due to the isentropic ascent forced by the strong low-

level jet into the Midwest, but was not located in the region that received the heaviest precipitation of the event. Precipitation began in the region of interest at approximately Midpoint 1 and was convective in nature. These two separate regions may have contributed to the dual peaks of average precipitation noted in the moisture budget calculations. As the system evolved and progressed through the domain, the moisture flux began to decrease (again near Midpoint 2). Precipitation continued to occur over the region of interest through the defined "event end", but according to Figure 52, the event end for October was possibly 6 hours later. This case illustrated the challenge of forecasting where the heaviest precipitation would occur. The convective rainfall associated with the cold front produced the heaviest amounts due to the frontogenetical forcing (as indicated by the Q-vector forcing) and the cell motion with respect to the frontal movement. Precipitation in the vicinity of the warm front, while moderate in intensity, lacked the frontogenetical forcing.

The April case had a similar pattern to the October case, a synoptic type. The heaviest precipitation was convectively driven. Precipitation within the domain was caused almost entirely by convection along the frontal train. Of the three cases, this case had the lowest AR moisture content (Figures 12k–o), which may have also contributed to the relatively lower vertical extent of moisture noted in Figure 50. Moisture transport was largely due to the upper-level PV anomaly as computed by the PV inversion in Figure 63. The moisture flux was greatest across the southern boundary, but an increase in moisture flux preceding the event did not occur like the heavy precipitation cases. The moisture flux began to decrease shortly after event onset as the system progressed through the domain quicker than the heavy precipitation cases. Negative total moisture flux occurred as the dry air following the cold front dominated the domain. Precipitation reached a peak around Midpoint 1 and did not exhibit a dual peak characteristic as in the previous two cases. The peak value of average precipitation was about half of that received in the heavy

precipitation cases, most likely due to less available moisture (indicated by lower PW values in the AR) and the faster system progression through the domain.

In conclusion, the upper-level PV anomaly was important for the focusing of the AR in two cases, October and April, which were both of the synoptic-type precipitation events. While these two cases were very similar, the outstanding difference was the preceding moisture flux increase. This occurred in the October and was largely due to an extensive reservoir and deep fetch of moisture-rich air that was able to be concentrated into an AR and pumped into the Midwest.

The surface temperature anomaly was important for moisture transport in one case, the March case, which was of the frontal-type precipitation event. This case also presented with a preceding moisture flux increase, making it a common feature between the two heavy precipitation cases. Even though the precipitable water content was slightly higher than the moderate precipitation case, it produced a peak value in average precipitation more than twice than that of the moderate precipitation case. The frontogenetical forcing was greater, as well as the duration of the event, resulting in a greater extraction of precipitation and making the March case a heavy precipitation event.

B. RECOMMENDATION FOR FUTURE RESEARCH

Future research is needed to refine the results obtained from three cases in this study. First, it would be helpful to better refine the interaction between the upper-level and low-level features on scales closer to those of the precipitation. A more fine scale data set may be able to provide more details of the mesoscale aspects of these particular cases, and others like it, and the characteristics of the precipitation processes.

Next, while this study addressed 3 years of data, a climatological approach using 10- or 30-yr data sets to examine all cases over a long period of time could be beneficial in determining the robustness of the two types of cases identified. This would help solidify the type of cases and their characteristic forcing.

LIST OF REFERENCES

Davis, Christopher A., Kerry A. Emanuel, 1991: Potential vorticity diagnostics of cyclogenesis. *Mon. Wea. Rev.*, **119**, 1929–1953.

Dirmeyer, Paul A., James L. Kinter, 2010: Floods over the U.S. Midwest: A regional water cycle perspective. *J. Hydrometeor*, **11**, 1172–1181.

Dirmeyer, Paul A., and J. L. Kinter III, 2009: The Maya Express—Late spring floods in the U.S. Midwest. *Eos, Trans. Amer. Geophys. Union*, **90**, 101-102.

Draxler, R.R. and Rolph, G.D., cited 2012. HYSPLIT (HYbrid Single-Particle Lagrangian Integrated Trajectory). [Available online at http://ready.arl.noaa.gov/HYSPLIT.php.]

Higgins, R. W., V. E. Kousky, P. Xie, 2011: Extreme precipitation events in the south-central United States during May and June 2010: Historical perspective, role of ENSO, and trends. *J. Hydrometeor*, **12**, 1056–1070.

Lackmann, Gary M., John R. Gyakum, 1999: Heavy cold-season precipitation in the northwestern United States: Synoptic climatology and an analysis of the flood of 17–18 January 1986. *Wea. Forecasting*, **14**, 687–700.

Maddox, R. A., C. F. Chappell, L. R. Hoxit, 1979: Synoptic and meso-α scale aspects of flash flood Events. *Bull. Amer. Meteor. Soc.*, **60**, 115–123.

Moore, Benjamin J., Paul J. Neiman, F. Martin Ralph, Faye E. Barthold, 2012: Physical processes associated with heavy flooding rainfall in Nashville, Tennessee, and vicinity during 1–2 May 2010: The role of an atmospheric river and mesoscale convective systems. *Mon. Wea. Rev.*, **140**, 358–378.

National Weather Service, cited 2011: Record floods of Greater Nashville: Including flooding in middle Tennessee and western Kentucky, May 1-4, 2010. [Available online at http://www.weather.gov/os/assessments /pdfs/Tenn_Flooding.pdf.]

Neiman, Paul J., F. Martin Ralph, Gary A. Wick, Jessica D. Lundquist, Michael D. Dettinger, 2008: Meteorological characteristics and overland precipitation impacts of atmospheric rivers affecting the West Coast of North America based on eight years of SSM/I satellite observations. *J. Hydrometeor*, **9**, 22–47.

Neiman, Paul J., F. Martin Ralph, P. Ola G. Persson, Allen B. White, David P. Jorgensen, David E. Kingsmill, 2004: Modification of fronts and precipitation

by coastal blocking during an intense landfalling winter storm in southern California: Observations during CALJET. *Mon. Wea. Rev.*, **132**, 242–273.

Ralph, F. Martin, Paul J. Neiman, George N. Kiladis, Klaus Weickmann, David W. Reynolds, 2011: A multiscale observational case study of a Pacific atmospheric river exhibiting tropical–extratropical connections and a mesoscale frontal wave. *Mon. Wea. Rev.*, **139**, 1169–1189.

Ralph, F.M., P.J. Neiman, G.A. Wick, S. I. Gutman, M. D. Dettinger, R. Cayan, and A. B. White, 2006: Flooding on California's Russian River: Role of atmospheric rivers. Geophys*. Res. Lett.*, **33**, L13801, doi:10.1029/2006GL026689.

Ralph, F. Martin, Paul J. Neiman, Gary A. Wick, 2004: Satellite and CALJET aircraft observations of atmospheric rivers over the eastern north Pacific Ocean during the winter of 1997/98. *Mon. Wea. Rev.*, **132**, 1721–1745.

Saha, Suranjana, and Coauthors, 2010: The NCEP climate forecast system reanalysis. *Bull. Amer. Meteor. Soc.*, **91**, 1015–1057.

Schumacher, Russ S., Richard H. Johnson, 2005: Organization and environmental properties of extreme-rain-producing mesoscale convective systems. *Mon. Wea. Rev.*, **133**, 961–976.

The Leaf Chroincle, cited 2010: Closings due to flood. [Available online at http://www.theleafchronicle.com/article/20100504/NEWS01/5040311/Closings-due-flood?gcheck=1.]

Zhu, Yong, Reginald E. Newell, 1998: A proposed algorithm for moisture fluxes from atmospheric rivers. *Mon. Wea. Rev.*, **126**, 725–735.

INITIAL DISTRIBUTION LIST

1. Defense Technical Information Center
   Ft. Belvoir, Virginia

2. Dudley Knox Library
   Naval Postgraduate School
   Monterey, California

3. Air Force Weather Technical Library (AFWTL)
   14th Weather Squadron
   Ashville, North Carolina

4. Air Force Institute of Technology (AFIT)
   Wright-Patterson AFB, Ohio